ADVANCED CURRENT COLLECTION RESEARCH

LEVEL II 12

Annual Technical Report for
Period Ending 28 February 1978

A052394

Code 473 SC

Submitted to

Advanced Research Projects Agency

Contract N00014-76-C-0683

ARPA Order No. 3153

D. L. Greene, J. L. Johnson, P. K. Lee,
I. R. McNab, C. J. Mole, J. J. Schreurs,
O. S. Taylor

AD A056273

AD NO. ____
DDC FILE COPY

Westinghouse R&D Center
1310 Beulah Road
Pittsburgh, Pennsylvania 15235

ADVANCED CURRENT COLLECTION RESEARCH

LEVEL II

12

Annual Technical Report for
Period Ending 28 February 1978

Submitted to

Advanced Research Projects Agency

Contract N00014-76-C-0683

ARPA Order No. 3153

D. L. Greene, J. L. Johnson, P. K. Lee,
I. R. McNab, C. J. Mole, J. J. Schreurs,
O. S. Taylor

Westinghouse R&D Center
1310 Beulah Road

UNCLASSIFIED
Security Classification

DOCUMENT CONTROL DATA - R&D

(Security classification of title, body of abstract and indexing annotation must be entered when the overall report is classified)

1. ORIGINATING ACTIVITY (Corporate author)
Westinghouse Electric Corporation
Research & Development Center
Churchill, PA 15235

2a. REPORT SECURITY CLASSIFICATION
UNCLASSIFIED

2b. GROUP

(10) D. L. Greene
J. L. Johnson
P. K. Lee
I. R. McNab
C. J. Mole

3. REPORT TITLE
(1) ADVANCED CURRENT COLLECTION RESEARCH *

4. DESCRIPTIVE NOTES (Type of report and inclusive dates)
(9) Annual Technical Report * For Period Ending 28 February 1978

5. AUTHOR(S) (First name, last name, initial)
Greene, D. L.; Johnson, J. L.; Lee, P. K.; McNab, I. R.; Mole, C. J.; Schreurs, J. J.; and Taylor, O. S.

6. REPORT DATE
(11) 19 April 1978

7a. TOTAL NO. OF PAGES
(12) 163p.

7b. NO. OF REFS

8a. CONTRACT OR GRANT NO.
(15) N00014-76-C-0683

b. PROJECT NO.
ARPA Order-3353

c.

d.

(14)

9a. ORIGINATOR'S REPORT NUMBER(S)
78-9B21-AMCOL-R1

9b. OTHER REPORT NO(S) (Any other numbers that may be assigned this report)

DISTRIBUTION STATEMENT A
Approved for public release
Distribution Unlimited

10. AVAILABILITY/LIMITATION NOTICES
Qualified requesters may obtain copies of this report from Defense Documentation Center, Cameron Station, Alexandria, VA 22314

11. SUPPLEMENTARY NOTES (Add'l Sponsor)
Office of Naval Research
800 N. Quincy Street
Arlington, VA 22217

12. SPONSORING MILITARY ACTIVITY
Advanced Research Projects Agency
Dept. of Defense, 1400 Wilson Blvd.;
Arlington, VA 22209

13. ABSTRACT

This report describes the work performed during the second year of ARPA/ONR Contract N00014-76-C-0683, with a scope of work expanded beyond that of the first year. The program is directed towards obtaining a greatly improved understanding of the physical factors which govern high current brush performance, leading to the development and demonstration of advanced brush materials. These materials are to be demonstrated at 7.75 MA/in^2 (5 kA/in^2) in a machine application as the ultimate goal of the program. Progress is reported in the attainment of this goal in the areas of materials characterization, brush/ring dynamics, brush heat transfer, atmosphere control, contact interface investigations, multi-element brush research, and monolithic brush material research. The participation of university researchers in the investigation of specific technology areas is also described.

SQ IN.

14. KEY WORDS	LINK A		LINK B		LINK C	
	ROLE	WT	ROLE	WT	ROLE	WT

INSTRUCTIONS

1. ORIGINATING ACTIVITY: Enter the name and address of the contractor, subcontractor, grantee, Department of Defense activity or other organization *(corporate author)* issuing the report.

2a. REPORT SECURITY CLASSIFICATION: Enter the overall security classification of the report. Indicate whether "Restricted Data" is included. Marking is to be in accordance with appropriate security regulations.

2b. GROUP: Automatic downgrading is specified in DoD Directive 5200.10 and Armed Forces Industrial Manual. Enter the group number. Also, when applicable, show that optional markings have been used for Group 3 and Group 4 as authorized.

3. REPORT TITLE: Enter the complete report title in all capital letters. Titles in all cases should be unclassified. If a meaningful title cannot be selected without classification, show title classification in all capitals in parenthesis immediately following the title.

4. DESCRIPTIVE NOTES: If appropriate, enter the type of report, e.g., interim, progress, summary, annual, or final. Give the inclusive dates when a specific reporting period is covered.

5. AUTHOR(S): Enter the name(s) of author(s) as shown on or in the report. Enter last name, first name, middle initial. If military, show rank and branch of service. The name of the principal author is an absolute minimum requirement.

6. REPORT DATE: Enter the date of the report as day, month, year; or month, year. If more than one date appears on the report, use date of publication.

7a. TOTAL NUMBER OF PAGES: The total page count should follow normal pagination procedures, i.e., enter the number of pages containing information.

7b. NUMBER OF REFERENCES: Enter the total number of references cited in the report.

8a. CONTRACT OR GRANT NUMBER: If appropriate, enter the applicable number of the contract or grant under which the report was written.

8b, 8c, & 8d. PROJECT NUMBER: Enter the appropriate military department identification, such as project number, subproject number, system numbers, task number, etc.

9a. ORIGINATOR'S REPORT NUMBER(S): Enter the official report number by which the document will be identified and controlled by the originating activity. This number must be unique to this report.

9b. OTHER REPORT NUMBER(S): If the report has been assigned any other report numbers *(either by the originator or by the sponsor)*, also enter this number(s).

10. AVAILABILITY/LIMITATION NOTICES: Enter any limitations on further dissemination of the report, other than those imposed by security classification, using standard statements such as:

(1) "Qualified requesters may obtain copies of this report from DDC."

(2) "Foreign announcement and dissemination of this report by DDC is not authorized."

(3) "U. S. Government agencies may obtain copies of this report directly from DDC. Other qualified DDC users shall request through _____."

(4) "U. S. military agencies may obtain copies of this report directly from DDC. Other qualified users shall request through _____."

(5) "All distribution of this report is controlled. Qualified DDC users shall request through _____."

If the report has been furnished to the Office of Technical Services, Department of Commerce, for sale to the public, indicate this fact and enter the price, if known.

11. SUPPLEMENTARY NOTES: Use for additional explanatory notes.

12. SPONSORING MILITARY ACTIVITY: Enter the name of the departmental project office or laboratory sponsoring *(paying for)* the research and development. Include address.

13. ABSTRACT: Enter an abstract giving a brief and factual summary of the document indicative of the report, even though it may also appear elsewhere in the body of the technical report. If additional space is required, a continuation sheet shall be attached.

It is highly desirable that the abstract of classified reports be unclassified. Each paragraph of the abstract shall end with an indication of the military security classification of the information in the paragraph, represented as *(TS), (S), (C), or (U)*

There is no limitation on the length of the abstract. However, the suggested length is from 150 to 225 words.

14. KEY WORDS: Key words are technically meaningful terms or short phrases that characterize a report and may be used as index entries for cataloging the report. Key words must be selected so that no security classification is required. Identifiers, such as equipment model designation, trade name, military project code name, geographic location, may be used as key words but will be followed by an indication of technical context. The assignment of links, rules, and weights is optional.

TABLE OF CONTENTS

TABLE OF CONTENTS (Cont'd)

TABLE OF CONTENTS (Cont'd)

LIST OF FIGURES

LIST OF FIGURES (Cont'd)

LIST OF TABLES

SECTION 1
INTRODUCTION AND SUMMARY

1.0 Background

After a year of advanced current collection research effort conducted under DARPA and ONR sponsorship (Contract N00014-76-C-0683), the program was modified to reflect the optimism that significantly higher current densities could be achieved for solid brush sliding electrical contacts than had been previously predicted. The modification of program direction also recognized the fact that the participation of university research specialists could contribute beneficially to the program, and that a portion of the program should be tailored to meet the needs of the ONR SEGMAG machine research effort.

The expected results of the ongoing advanced current collection research work will contribute to many sectors of DOD where high power density equipment is utilized. For example, in electrical machine designs requiring current transfer from a rotating member to a stationary member, a high current density collector can substantially reduce overall machine weight and volume.

1.1 Objectives

The objectives of the advanced current collection research program are keyed to measure success in both the SEGMAG machine research effort and the brush interface and material research effort.

For the SEGMAG machine research effort, the program seeks to:

1. Characterize the broad spectrum of SEGMAG candidate brush materials for operation at current densities up to $2.3 \cdot 10^6$ A/m^2.
2. Establish optimal design data for brush/ring system dynamics.

3. Create a theoretical brush interface heat transfer model, and test it experimentally.

4. Establish limits of debris concentration in machine atmosphere for satisfactory operation.

For the brush interface and material research effort, the principal objective is to improve brush current density from the present level of 1.55 MA/m^2 to 7.7 MA/m^2, with an interim goal of 3.1 MA/m^2. Successful achievement of these goals will require major improvements in brush materials. The values of critical parameters which are established for a nominal operating requirement for the interim and ultimate current density goals are shown in Table 1.1 below.

TABLE 1.1 - RESEARCH PROGRAM GOALS FOR CRITICAL PARAMETERS

Parameter	Interim Goal	Ultimate Goal
Current Density (MA/m^2)	3.1	7.8
Collector Surface Velocity (m/s)	25-75	25-75
Brush Material Life (max. velocity) (hr/in)	1400	1400
Demonstration Period (hr)	300	500
Losses (w/A)	.25	.25

In order to demonstrate the results of the current collection research program, a model of a practical application will be selected, designed, constructed, and tested in the program. The objective will be to show the impact of the technology advancement in a defense role.

1.2 Prior and Related Work

Prior work under Contract N00014-76-C-0683 was reported in the first annual report and is summarized below.

The conduct of the test program required the use of five conventional test rigs and two sophisticated test rigs specifically

designed for the program. These include four laboratory rigs for the initial screening of materials and environments, one laboratory rig for the testing of fiber brushes and two high speed, cooled rotor rigs for the close simulation of developmental machine performance. All of these rigs were operated in a comprehensive screening program to identify materials capable of operating at high current densities.

Brush material screening tests resulted in the selection of four candidate materials for continued testing at high speed on the cooled rotor test rigs, including three silver-graphite and one copper graphite grades. Tests of various ring materials indicate that copper and silver based alloys result in the lowest net power loss and longest life for brush operation.

The development of a multi-fiber shunt was continued through two iterations in preparation for dynamic tests against an operating brush. Static tests correlated well with a mathematical description of the voltage drop. These shunts were for replacement of conventional braided shunts which are too bulky in high current density applications.

Five non-oxidizing gases, combined with water vapor, were tested as the atmosphere for the operation of copper graphite brushes on copper slip rings. Simiarly, a series of tests employing atmospheres of CO_2 with hydrocarbon vapor addition was run to examine the impact of various vapors on the lubricating properties of graphite. Brush performance was found to be dependent on the selection of the non-oxidizing gas as well as on hydrocarbon molecular weight and vapor concentration.

It was recognized that multiple-contact brushes and fiber brushes particularly were required, if substantially higher current densities were to be realized. In the fiber brush work, principal efforts were conducted in the areas of carbon fiber metallization and fiber brush construction. A fiber brush test rig was commissioned and testing undertaken. Tests were accomplished with various atmospheres, but with no forced cooling.

Fundamental research projects were divided into three areas: a general state-of-the-art review, development of contact phenomena information, and the establishment of technologically promising approaches for the future of the program.

In order to base the material research and development efforts on the most up-to-date information, a literature review was conducted in the relevant areas of the chemical and physico-chemical properties of lamellar solids (mainly graphite and various dichalcogenides) and their interactions with metal surfaces.

The impact of hydrocarbon vapors or water vapor present in the atmosphere of graphite and metal-graphite contact systems was measured experimentally. Resistance values as a function of contact force were determined, and a power-law relationship was established.

Based on the results of screening tests, contact phenomena experiments, atmosphere variation tests and the literature review, the directions for new material developments were identified, with the objective of reaching the program goals in the most effective manner. Avenues to be pursued were shown to be promising in both new materials and new structures for brushes, as well as advanced cooling, shunting, and loading techniques.

1.3 Summary of Current Progress

1.3.1 Materials Characterization

Brushes which were selected on the basis of earlier work were subjected to longer duration, higher speed tests to confirm their applicability to the segmented magnet (SEGMAG) machine program. The focus was on silver-graphite brushes of a 75% by weight metal content. Additional tests included high-speed screening of other compositions, determination of brush material mechanical properties and operation of multiple brushes in the same track to observe current sharing performance. In the brush tests, operation of silver graphite brushes was achieved with losses 2-2.5 times the ultimate desired level for operation in the

3000 hp SEGMAG demonstration machines. The parallel operation tests demonstrated the ability of a large number of brushes to operate successfully at high current density in the same track.

1.3.2 Brush/Ring Dynamics

The conventional brush holder heuristic design restrictions have been reduced to theoretical limitations by revealing brush performance sensitivity to variations in contact load. Graphs of loss amplification factors are supplied for the design engineer to apply to brush loss calculations to account for load variations.

A theoretical model is presented to explain the electrical performance of the Multiple Finger Shunts (MFS). The model follows the fundamental contact theory of Holm and is presented with supporting data.

A brush actuation system prototype has been developed for experimental use on the Advanced Brush System (ABS) test stand. The actuation system utilizes pneumatic cylinders for lifting and constant force springs for fail-safe loading.

1.3.3 Brush Heat Transfer

No work was scheduled in this task area during the reporting period. Preliminary efforts are reported.

1.3.4 Debris Removal/Atmosphere Control

A debris removal system prototype has been designed and built for experimental use on the Machine Environment Brush (MEB) system test stand. The system utilizes the machine cover gas to transport the airborne brush debris outside the machine where the gas is filtered, cooled, humidified, and then returned to the machine.

1.3.5 Contact Interface Investigation

An evaluation of experimental data for a range of silver-graphite brush materials run on copper slip rings in non-air atmospheres has been undertaken. The major contribution to the electrical contact resistance was found to be provided by the constriction resistance, with the film resistivity being relatively small ($< 6 \times 10^{-13}$ ohm m^2). The frictional behavior, based on the assumption of an adsorbed water film, was consistent with an average film thickness of one or two monomolecular layers. The most notable unexplained feature was that the brush wear rate changed by a factor of a hundred (from 0.7 mm^3/Mm to 70 mm^3/Mm) as the brush metal mass friction was doubled from 0.45 to 0.90. To date, a fully satisfactory explanation for this has not yet been developed, although a model is at present under development.

Experimental studies, using Auger techniques, confirmed that some portions of the bulk slip ring were within 10 Å of the film surface. Further studies using high vacuum techniques are presently underway to further elucidate the mechanism of film formation.

1.3.6 Multi-Element Brush Research

Techniques have been developed for coating and assembling brushes using carbon fibers. Experimental tests with these brushes have been undertaken in a variety of atmospheres and levels of humidity at current densities up to 4.65 MA/m^2. Extensive tests at lower current densities 1.55 MA/m^2 showed that a significant polarity difference (with the positive voltage drop being 3 to 5 times greater than the negative voltage drop) was present in "wet" air atmospheres, but not in "dry" (i.e., low humidity) conditions. In helium atmospheres, polarity effects were less evident, for reasons which have not yet been determined.

Development of a general theory for multi-element brushes is presently underway. The results obtained to date demonstrate a clear advantage for the multi-element approach so far as contact resistance is concerned. The development of a model for friction and wear in

multi-element contacts has also been initiated, and is described here. In parallel with this theoretical development, an experimental multi-element brush unit has been built and is being prepared for testing.

1.3.7 Monolithic Brush Material Research

During this reporting period, efforts were primarily devoted to the preparation and evaluation of metal-coated graphite, oleophilic graphite and phosphate-impregnated graphites. After metallization, bulk resistivities which were significantly lower than those of brushes produced by powder metallurgy techniques or metal infiltrated graphites were measured, as a result of the three-dimensional metal matrix within the brush.

Slip ring tests with a variety of powder-metallurgy produced brushes were undertaken at current densities up to 2.3 MA/m^2 (and, more recently, at current densities up to 10.85 MA/m^2 -- a level 40% beyond the ultimate goal for this program). Emphasis is now directed towards reducing electrical and frictional losses and reducing wear rates.

1.3.8 University Investigations

During the period covered by this report, investigations have been initiated at three universities -- Northwestern, MIT, and Syracuse. The efforts at each location emphasize differing, but complementary, aspects of the major program goal. Work at NWU centers around an extension of thermo-elastic stability studies to brush conditions, and an initial study has been completed. Emphasis at Syracuse will be on investigations of surface films using advanced diagnostic techniques, and existing Auger apparatus is presently being modified for this purpose. Work at MIT is directed towards materials science aspects of friction and wear with metal-graphite materials under representative conditions of current transfer.

Substantial and significant contributions to the program are expected from these investigations in the next contract period.

1.3.9 Demonstration Machine Program

Initial contacts were made with U.S. Army TARADCOM for assistance in preparing for the selection of candidate platform characteristics which will define a current collection demonstration model. It is expected that appropriate vehicles will lie in the 650-1000 hp engine power class.

SECTION 2
BRUSH APPLICATION (SEGMAG) RESEARCH

This research program supports the Segmented Magnet (SEGMAG) Machine Research Program sponsored by the Office of Naval Research by providing current collection system design data and experimental verification of current collector system performance estimates. To fulfill these requirements, task efforts have been undertaken in the areas of brush testing, brush/ring dynamics, brush heat transfer, and brush debris removal and atmosphere control. All of these areas will require significant analytic and experimental effort to provide full confidence in the operation of the first demonstration SEGMAG machines, a motor and generator at 3000 HP.

Of greatest significance during the reporting period was successful testing of prototypic brushes in a demonstration machine. The initial development of high-power-density homopolar motors requires brushes with a continuous running capability of 155 A/cm^2 (1 kA/in^2), a large percentage ring cover by the brushes, and many parallel brushes transferring large total current loads. Testing was achieved with a unique machine environment brush tester, the only known electrical machine in the world that uses brushes at 155 A/cm^2 continuously. Evaluation runs of up to 170 h were made with a full complement of silver-graphite brushes (92 brushes; 46 parallel brushes/polarity) and with a total load current near 10,000 amperes. Successful brush-slip ring performance is attributed to a careful selection of brush materials, to running in an oxygen-free gas environment, and to efficient use of brush-ring cooling. Continuous operation of monolithic brushes has been successfully advanced from 12 A/cm^2 (80 A/in^2) to 155 A/cm^2 (1 kA/in^2), with significant improvements in the interface energy loss and contact life. Neither energy loss density nor wear were degraded as the number of test brushes was increased to the

full complement level. Over one year average brush life was demonstrated under conditions of 42 m/s (8300 ft/min) collector ring velocity and 52% ring coverage by the brushes.

While work is continuing to develop unconventional brush materials leading to more efficient current transfer and to meet a new higher current density goal of 230 A/cm^2 (1.5 kA/in^2), the present brush performance results are of principal significance in relationship to the developments of the high-power-density dc SEGMAG machines.

The following sections describe more fully the work accomplished in all the tasks associated with providing current collection systems appropriate to the design of SEGMAG machines.

2.1 Materials Characterization

2.1.1 Objectives

The objective of this task is to conduct screening and long duration tests of brush materials which are candidates for operation in SEGMAG machines. The ultimate goal is support of current collection systems with 2.3×10^6 A/m^2 (1500 apsi) interface capability. The interim goal is to support current collection systems for a 3000 hp SEGMAG motor and generator with a $1.5 \cdot 10^6$ A/m^2 (1000 apsi) interface capability.

2.1.2 Prior and Related Work

In work reported previously, large numbers of commercially available brush materials were screened to identify the most promising candidates for further high current tests. The grades which yielded the best combination of low wear and low losses were metal-graphite grades with compositions containing metal weight percentages between 55 and 80. A composition of silver-graphite with 75% silver by weight was particularly attractive in prior tests. This material was considered the prime SEGMAG candidate after the first year's effort. However, it is recognized that lower cost materials will be necessary in the long-term and must be developed.

2.1.3.1 Material Properties

A desire in high current density solid brush current collection is to theoretically predict the performance based on operating conditions, geometry, and material properties. The purpose of the material properties investigation was to provide the mechanical strength portion of the material properties for a group of metal graphite brushes. There were seven grades of copper graphite and seven grades of silver graphite brush materials examined, both metals ranging in weight percent from fifty-five to eighty-five in five percent increments.

The metal graphite brush materials were very brittle (maximum compressive strains were generally less than 1%) and exhibited non-linear stress-strain relations, much like very soft copper. Therefore, it is impractical to determine elastic properties (modulus and Poisson's ratio) for these materials without specifying the load. The yield stress should be defined at a given strain, rather than any offset value.

From the test results and a consideration of material use, the hardness measurement of the material is the most desired and economic mechanical property to be measured. Also, the 15-W Rockwell superficial scale is the most suitable to cover the material hardness.

2.1.3.2 Test Results

The significant test efforts conducted during the reporting period were aimed at demonstrating the operation of brushes under machine sliding speed and current density conditions and at demonstrating the ability to operate multiple brushes in the same track with good current sharing. The highlights of the test results are described below.

A. Machine Speed and Current Density Tests. For these tests, the Advanced Brush System (ABS) Tester and the Machine Environment Brush (MEB) tester were employed in a series of tests which simulated the 3000 hp SECMAG motor and generator speeds and current densities. In the ABS tester, current is supplied by a full wave rectifier dc source and the rig is powered by a variable speed dc motor. The MEB tester is a drum-type

homopolar machine, driven by a wound-rotor induction motor. Silver-graphite brushes of metal weight percentage ranging from 55 to 85% were tested during the reporting period. The MEB rotor is a smooth copper drum, while the ABS rotor has been slotted to simulate the bar arrangement of the 3000 hp SEGMAG machines. In the ABS, the brushes were mounted as shown in Figure 2.1, with the brushes at a 15° trailing angle; that is, the brush longitudinal axis made a 15° angle with the radius of the rotor. The ABS utilizes four brushes per holder, and there are two holders in the test chamber, one for each polarity. The brush current is transferred to the holder by a Multiple Finger Shunt (MFS).

In the MEB tester, the brushes are supported radially, with no lead or trail angle. Brush current is transferred from the brush to the stator through "pigtail" shunts of copper wire tamped into the brush. There are two brush tracks per polarity, with a capacity of 23 brushes per track.

The use of the ABS and MEB rigs permitted testing at sliding velocities which duplicate the 3000 hp SEGMAG motor (35.5 m/sec, 7000 ft/min) and generator (71.1 m/sec, 14,000 ft/min) full load conditions. The brush pressures were varied from 104.5 kPa (15.2 psi) to 52.3 kPa (7.6 psi) to investigate the effect of loading on performance. Figures 2.2 and 2.3 reflect the results of the high speed, $1.5 \cdot 10^6$ A/m^2 (1000 apsi) tests. As indicated on these figures, the best loss performance results obtained in the reporting period were within 2-2.5 times the goals established in the SEGMAG machine program. As was the case in the earlier, slow-speed screening tests, the best performance was obtained with silver-graphite brushes in the metal weight percentage range of 65-80%.

Subsequent to achieving the loss level described above, planning and analysis were undertaken to establish the necessary directions for reducing the brush losses by one-half. The most obvious direction was the reduction in friction loss which would accrue to the use of reduced brush pressure, since the distribution of the losses has generally shown the friction loss to be more than one-half of the total. The difficulty

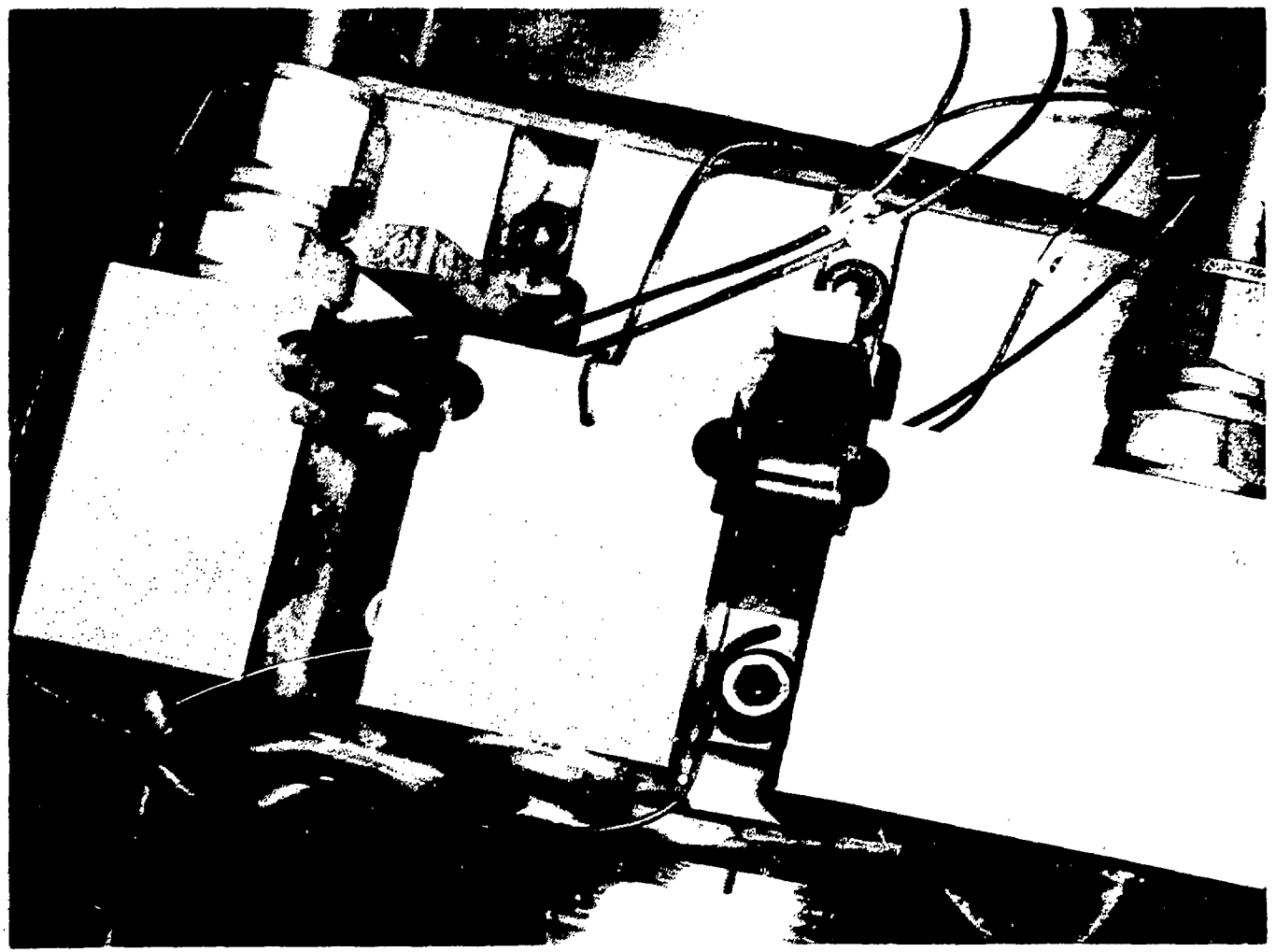

FIGURE 2.1. Advanced Brush System (ABS) test stand brush holder.

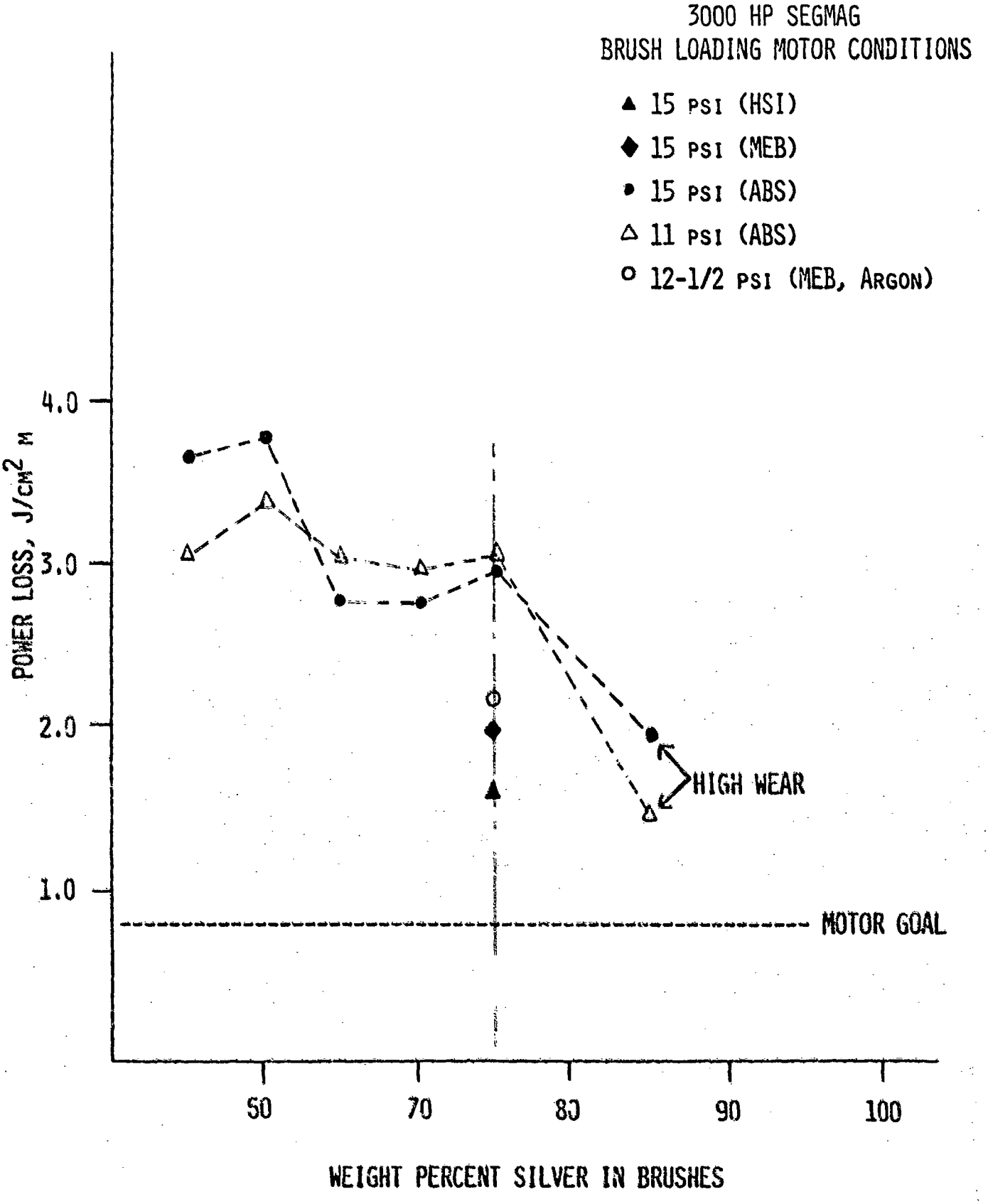
3000 HP SEGMAG
BRUSH LOADING MOTOR CONDITIONS
15 PSI (HSI)
15 PSI (MEB)
15 PSI (ABS)
11 PSI (ABS)
12-1/2 PSI (MEB, ARGON)
POWER LOSS, J/CM2 M
4.0
3.0
2.0
1.0
HIGH WEAR
MOTOR GOAL
50
70
80
90
100
WEIGHT PERCENT SILVER IN BRUSHES

FIGURE 2.2

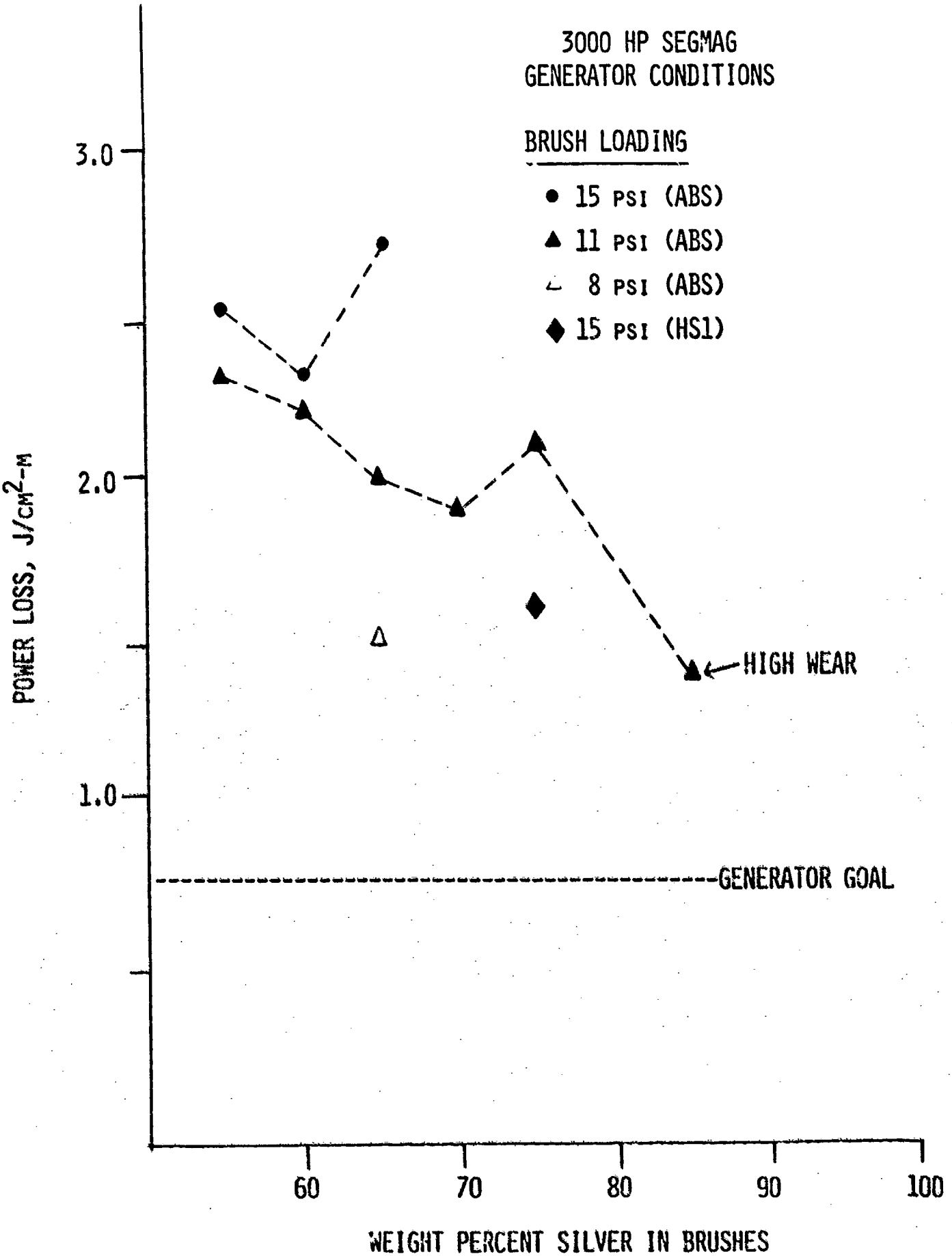
3000 HP SEGMAG
GENERATOR CONDITIONS
BRUSH LOADING
15 PSI (ABS)
11 PSI (ABS)
8 PSI (ABS)
15 PSI (HS1)
3.0
2.0
1.0
POWER LOSS, J/CM2-M
HIGH WEAR
GENERATOR GOAL
60
70
80
90
100
WEIGHT PERCENT SILVER IN BRUSHES

FIGURE 2.3

in reducing brush pressure in high speed systems lies in dynamic factors which result in an inability of the brush to follow the ring closely, resulting in a widely fluctuating loading pressure. In the ABS and MEB tests, operation below 8 psi resulted in a fluctuating contact voltage drop, indicating a loading pressure variation which approached the spring-applied loading pressure. The ABS tester was then instrumented to establish the dynamic pattern of load variation, with the intent of correcting this load variation to permit reduction of the applied pressure. A literature search for experience in the area of brush loading stability was undertaken, resulting in the bibliography of references 2.1-2.13, many of which required translation. The dynamics of the brush/ring system are under investigation as described in Section 2.2; however, utilizing the analytic approach developed there, it was possible to speculate on the performance improvement which would be possible, if the load variation could be controlled. The accelerometers on the ABS also showed that some stiffening and realignment of the test rig was necessary to correct vibration of the stand and holders. This vibration, coupled with poor dynamic coupling of the brush/ring system was identified as the major source of the inability to achieve stable, low loading pressure performance.

In order to predict the improvement possible with reduced load variation, it was assumed that at 50 kPa (7.5 psi) arcing occurs, due to the brush momentarily leaving the rotor surface. From the techniques described in Section 2.2, a variation in load of 50 kPa would result in an estimated contact force variation of 67% at 104.5 kPa and 50% at 78.5 kPa. The corresponding average voltage drop increases are 26% and 12%, respectively. For the test data in Figure 2.3, the loss associated with operation of 65% by weight brush at 104.5 kPa would thus be 1.9 $J/cm^2 \cdot m$, vice 2.3, if all variation was removed. The loss associated with operation of the 70% by weight brush at 78.5 kPa would be 1.8 $J/cm^2 \cdot m$, vice 1.9. The combined elimination of load variation and reduction in load pressure from 78.5 to 50 kPa would result in a loss of about 1.8 $J/cm^2 \cdot m$ (700 W/in^2), which has been demonstrated in this pressure range.

A second factor which prevented reduction in brush losses during the reporting period was a higher than predicted contact voltage drop, apparently due to the establishment of a silver film on the slip ring surface which was heavier than the optimum. At the beginning of the tests, contact voltage drops were typically .2V (avg. positive and negative), which was somewhat higher than had been achieved on the smaller rigs (.1-.15V avg.), and this drop increased as a test series proceeded, at times reaching .3 V avg. It was felt that some control over the film growth could be obtained with the addition of a small amount of cleaning material in the brush body. Preparations were made for the supply of silver-graphite brushes containing such additives for testing early in the next reporting period.

It was concluded at the close of the reporting period that, in order to reach the design goal for losses in the 3000 hp SEGMAG motor and generator, it would be necessary to insure stable dynamic brush performance, reduce the loading pressure below 50 kPa, and control the film thickness. Additionally, some other additives, notably the dichalcogenides described in Section 3.3, under the material research portion of the program, will be utilized to improve the friction characteristics of brush performance.

B. Tests for Operation of Many Brushes in Parallel. These tests were conducted with the Machine Environment Brush (MEB) tester, which is a homopolar machine previously described in the First Annual Report. Graphite brushes containing nominal 0.75 weight fraction silver were tested during the reporting period. This brush composition was selected because previously determined performance of similar material brushes was judged to be near the optimum, based on smaller scale (one brush per polarity), lower peripheral speed (13 m/s), and lower current (78 A/cm^2) laboratory tests. The first MEB brush test run was made with only four brushes per polarity or ring (9% circumferential coverage). Subsequent tests were made with greater numbers of parallel-connected brushes, to a maximum of 23 brushes per ring (52% coverage). Finally, a full machine complement of brushes (92) was tested, involving 23 brushes per ring and 2 rings per polarity.

The total brush load current was increased as the number of test brushes was increased to achieve a constant current density (155 A/cm^2), the 3000 hp machine goal. The test runs reported here were relatively short in duration (6 h), but most were duplicated. Longer duration runs (48 to 170 h) were made with 15 brushes per ring, because that operating condition represents typical ring coverage (34%) for the advanced design homopolar machines of interest. Other pertinent test operating conditions are presented along with the performance curves.

The results of these tests are summarized in Figures which serve to illustrate the excellent current sharing capability of the brushes operating at high current density in a controlled environment. The principal findings of this test series can be described as follows:

a) Both total contact resistance (Figures 2.6 and 2.5) and contact resistance per brush (Figure 2.6) decreased as the number of brushes per ring was increased. This was possibly due to the greater silver transfer to the copper ring as the number of brushes (and load current) were increased.

b) It was observed that quite uniform silver films were deposited on the chrome-copper alloy drum by the brush operation. In general, the film is thicker on the cathodic ring track. This surface is the one which would be favored by ionic conduction of positive silver ions.

c) The percentage of the total interface loss which is attributed to the electrical component, vice the friction component, decreases as the number of brushes per ring is increased. As the number of brushes per ring was varied from 4 to 23, the percentage of the total loss due to the electrical effects decreased from 42 to 23% and 28 to 11% for the anodic and cathodic brushes, respectively.

d) Comparison of short time (4-6 hrs) and long time (48 hrs) test results showed similar contact drop and friction coefficient values. Brush life values for long-term runs were on the order of 20,000 hr/in cathodic and 10,000 hr/in anodic.

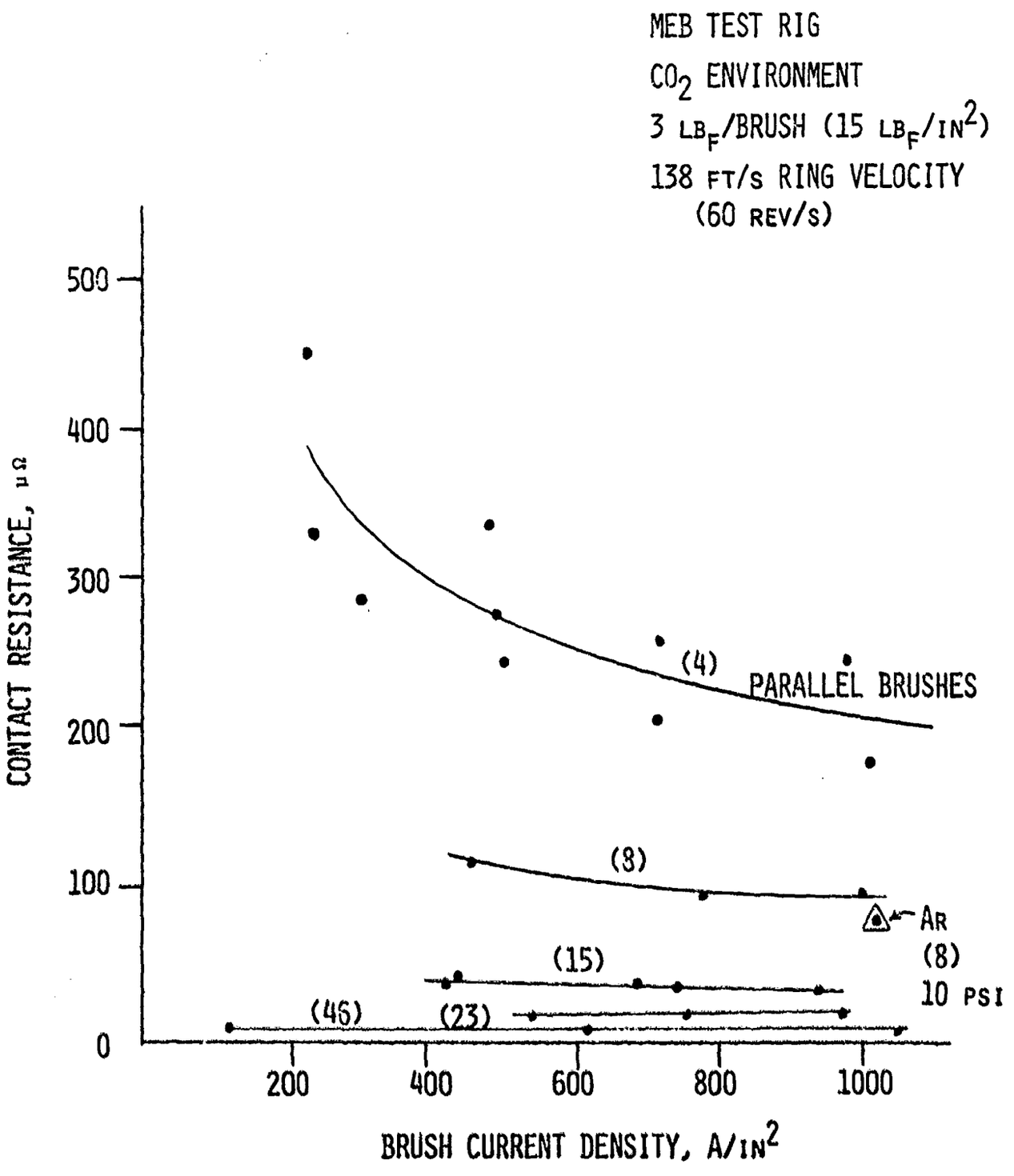
MEB TEST RIG
CO_2 ENVIRONMENT
3 LB_F/BRUSH (15 LB_F/IN^2)
138 FT/S RING VELOCITY
(60 REV/S)
CONTACT RESISTANCE, μΩ
500
400
300
200
100
0
200
400
600
800
1000
BRUSH CURRENT DENSITY, A/IN^2
(4) PARALLEL BRUSHES
(8)
AR
(8)
10 PSI
(15)
(46)
(23)

FIGURE 2.4

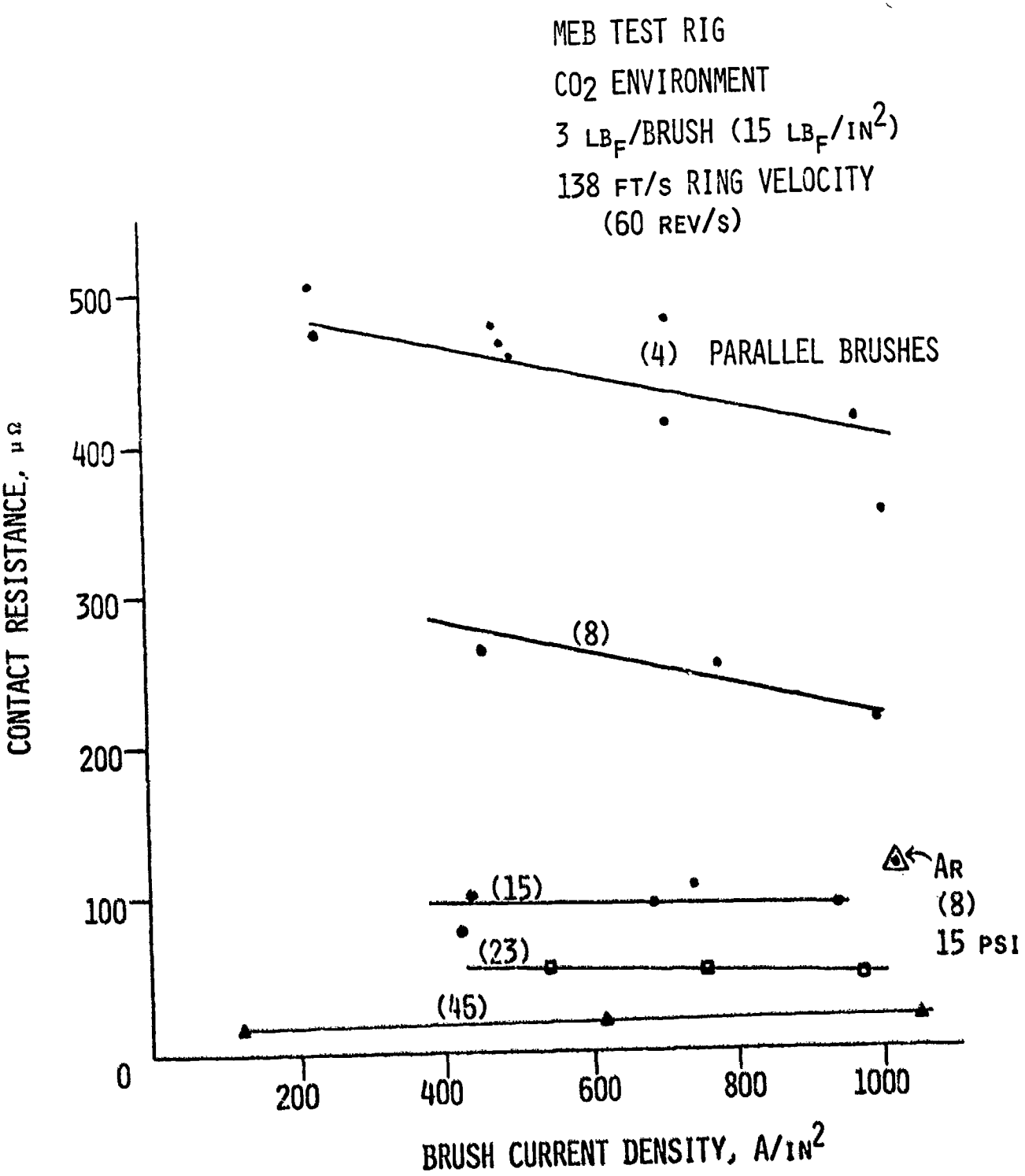
MEB TEST RIG
CO_2 ENVIRONMENT
3 LB_F/BRUSH (15 LB_F/IN^2)
138 FT/S RING VELOCITY
(60 REV/S)
CONTACT RESISTANCE, μΩ
500
400
300
200
100
0
(4) PARALLEL BRUSHES
(8)
(15)
(23)
(46)
AR
(8)
15 PSI
200
400
600
800
1000
BRUSH CURRENT DENSITY, A/IN^2

FIGURE 2.5

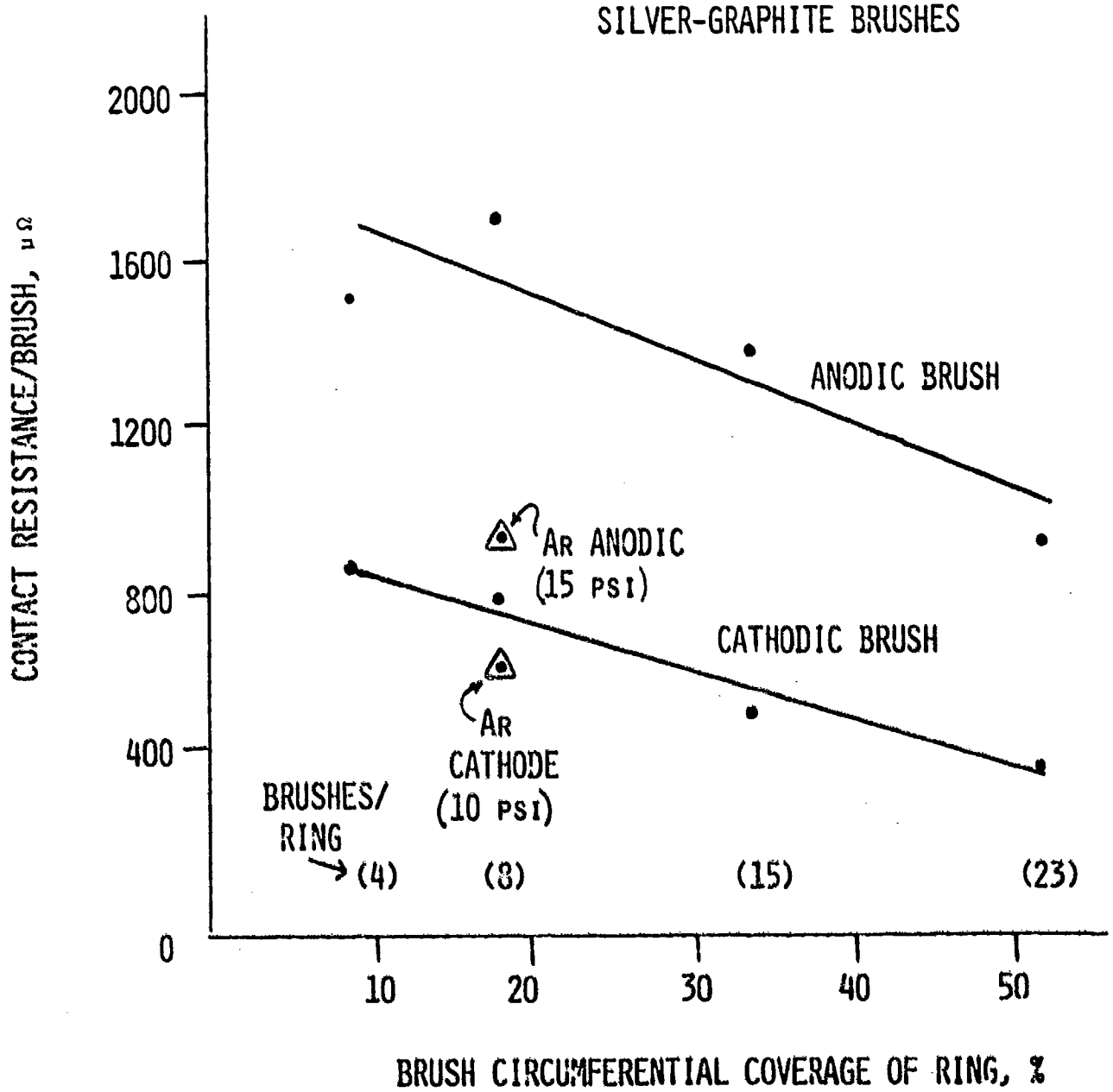
MEB TEST RIG
CO_2 ENVIRONMENT
138 FT/S RING VELOCITY (60 REV/S)
15 LB_F/IN^2 (3 LB_F/BRUSH)
1000 A/IN^2 (195 A/BRUSH)
SILVER-GRAPHITE BRUSHES
CONTACT RESISTANCE/BRUSH, μΩ
2000
1600
1200
800
400
0
ANODIC BRUSH
AR ANODIC
(15 PSI)
CATHODIC BRUSH
AR
CATHODE
(10 PSI)
BRUSHES/
RING
(4)
(8)
(15)
(23)
10
20
30
40
50
BRUSH CIRCUMFERENTIAL COVERAGE OF RING, %

FIGURE 2.6

e) A test run was conducted in humidified argon gas to verify earlier low-loss experience with this atmosphere. The results are shown on Figures 2.4 and 2.5, and a 22% loss reduction was indicated by the test. This suggests that a mixture of CO_2 for arc suppression and A for improved brush performance may be the preferred SEGMAG machine environment.

2.2 Brush/Ring Loading

2.2.1 Objectives

The objective of the brush/ring loading research is to develop a method to control brush loads to acceptable values. Selection of proper mechanical loading is necessary to assure satisfactory brush operation in rotating electrical machines. Irregularities in the moving surface produce forces such as brush inertia and holder friction which alter the contact force. The range of force variation depends upon controllable factors in the brush system design.

2.2.2 Prior and Related Work

Most of the previous work was done in the area of current transfer from the brush to the holder (brush-to-holder shunt). The conventional shunt size cannot be maintained with brush body current densities in the range of 1.55 MA/m^2 (1000 A/in^2) and higher. The large shunts which are necessary to preserve low voltage drops and acceptable temperatures are found to be heavy and stiff. Brush body voltage drop may also become a significant contributor to electrical power loss. With bulky shunt leads, it is difficult to avoid adverse mechanical restraint of the brush by the shunt, and this in turn prevents achievement of the contact load control necessary for good brush performance.

The electrical shunts have progressed through two generations of development. The first generation shunt was described in a similar report submitted to ARPA in September 1976.[2.14] This shunt configuration was composed of circular brass fibers drawn into brass blocks and then silver plated. The bundles of brass fibers were found to be too stiff and, as a result, only a friction of the fibers carried the current. A second

generation shunt was developed to obtain a more flexible contact. The second generation shunt performance, as well as the supporting theory was presented in the first annual technical report submitted to ARPA for the period ending 28 February 1977. Additional information pertaining to a third generation shunt that was developed for a particular machine application can be found in reference 2.15. A general review of the multiple contact theory along with appropriate data can be found in reference 2.16.

2.2.3 Current Progress

2.2.3.1 Finger Contacts

A multiple finger shunt (MFS) has been developed for use in the Advanced Brush System (ABS) test stand. A photograph of this shunt is shown in Figure 2.7 and a photograph of the shunt as positioned in the ABS brush holder is shown in Figure 2.1. The shunt and holder arrangement is shown schematically in Figure 2.8.

The MFS shunt has endured hundreds of hours of operation on ABS brushes operating at 1.55 MA/m^2 (1000 A/in^2). No measurable indications of wear were found either on the shunt contacts or the brush. There was, however, a change in surface texture that identified the path of the contact points on the side of the brush. The long-term shunt wear is expected to be low because both the contact load and the travel distance are small.

The high current density brush testing has demonstrated an advantage of using the MFS in the simplification of the brush manufacture and the ease of brush replacement. Without the conventional "pigtail" shunt, the brushes are simply rectangular blocks of brush material. Lead times on new brush materials has been reduced since shunt fabrication has been eliminated. The MFS is also easily removed for inspection or replacement since a simple bolted assembly is used for installation.

The MFS shown in Figure 2.7 was made from commercially available strips of silver-plated beryllium copper contact fingers. The finger contact strips were stacked and soldered to copper spacers to form an

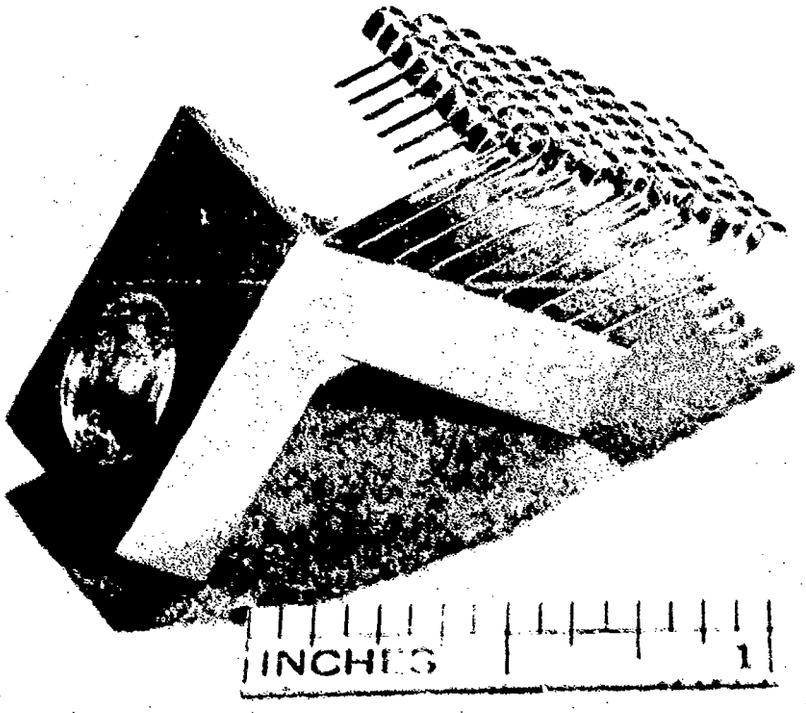

FIGURE 2.7. Multiple Finger Shunt (MFS)

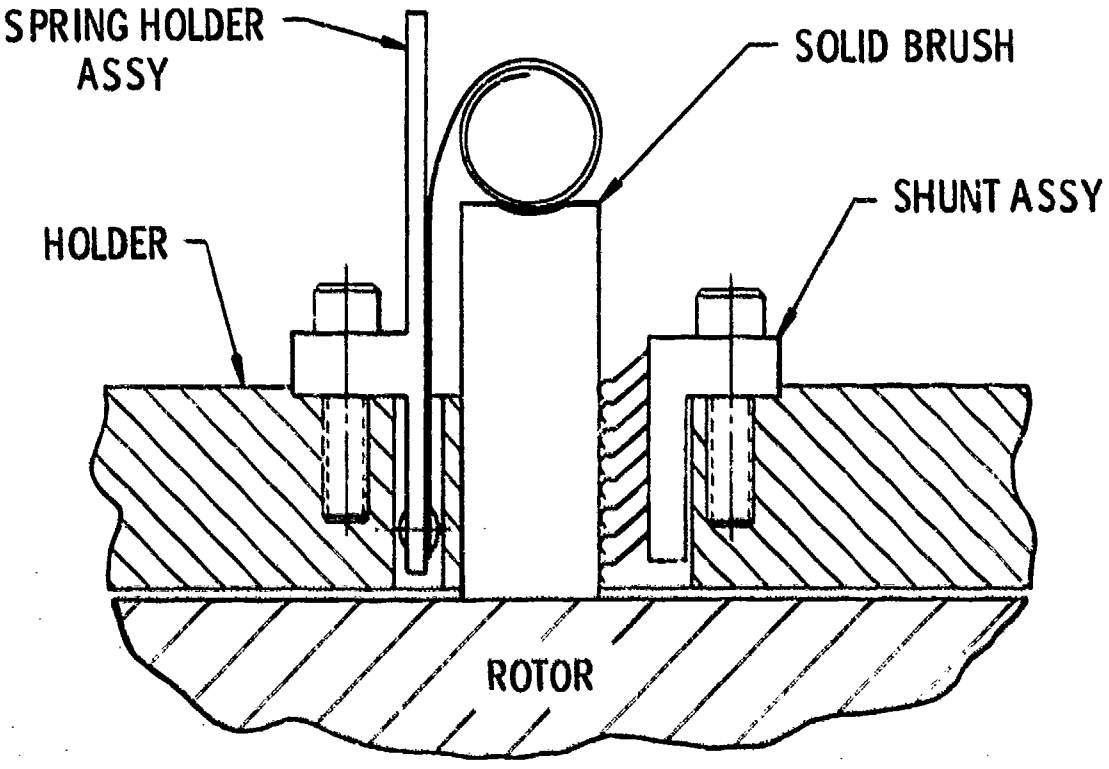

FIGURE 2.8

;LIDING CONTACT SHUNT APPLICATION

array of 72 contact points in a 21 mm (0.84 in) by 13 mm (0.50 in) area.

Since the first annual report (for the period ending 28 February 1977) much has been learned about the fundamental nature of the contact. Static test results from the MFS reveal that the contact resistance should be modeled as two resistance components rather than one as was previously done.

The electrical contact between two solid conductors is understood to occur through a number of very small areas which are part of the mechanical interface of the two mating surfaces. The electrical contact resistance is composed of a constriction resistance plus the effect of any film that may exist at these conducting locations. For a given material and film, the resistance depends on the number and size of these contacts. For metallic surfaces, the resistance has been demonstrated to follow an inverse power relationship with applied force:[2.17,2.18]

$$r_1 = C_1 f^{k_1} \tag{2.1}$$

$$r_2 = C_2 f^{k_2} \tag{2.2}$$

where r is the component of contact resistance corresponding to the contact force f, and C and k are constants which depend on material properties and the nature of the surface. The subscripts are "1" for constriction and "2" for film.

If two or more sets of these contacts are electrically connected in parallel, they will share the current just as parallel resistors in a circuit. For n identical contacts with a total force F = nf, the overall resistance will be:

$$R = (r_1 + r_2)/n \tag{2.3}$$

From Equations (1), (2), and (3), the resistance becomes:

$$R = \left[C_1 F^{k_1} \Big/ n^{1+k_1} \right] + \left[C_2 F^{k_2} \Big/ n^{1+k_2} \right] \qquad (2.4)$$

It can be seen, that for values of k less than 1, an increase in the number of contacts will reduce the total contact force required to achieve a given value of resistance. For certain contact geometries, Holm[4] has found values of $k_1 = -1/3$ and $k_2 = -2/3$ for light (elastic) loading and $k_1 = -1/2$ and $k_2 = -1$ for heavier loads where plastic flow determines the real contact area. The gross shape or conformability of the individual contacting members may influence the distribution and number of contact points at a given load. For closely mated or flexible bodied members, the number of contacts may increase with load, and this will result in larger negative values for k.[2.19,2.20] The flexibility of the asperities, the average separation distance, and the conformability of the contact members will determine this relationship.

Static tests were performed on a shunt like the one shown in Figure 1. The silver contact surfaces were cleaned with acetone followed by ethyl alcohol and a water rinse, a few hours prior to testing. Steel wool was used with the acetone to lightly abrade the surface film in order to assure consistent test conditions. Clean paper towels were used to dry the contacts. For comparison, a test series was performed on a shunt assembly which was not abraded with the steel wool but had been exposed to laboratory air for at least three months prior to the test to allow build-up of surface film. No significant difference was observed in the resulting measurements.

Figure 2.9 is a schematic of the test arrangement for the sliding contact shunt. The shunt was attached to a stationary metallic heat sink. The mating contact member for the test shunt was another heat sink and was silver plated. This member was suspended by a cable which permitted motion normal to the shunt without introduction of measurable force. The contact load, F, was measured with a strain gauge mounted on a

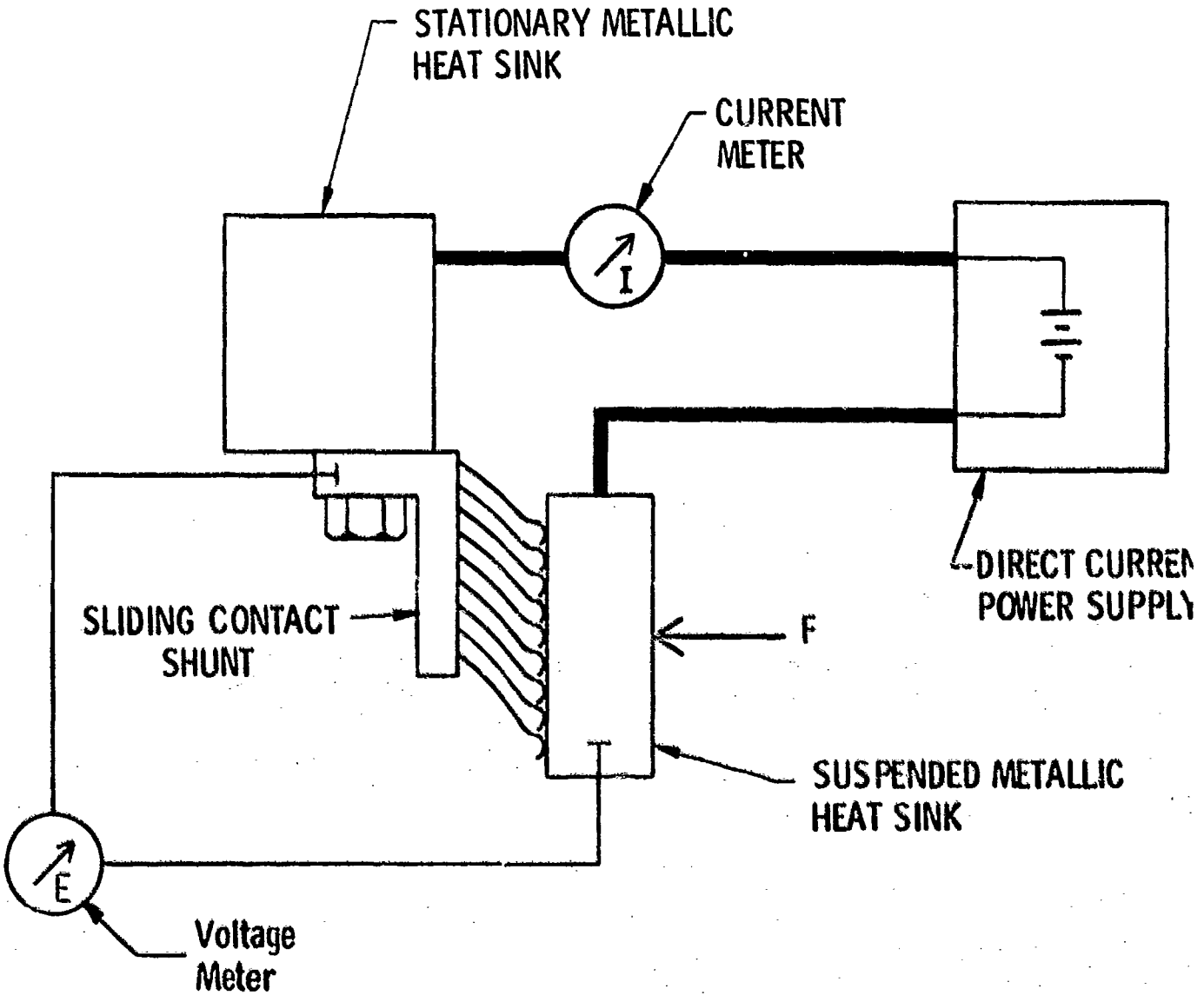

FIGURE 2.9

SLIDING CONTACT SHUNT TEST SCHEMATIC

cantilever. Direct current was supplied by a regulated power source. The sliding contact shunt resistance was determined from voltage and current measurements indicated in the Figure 2.9 schematic.

The results of the testing are shown in Figures 2.10, 2.11, and 2.12. Figure 2.10 shows typical measurements of shunt voltage drop versus current at three contact loads. The contact drop was measured for both increasing and decreasing current levels at each value of contact load. Figure 2.11 shows the measured values of resistance as well as the theoretically predicted relationship. Each point shown on Figure 2.11 represents the average of four points of data at each load value. The theoretical values of resistance are shown to be composed of a constant body resistance plus load-dependent film and constriction resistance components.

To separate the resistance components, the body resistance of the fingers was first determined by direct measurement. This was achieved by soldering the contact surfaces to a metal plate so that film and constriction resistances were eliminated. The constriction resistance was then calculated for each test value of shunt load, and the film resistance was determined as the remaining balance.

For the spherical contact of the finger loaded against the flat plate, the radius of the contact area for each finger is:[2.17]

$$a = 1.1 \left(\frac{f x}{E} \right)^{1/3} \qquad (2.5)$$

where x is the spherical radius of curvature (0.047 in, 1.2 mm) and E is the elastic modulus (11×10^6 lb/in^2, 7.6×10^{10} N/m^2).[2.21] This model is based on elastic theory and assumes that the silver plating determines the material characteristics of the interface.

The constriction resistance is:[2.17]

$$r_1 = \frac{\rho}{2a} \qquad (2.6)$$

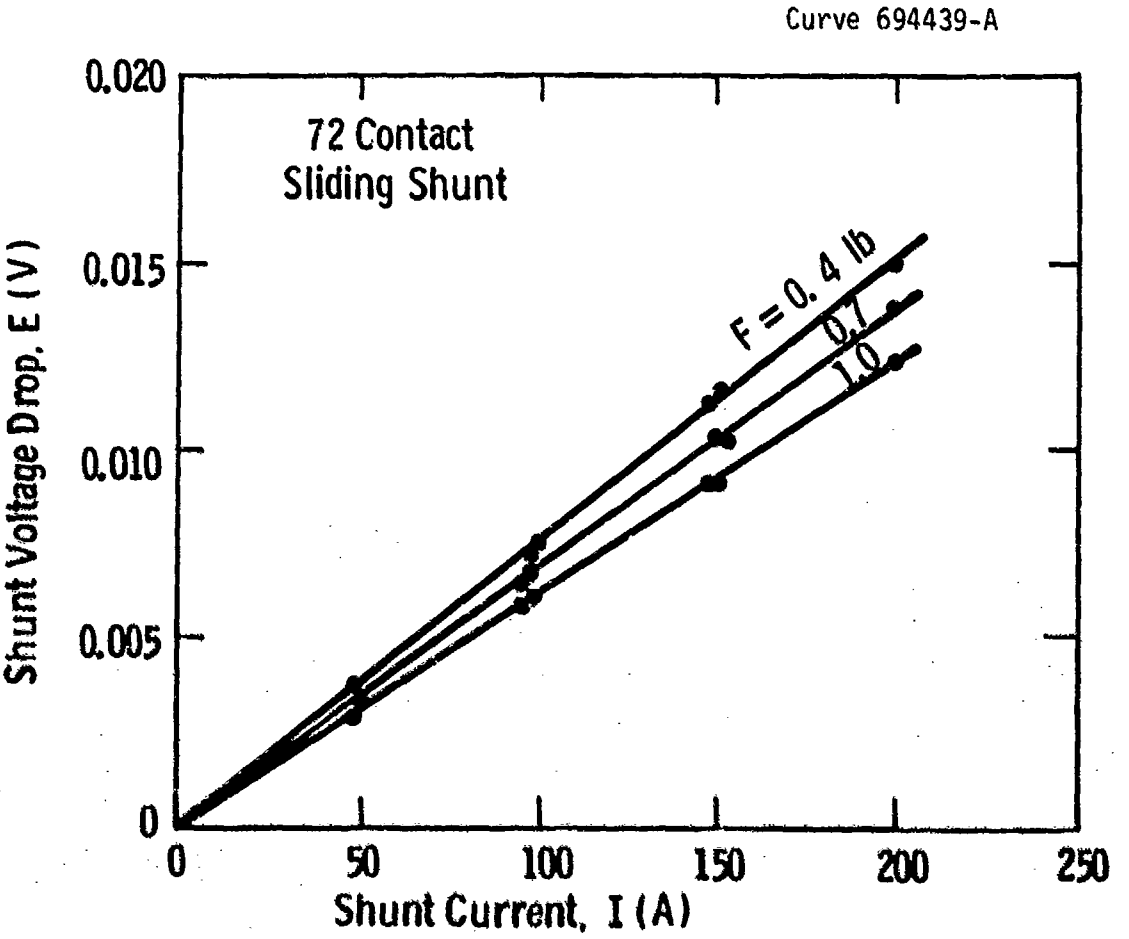

Fig. 2.10 – Shunt voltage drop versus current at various loads

Curve 694438-A

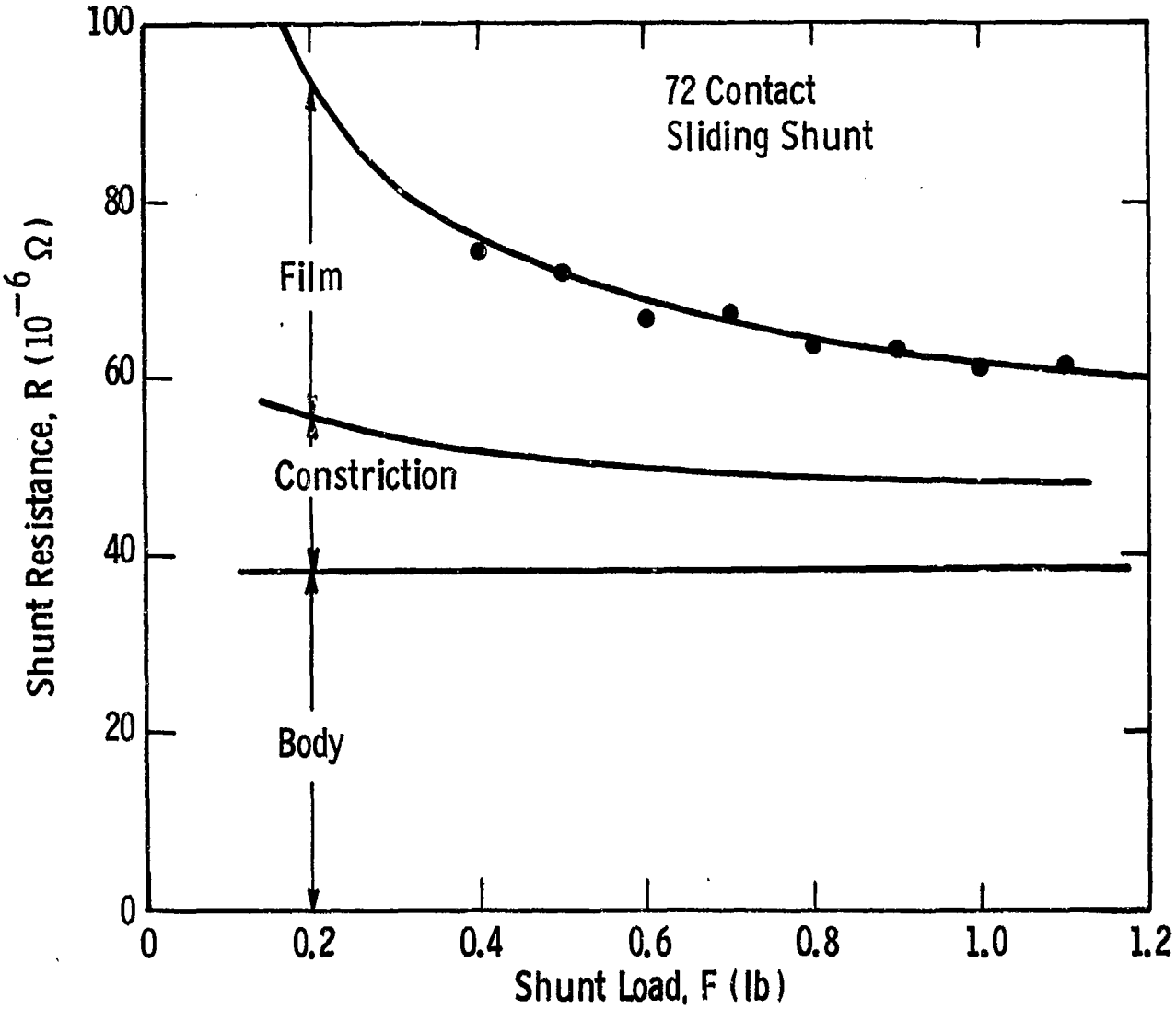

Fig. 2.11 – Shunt resistance versus contact load

Curve 694437-A

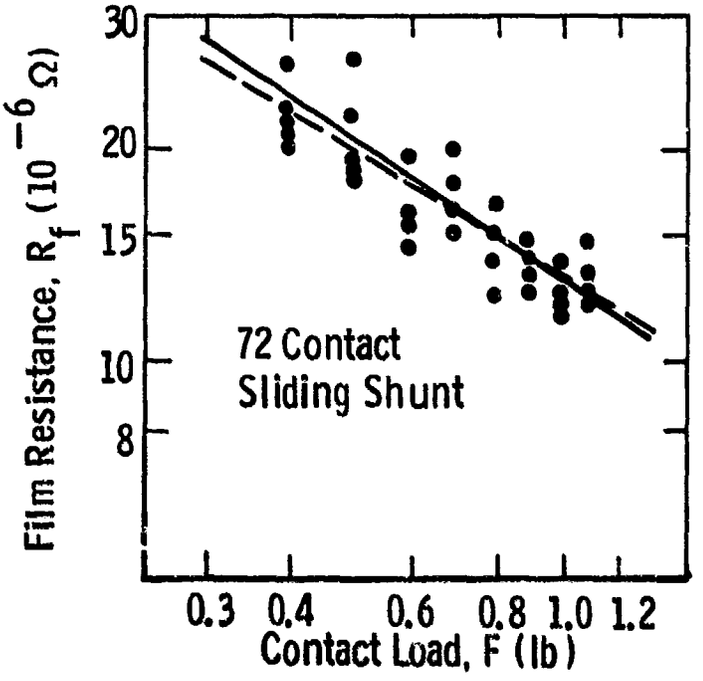

Fig. 2.12 – Film resistance versus contact load

where ρ is the electrical resistivity of the contact material (0.63×10^{-6} Ω in, 1.5×10^{-6} Ω cm).[8] Equations (2.5) and (2.6) are combined to determine the following constants for Equation (2.1)

$$C_1 = \frac{\rho}{2.2} \left(\frac{E}{x}\right)^{1/3} \tag{2.7}$$

$$k_1 = -1/3 \tag{2.8}$$

These constants were used to calculate the constriction resistance for each point of data and the resulting values of film resistance by difference, are shown in Figure 2.12. The broken line represents a linear regression analysis curve fit for the actual data. The regression coefficient for this analysis is 0.88.

The film resistance is:

$$r_2 = \frac{\epsilon}{\pi a^2} \tag{2.9}$$

where ϵ is the film tunnel resistivity. Equations (2.5) and (2.9) are combined to determine the following constants for Equation (2.2):

$$C_2 = \frac{\epsilon}{1.21\,\pi} \left(\frac{E}{x}\right)^{2/3} \tag{2.10}$$

$$k_2 = -2/3 \tag{2.11}$$

As a result of the regression analysis, the value of tunnel resistivity was found to be $\epsilon = 5.5 \times 10^{-10}$ Ω in^2 (3.6×10^{-13} Ω m^2) at the 1.0 lb (4.4N) load point. The solid line in Figure 2.12 was then determined from the theoretical relationship for the film component of Equation (2.4) using the above value of resistivity and n = 72 contacts. Based upon the correlation of the experimental results with the theoretical values of $k_1 = -1/2$ and $k_2 = -2/3$ for elastic conditions, the theoretical relationships using these values are shown for the film and constriction components in Figure 2.11.

Equation (2.4) shows that the film component becomes a larger fraction of the total contact resistance as the number of contacts increase and as the total contact force decreases. The relative importance of the film as well as the body resistance components can be seen in Figure 2.11. The experimental results conform to the theoretical relationships which correspond to elastic contact theory ($k_1 = -1/3$, $k_2 = -2/3$). Figure 2.13 displays the theoretical effect of the number of contact fingers on the component resistances. It can be seen that increasing the number of contacts beyond 75 to 100 produces only a small reduction in the silver-on-silver contact resistance. The same contact resistance values would occur at a slightly greater number of contacts with the higher resistivity brush material.

The film resistance was found to be quite small, even for one sample that was not abraded with the fine steel wool during cleaning. This is probably due to the soft nature of films on silver and due to the slight sliding motion that occurs between the contacting surfaces as the fingers are bent during the application of load. Reversal of the current direction had no effect on the measured contact resistance. Methods to further reduce all three resistance components are desirable and are presently being pursued. The body resistance of the fingers can be reduced by silver plating. If the brush is not silver plated, the film and constriction resistance can be reduced by increasing the number of contact points. In the application of the shunt to a typical high metal graphite brush material, the constriction and film resistance are expected to be somewhat larger than the values determined for the silver-plated test contact.

When two different contact material are used, Equations (2.7) and (2.10) can still be used except that the following material properties should be substituted:

$$E = 2 E_s E_b / (E_s + E_b) \qquad (2.12)$$

$$\rho = (\rho_s + \rho_b)/2 \qquad (2.13)$$

Curve 694509-A

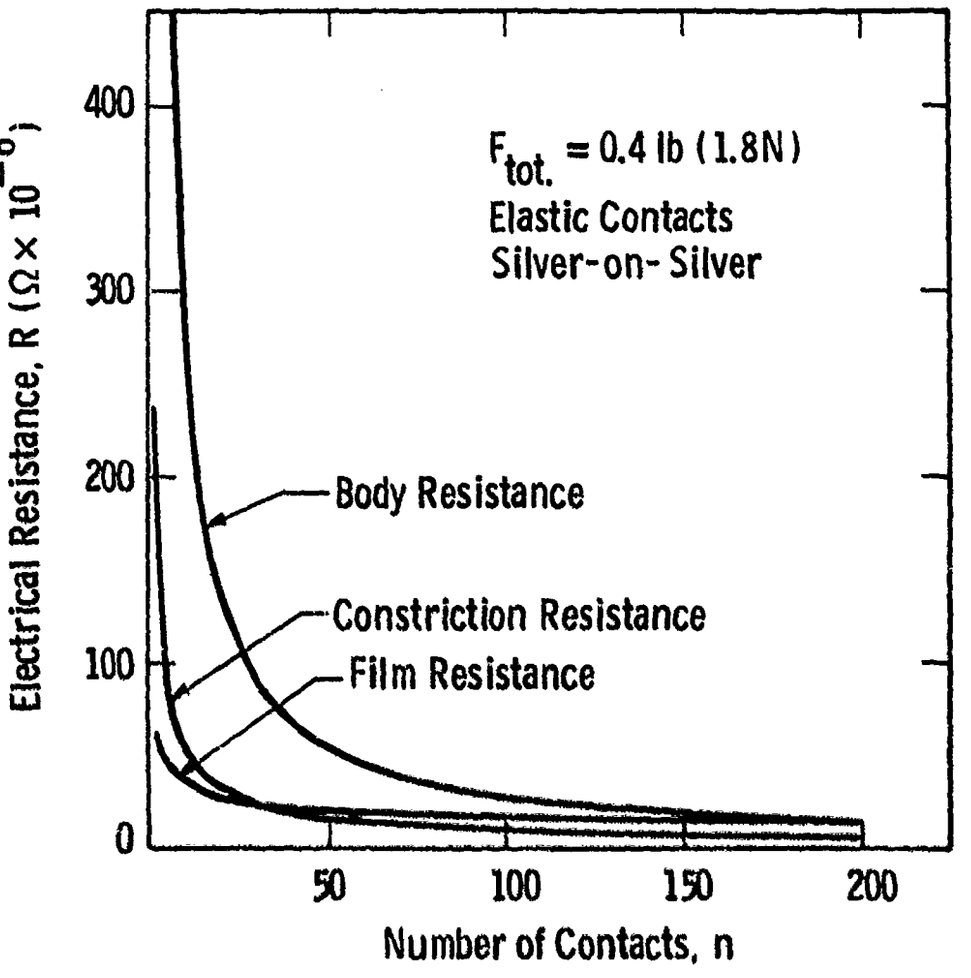

Fig. 2.13– Shunt component resistance versus number of contacts

where the subscripts s and b refer to the shunt (silver) and the brush materials, respectively. (Poisson's ratio is assumed to be 0.3 for both materials, since the importance of this variable is small.)

2.2.3.2 Variation in Load

For a given brush system configuration, selection of proper brush mechanical loading is necessary to assure satisfactory operation and to minimize brush power loss. Generally, brush contact loads are designed to remain reasonably constant during machine operation. However, in the real application, rotor eccentricity and irregularities in the moving surface produce forces such as brush inertia and holder friction which alter the net contact force. A method has been developed[2.22] to determine the brush performance sensitivity for contact force variations.

Power loss at the brush interface is composed of frictional and electrical components. The electrical loss can be differentiated further to that caused by constriction and film voltage drops. With increasing brush loading, frictional power loss increases, but electrical losses are found to decrease, due to the greater real contact area. The total loss, which is the sum of these two components, will have a minimum value for the optimum contact load.

As shown below for metallic brushes, the various components of brush interface power loss, P, may each be expressed in the form:

$$P = CF^k \qquad (2.14)$$

where C and k are constants and F is the force at the sliding contact.

For example, the brush frictional power loss, P_f, is:

$$P_f = \mu v F \qquad (2.14)$$

where μ and v are friction coefficient (assumed to be independent of force) and sliding velocity, respectively. In this case, $C = \mu v$ and $k = 1.0$ when expressed in the form of Equation (2.14).

It would be expected that the mechanism of current transfer at a sliding contact interface is fundamentally similar in nature to that of a static contact.[2.17,2.18] That is, the current transfer still passes through a few very small "bridges" (which may continually vary in position on the brush face) which occur as part of the total contacting surface. The film and constriction resistance occur at these "bridges". The same analytical model may be used, therefore, as is used to define static contact resistance. For light brush loads (elastic contacts), the constriction resistance R_1 may be expressed as:[2.17]

$$R_1 = a_1 F^{-1/3} \tag{2.16}$$

where a_1 is a constant which depends upon the contact materials and surface geometry. The corresponding electrical power loss due to constriction is:

$$P_1 = I^2 a_1 F^{-1/3} \tag{2.17}$$

where I is the electrical current passing through the brush. For the elastic constriction, the constants in Equation (1) become $C = I^2 a_1$ and $k = -1/3$.

In the theoretical models for contact resistance, the film resistance is shown to be inversely proportional to the area of the local contact spot, whereas the constriction resistance is inversely proportional to the radius of the assumed circular contact area. This leads to the following form for the film resistance expression:

$$R_2 = a_2 F^{-2/3} \tag{2.18}$$

where a_2 is a constant for the specific brush interface. The film resistance then results in a power loss of:

$$P_2 = I^2 a_2 F^{-2/3} \tag{2.19}$$

and the constants in Equation (2.14), for elastic film resistance, are $C = I^2 a_2$ and $k = -2/3$. When the local contact points are assumed to be fully plastic, the constriction and film resistance becomes:

$$R_1 = a_1 F^{-1/2} \tag{2.20}$$

and

$$R_2 = a_2 F^{-1} \tag{2.21}$$

The corresponding power loss expressions are:

$$P_1 = I^2 a_1 F^{-1/2} \tag{2.22}$$

and

$$P_2 = I^2 a_2 F^{-1} \tag{2.23}$$

The constants for use in Equation (2.14) for these and the previous expressions are summarized in Table 2.1.

TABLE 2.1

CONSTANTS FOR USE IN EQUATION (2.14)

Type of Loss	Contact Model	C	k	k'
Frictional		μV	1.0	-
Electrical Constriction	elastic	$I^2 a_1$	-1/3	-3/5
	plastic	$I^2 a_1$	-1/2	-3/4
Electrical Film	elastic	$I^2 a_2$	-2/3	-4/5
	plastic	$I^2 a_2$	-1	-1

In the contact models used above, the number of contact spots has been assumed constant and independent of load. In reality, the number of contacts probably increases with increasing load and this alters the apparent values of k. Archard[2.19] has proposed a model in which both the number of contacts and the area of each contact increases with increasing load. His model predicts higher negative values of k when the number of

contacts increases with load. These values are presented as k' in Table 2.1. A more complex model[2.20] presented in later publications yields even higher values of k approaching negative one. One can, however, empirically determine C and k if variations in load are held below certain values as will be shown later.

The instantaneous power loss, Equation (2.14) will vary if the contact force varies either as a function of time or geometric position. The average power loss may be determined for various force relationships and different values of k.

Average power loss is considered for two brush applications: first, a commutator, and then a slip ring application. For a commutator application or a single brush on a slip ring, the current is considered to be collected at a single point on the rotor circumference. Assume also that the current I, is constant since the collection site is electrically connected in series to other brush sites and the overall circuit impedance is dominated by other components of the machine system. The brush interface power loss, P, can be expressed as:

$$P = I^2R \tag{2.24}$$

where R is the contact resistance. Contact load variation will produce a corresponding resistance variation as a function of time, t. The average power loss, $\bar{P}$, can then be found as:

$$\bar{P} = \frac{1}{t}\int_0^t P(t)\,dt \tag{2.25}$$

As shown previously in Equations (2.17), (2.19), (2.22), and (2.23), the general expression for the components of electrical power loss is:

$$P = I^2 a F^k \tag{2.26}$$

We will first examine a sinusoidal load variation as a function of time:

$$F = F_o (1 + X \sin \omega t)^k \tag{2.27}$$

where F_o is the nominal brush load, ω is the frequency of the force variation, and X is the amplitude of force variation as a fraction of nominal load. This varying force may be substituted into Equation (2.26) to yield an expression for the power loss as a function of time:

$$F = I^2 a F_o^k (1 + X \sin \omega t)^k \tag{2.28}$$

The average power loss, Equation (2.25), becomes:

$$\bar{P} = I^2 a F_o^k \frac{\omega}{2\pi} \int_0^{2\pi/\omega} (1 + X \sin \omega t)^k \, dt \tag{2.29}$$

where the integral is taken over the time interval for one typical complete cycle. Then:

$$\bar{P} = P_o Y \tag{2.30}$$

where P_o is the power loss for a constant brush load, F_o and:

$$Y = \frac{\omega}{2\pi} \int_0^{2\pi/\omega} (1 + X \sin \omega t)^k \, dt \tag{2.31}$$

The term Y, which is a function of k (the exponent on force) and X (the magnitude of the force variation), is seen to be an amplification factor by which the nominal power lo is multiplied to account for variable load.

For the slip ring application, the current collection is assumed to be distributed around the full rotor circumference. For simplicity, the voltage drop between the rotor and the brush is assumed to be constant. The resistance will vary along the circumference of the rotor slip ring as a function of the angle, θ, when the contact force varies due to such

things as rotor eccentricity coupled with brush inertia. For a given rotor eccentricity, the force distribution relative to the rotor will be constant, although it will rotate relative to the stationary frame of reference.

Since the voltage is assumed constant and the resistance varies along the circumference, the current will redistribute and reduce the significance of the resistance variation. The effective resistance will be the inverse of the cumulative conductance along the slip ring circumference. If the distributed resistance, σ, is used for either the constriction of film components, then the cumulative conductance will be:

$$I/R = \int_0^{2\pi} \frac{dA}{\sigma(\theta)} \tag{2.32}$$

where A is the slip ring collection area. Then, since:

$$dA = \frac{d\theta}{d\pi} A \ , \tag{2.33}$$

the effective resistance is:

$$R = \frac{2\pi}{A} \Big/ \int_0^{2\pi} \frac{d\theta}{\sigma(\theta)} \tag{2.34}$$

As in the force relationships shown above, the following general relationship may be found for distributed resistance:

$$\sigma = c\, p^k \tag{2.35}$$

where c is a constant and p is the contact pressure. For a sinusoidal variation of pressure along the circumference, the average power loss for this geometric variation is found from Equations (2.24), (2.34), and (2.35).

$$\overline{P} = P_o \ 2\pi \Big/ \int_0^{2\pi} \frac{d\theta}{(1 + X \sin\theta)^k} \tag{2.36}$$

where $P_o = I^2 (c\, p_o^{\,k}/A)$.

We may now define an amplification factor Z such that:

$$P = P_o Z \tag{2.37}$$

In Figures 2.14 and 2.15, values of Y and Z are plotted as a function of k and X for a sinusoidal force variation. For the commutator application in Figure 2.16, the ordinate has been expanded to clarify the relationship for values of k in the zero to positive one range. Values of k beyond the range of those shown in Table A are presented to demonstrate the mathematical relationship.

Figures 2.17 and 2.18 are plots of $Y_{\square}$ and $Z_{\square}$, respectively, as functions of k and x where the force variation is a step function, that is, a square wave relationship. Sinusoidal variations are typical of brush inertia effects while step variations are caused by brush side friction. If one assumes a load variation that is a square-wave relationship, typical of brush holder friction, the commutator power loss is expressed as:

$$\overline{P} = P_o Y_{\square} \tag{2.38}$$

and the slip ring power loss is

$$\overline{P} = P_o Z_{\square} \tag{2.39}$$

In this case, the amplification factors are:

$$Y_{\square} = \frac{(1 + X)^k + (1 - X)^k}{2} \tag{2.40}$$

and

$$Z_{\square} = \frac{2}{(1 + X)^{-k} + (1 - X)^{-k}} \tag{2.41}$$

As an example, assume an electrical contact loss is inversely proportional to contact force (k = -1.0) in a commutator application. Also, the brush system is designed such that the brush inertia coupled with the rotor eccentricity yields a variation in contact load of $\pm$75%.

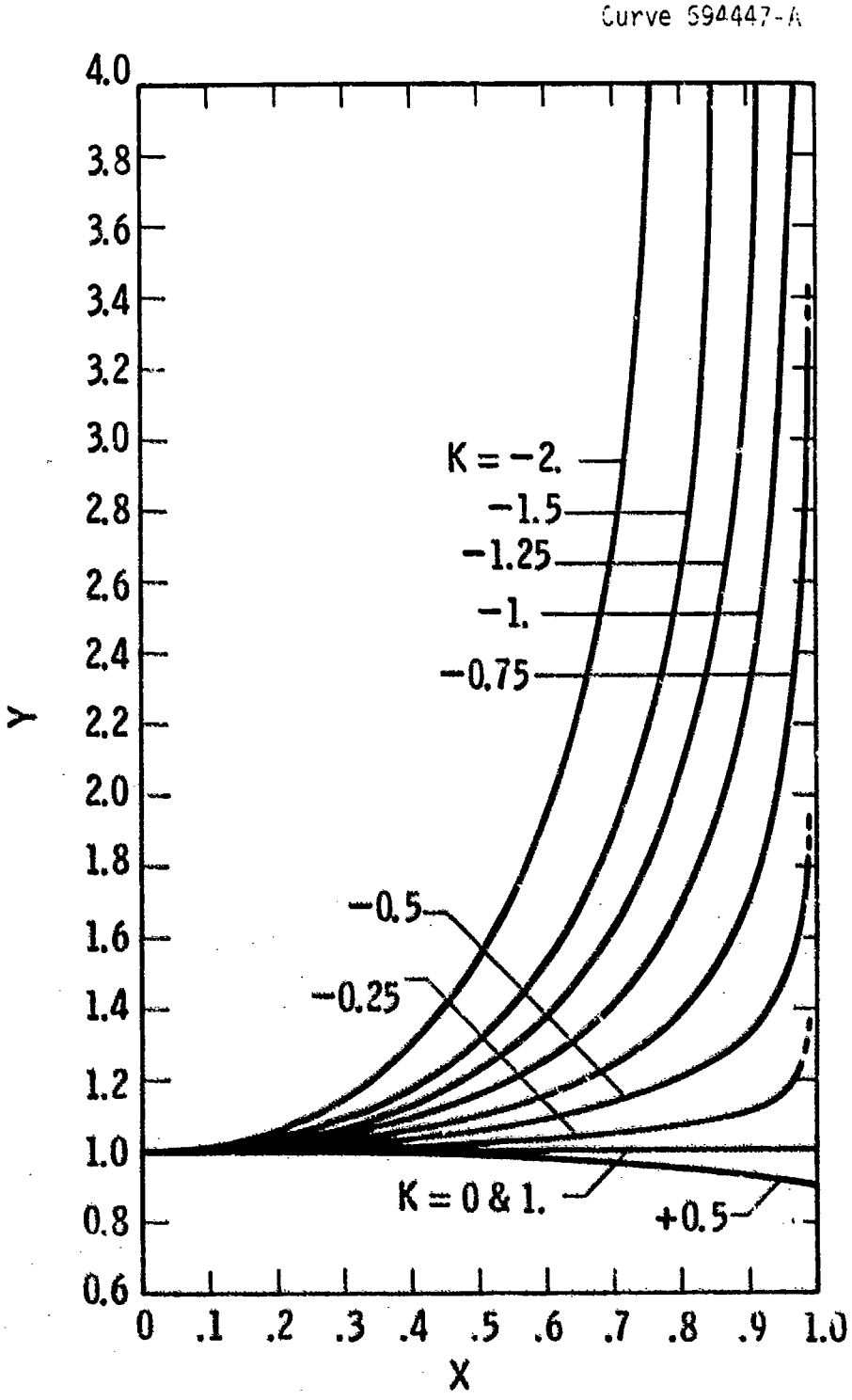

Fig. 2.14—Commutator application — sinusoidal variation

Curve 694448-A

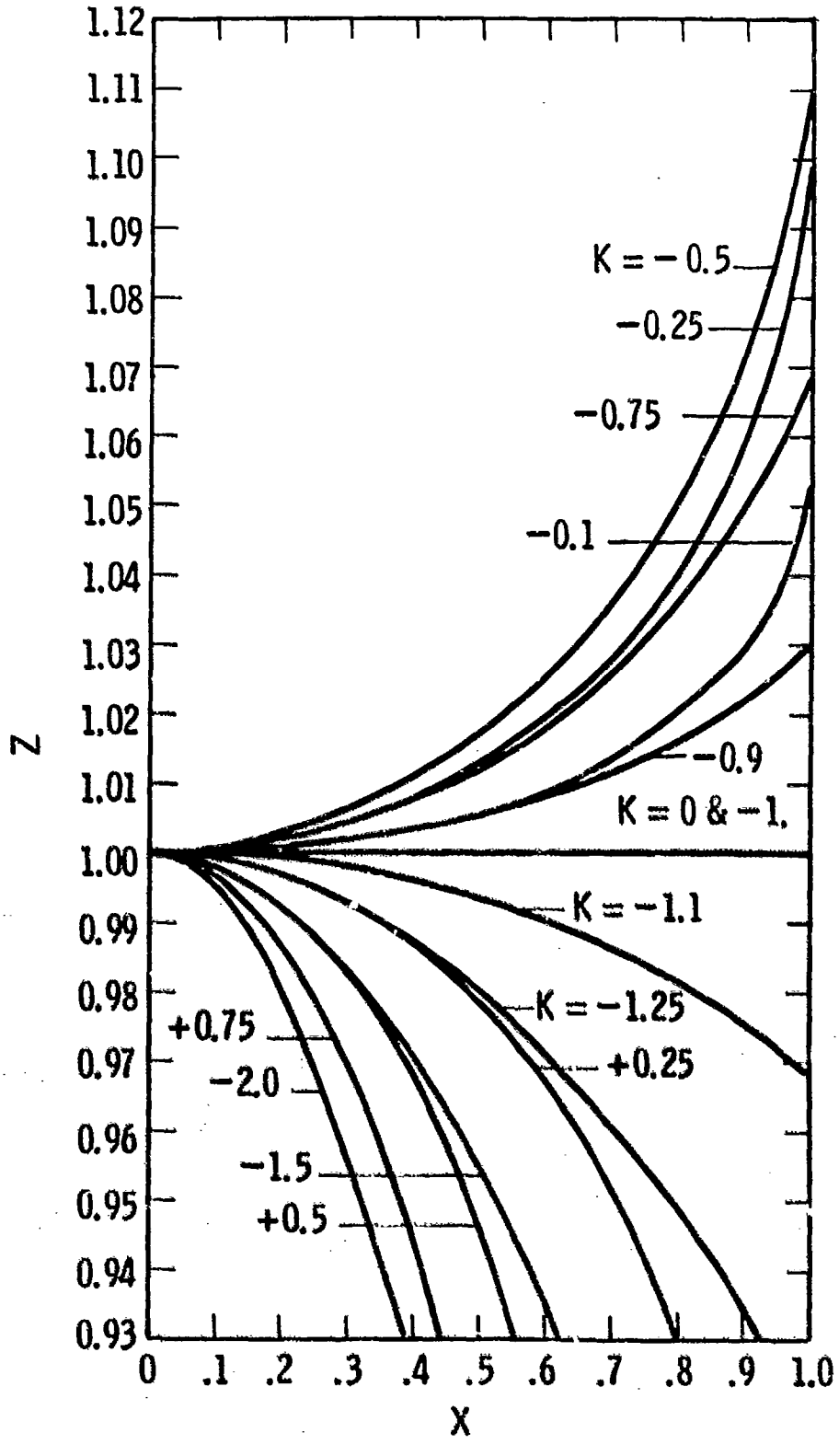

Fig. 2.15– Slip ring application – sinusoidal variation

Curve 694444-A

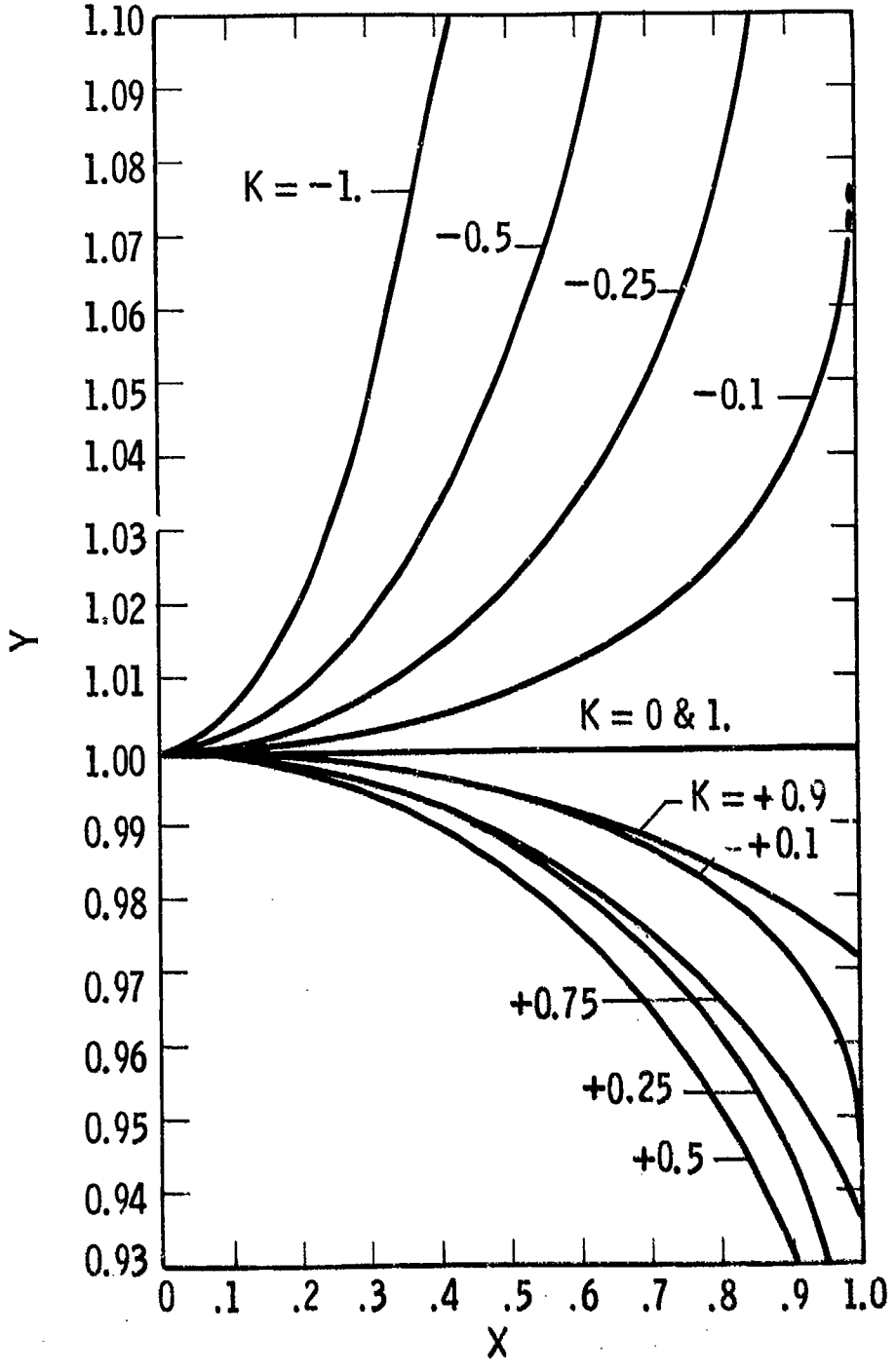

Fig. 2.16 – Commutator application – sinusoidal variation

Curve 694445-A

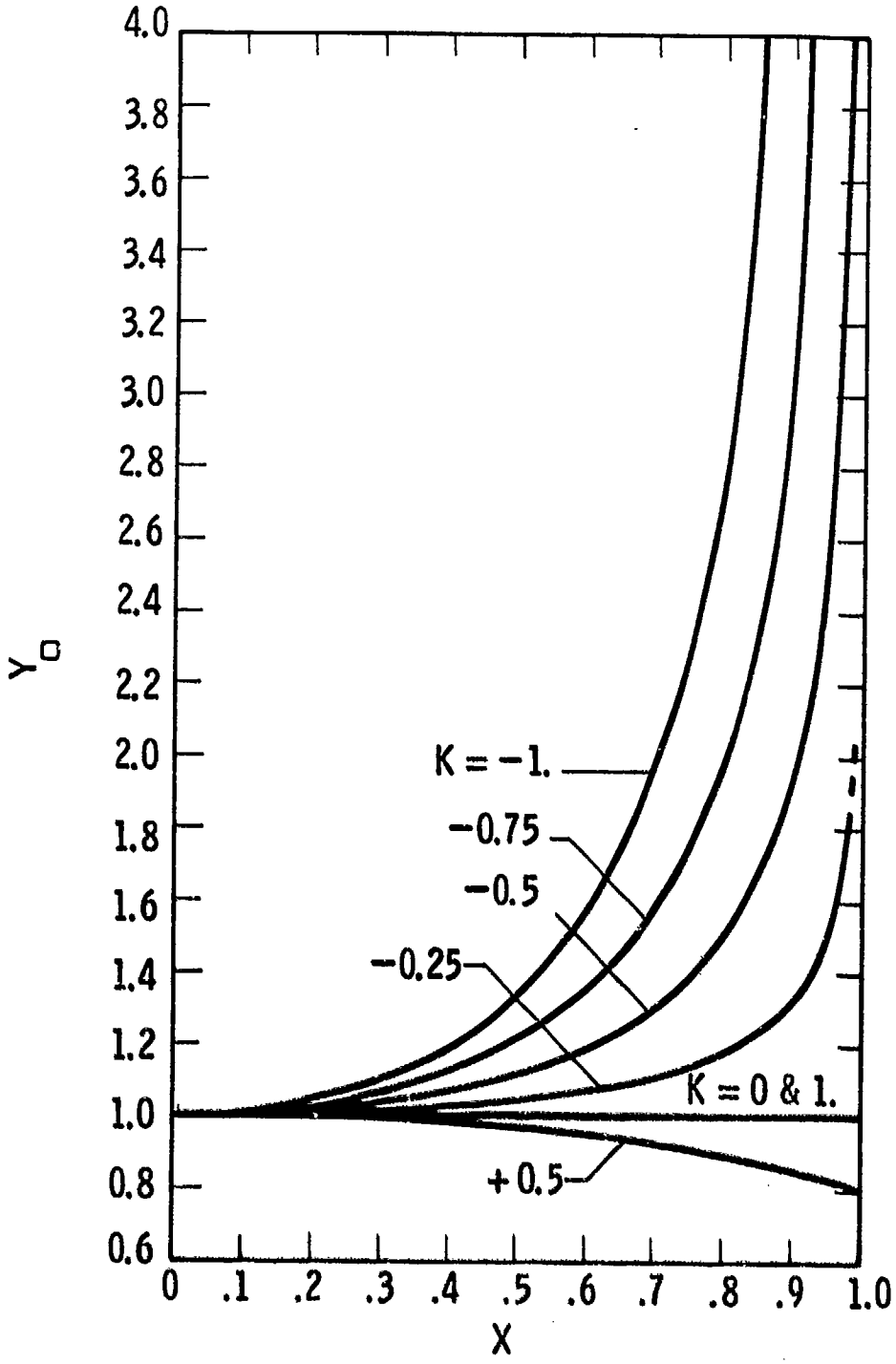

Fig. 2.17– Commutator application – step variation

Curve 694446-A

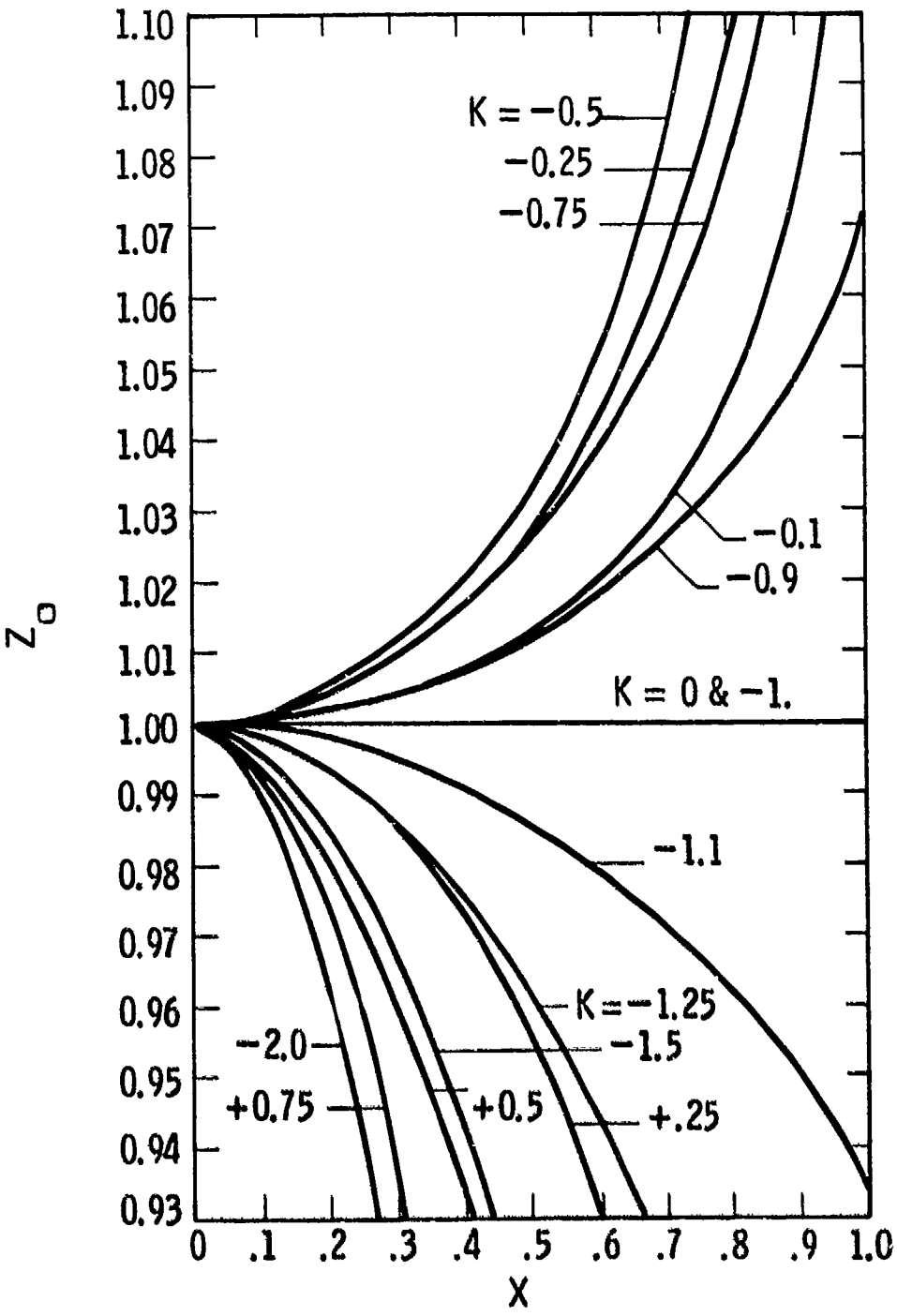

Fig. 2.18 – Slip ring application – step variation

That is, if the average brush pressure were 2 psi, the maximum would be 3.5 psi and the minimum would be 0.5 psi. From Figure 2.14 at X = 0.75 and k = -1.0, Y is found to be 1.5. The corresponding electrical power loss associated with a 75% variation in load is 50% higher than the loss for a constant load.

It is seen in Figures 2.14 through 2.18 that a limit to brush contact force variation may occur prior to physical separation and arcing, since interface power loss and contact drop may become excessive. However, careful brush system design will limit the amplification of power loss. For example, inertial forces can be reduced by reducing the brush length and the effective mass of the shunt and the brush loading system. Close control in the machining, inspection and balancing of the rotating current collection surface, and in selection of the bearings to maintain concentric smooth rotation, will minimize the amplitude of brush acceleration. Holder friction should be minimized provided that the brush mechanical stability can be maintained. The benefit of brush segmentation will theoretically depend upon the wavelength of the surface irregularities, since a thicker brush may bridge very local surface irregularities.

It should be noted that abrupt surface irregularities or high-frequency variations such as that caused by tool chatter during machining will have a greater effect than an equal amplitude of variation which occurs only once per revolution (such as that due to rotor eccentricity). If the brush does not bridge the irregularity, the acceleration force will be proportional to the square of frequency. For example, a sinusoidal variation of amplitude e, which completes a full cycle in one revolution of the collector surface, will result in a contact force variation of:

$$\Delta F = m\, e\, (n\omega)^2 \qquad (2.42)$$

where ω is the rotational speed, and m is the effective mass of the brush, shunt, and loading system. To demonstrate the significance of the frequency effect (n^2), consider eight sinusoidal geometric disturbances

around a slip ring surface. For this slip ring, an eccentricity amplitude of only 0.08×10^{-5} m (0.032×10^{-3} in) would produce a force variation equal to that of a one-per-revolution eccentricity of 5.1×10^{-5} (2.0×10^{-3} in). The strong effect of angular speed on the force variation and, therefore, on the value of X in Figures 2.14 through 2.18, is a probable factor in the increased brush voltage drop that has been observed with increasing rotor speed. For the same reason, if the friction coefficient is not constant as assumed in Equation (2.15), but is a function of force, then a variation of friction coefficient with speed may be predicted.

For the experimental evaluation of new brush and slip ring materials, or new brush holders, it is often convenient because of cost or material availability to use smaller slip ring diameters than that of the machine application. This is generally compensated by increasing the rotor speed to achieve the same sliding velocity, so that the brush frictional power loss is duplicated if the brush contact pressure is maintained. As shown in Equation (2.42) above, this increase in angular speed can increase the inertial force variation unless the eccentricity is greatly reduced, and this will result in higher observed brush voltage drop and power loss.

In applications where both the inertial and holder friction modifications of contact load are found to be significant, the values of Y or Z cannot be added linearly to obtain an accurate combined effect. Instead, the combined function of contact force, raised to the power k, must be integrated as was done for the sinusoidal relationship of Equation (2.29). Similarly, when both film and constriction components are significant for a slip ring application, the current will redistribute on the basis of the series resistance variation along the circumference. Therefore, the value of Z for the film and constriction components cannot be applied on an individual basis. Elastic deformation of heavy conventional shunts will produce a sinusoidal change in contact force that is 180 degrees out of phase with the inertial force. Also, since rotor irregularities need not be sinusoidal, integration of the actual force-time function would be necessary to establish accurate values of real

power loss. However, the curves of Figures 2.14 through 2.18 should still be useful in establishing relative sensitivity for design purposes.

It should be noted that while the values of Y may be used for either frictional or electrical power loss, provided that the proper value for k is used, the values of Z apply only to electrical losses and compensate for the current redistribution along the slip ring circumference. For frictional power loss on a slip ring, there is no redistribution effect, and the same values of Y may be used as those for the commutator application.

In place of the values shown in Table 2.4, these constants may be determined experimentally. For electrical losses, the total resistance, which is the sum of constriction and film components, is measured as a function of load and should follow the model relationships shown in Equations (2.16) and (2.18):

$$R = a_1 F^{k_1} + a_2 F^{k_2} \tag{2.43}$$

The four constants to be determined (a_1, k_1, a_2, and k_2) require that data be obtained for at least four different values of load. This will yield four equations which may be solved (reduced) by computer or trial-and-error techniques, to determine the constants.

For conditions where the film resistance is relatively small, the constants a_1 and k_1 are obtained from at least two measurements, through the use of the following relationships:

$$k_1 = \frac{\ln (R'/R)}{\ln (F'/F)} \tag{2.44}$$

and

$$a_1 = \frac{R}{(F)^{k_1}} \tag{2.45}$$

where the prime superscript denotes values for the second data point. These tests must be conducted under conditions where the magnitude of

force variation X is either small or known. For values of k between zero and minus one, a 30% sinusoidal variation in load (X = 0.3) would result in a resistance increase of not more than 5% (Y = 1.05).

Although Archard and others have also applied the quasi-static model that we have used to establish sliding contact area, it is quite possible that the tangential motion modifies the contact load relationship to real area. We are presently investigating this phenomenon for specific brush materials so that a more accurate estimate may be made of the constant k, for the dynamic condition. One might speculate that, since the mechanical contact points at asperities must alternate due to the tangential motion, each of these contacts sees a variable force, and although the current will redistribute, the result is similar to the effect of an eccentric slip ring where the average resistance will increase by the factor Z.

2.2.3.3 Brush Actuation

Brush actuation is the area of current collection that utilizes lifting or loading of brushes in order to improve the overall mission efficiency. If, for instance, the current collection scheme is designed for 1000 apsi at full load and at a part load condition the current density is 500 apsi, only half the brushes are needed to obtain the original design conditions of 2.55×10^6 A/m^2 (1000 apsi). By alternating groups of brushes to collect current at different times the overall brush life is increased.

The most attractive brush actuation system concept is that shown in Figure 2.19. This conceptual brush holder was designed for use in a 19.6 MW SEGMAG generator for the Office of Naval Research under Contract No. N00014-77-C-0307. The actuation system utilizes contact force springs to load the brush toward the rotor. To lift the brush, a pneumatic cylinder is activated and the brush is lifted but not taken out of the holder brush slot. As the brush wears, the spool contained inside the constant force spring coil can move freely in the slot provided in the

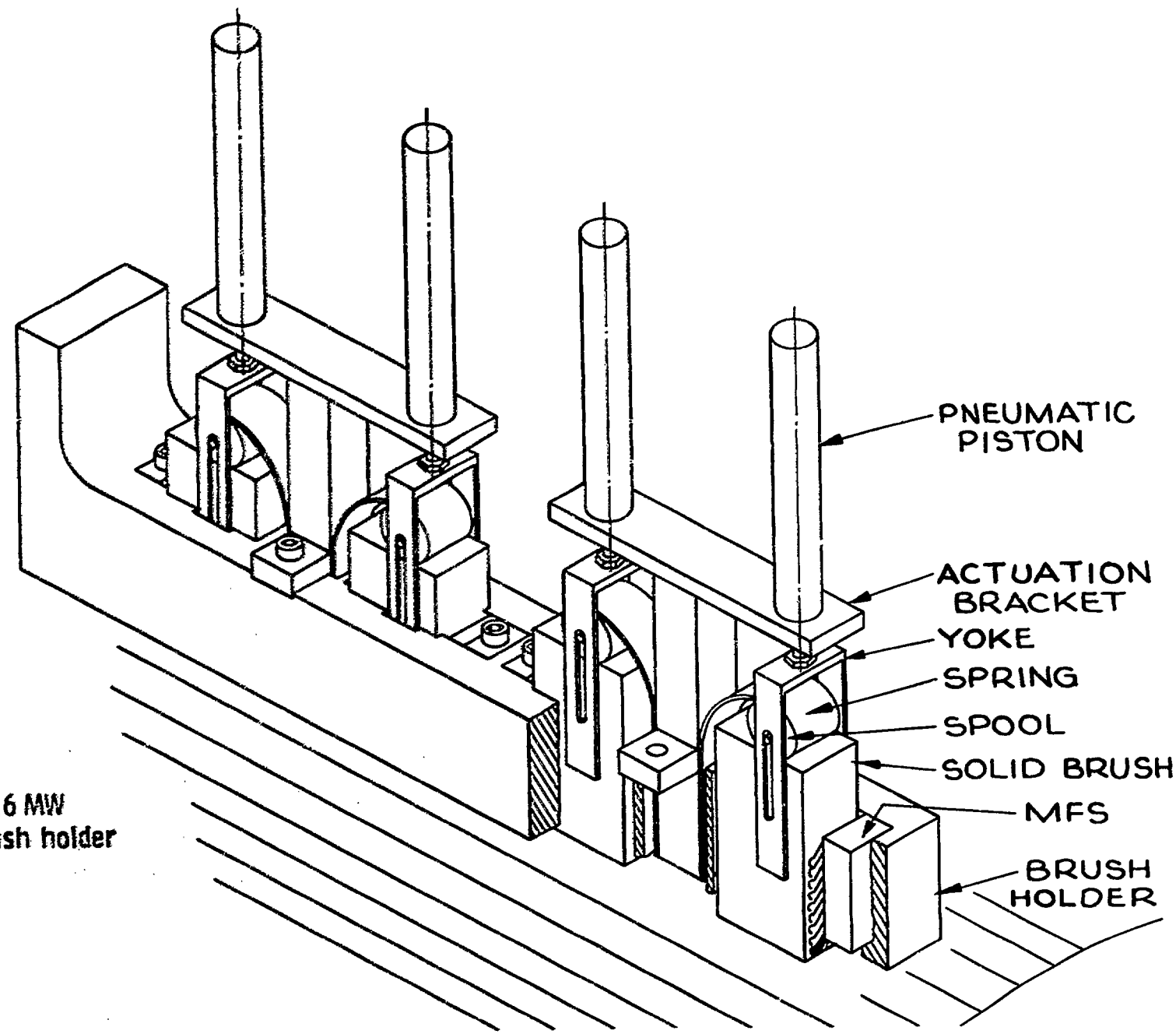

Fig. 2.19 – 19.6 MW generator brush holder

yoke. The length of this slot is equal to the allowable brush wear length. The pneumatic piston is a double acting piston that lifts the brush as the working gas pressure is increased. If the pneumatic working gas pressure is lost, the constant force springs will load the brushes to the rotor in a fail-safe mode.

Figure 2.20 shows photographs of a brush actuation system that has been designed and built for testing on the Advanced Brush System (ABS) test stand. In Figure 2.20a, the brushes are shown as they would appear when first installed or when lifted. In Figure 2.20b the brushes are recessed into the holder slot to show how the loading system moves with brush wear. In Figure 2.20c, the brushes are shown protruding out from the bottom of the holder to reveal the brush wear length. And in Figure 2.20d, the actuation system components are shown for one complete cluster of brushes. The cluster is composed of four brushes that are each .016 m (.62 in) wide by .0079 m (.31 in) thick by .051 m (2.0 in) long. The cluster of brushes is held together by a neoprene pad that is cemented to the top of the brushes. On top of the neoprene is a metal plate that attaches to the stem of the pneumatic cylinder. Above the metal plate is a micarta plate that has a concave surface to keep the springs in line as brush wear is accommodated.

The brushes are supported on the leading and trailing sides by the copper surface of the holder. On the brush ends (axial with respect to the rotor) the support is only on the corners since the multiple finger shunts (MFS) are located along those sides of the brush. The spring holders are bolted into the holder on either a leading or trailing brush side depending on which direction the rotor is turning. Since the brushes are radial (brush axis is perpendicular to the rotor tangent), the rotor forward and reverse directions are the same. An adjustable bracket is mounted on the spring holders in order to support the pneumatic piston. Since the piston breakaway fraction is negligible relative to the brush load, the piston is attached directly to the brush assembly. In Figure 2.19, the piston is attached to the brush assembly through a yoke that allows the brush assembly to move independently of the piston.

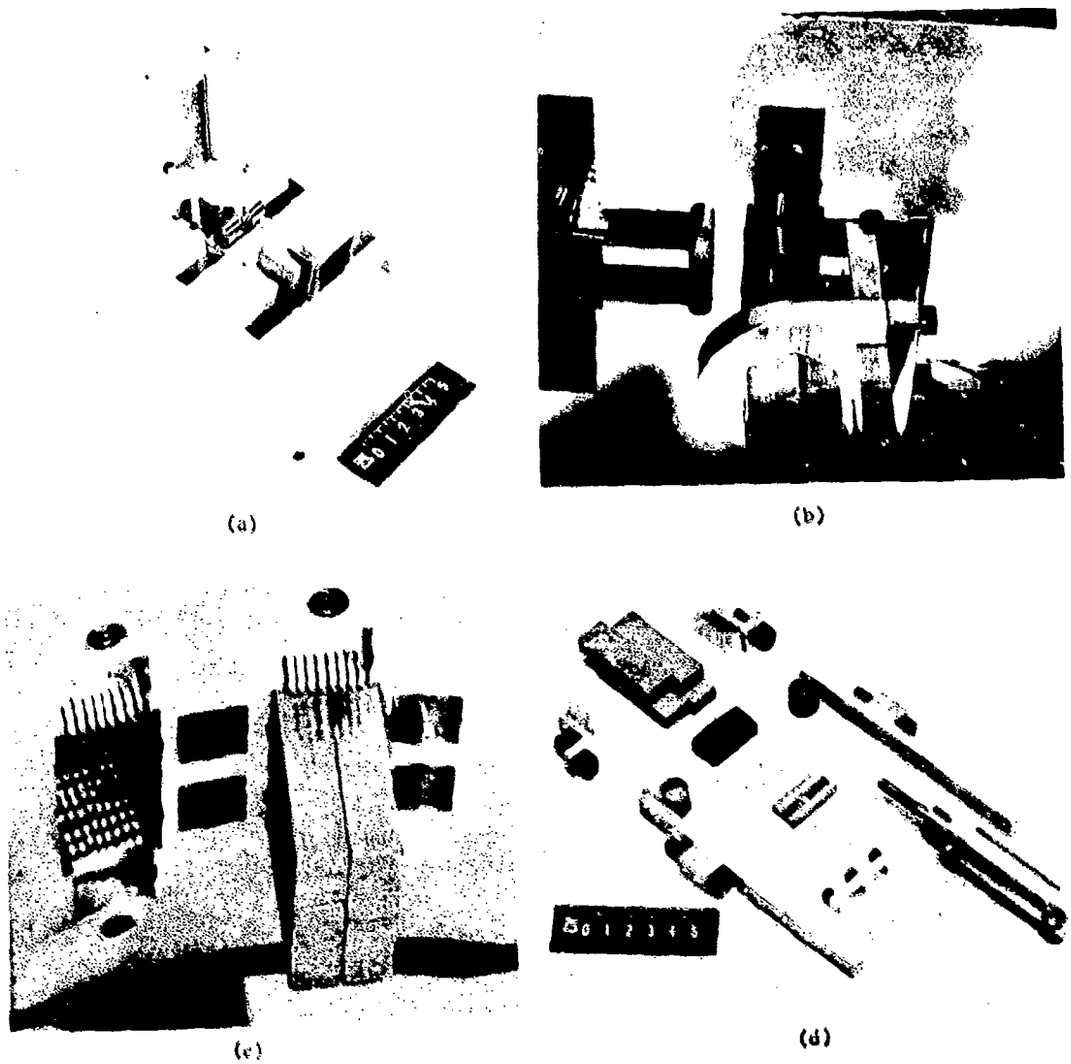

(a) (b)

(c) (d)

FIGURE 2.20. Brush Actuation System

The new system, shown in Figure 2.20, has the piston attached directly to the brush assembly but attached through the neoprene damping pad. The low piston loads coupled with the spring-damping of the neoprene pad will have negligible effects on the normal brush performance.

2.3 Brush Heat Transfer

2.3.1 Objectives

The objective of the brush heat transfer program is to determine the thermal characteristics of the high current density brush systems. These heat transfer characteristics will be correlated with the solid brush objectives in order to determine high current density brush holder heat transfer design requirements and procedures.

2.3.2 Prior and Related Work

The brush holder heat transfer characteristics of the High speed brush tester (HS1) and the Machine-Environment Brush (MEB) tester were analyzed. It was found that the thermal resistance between the brush and the holder was the major thermal barrier of the system. This thermal resistance is complicated and can vary significantly depending on brush position in the holder, clearance, brush loading, geometry, surface finish, material properties and atmospheric properties of the brush holder environment. The brush holders and brushes were instrumented to determine the thermal resistance. The experimental data was then correlated with theory in an effort to understand the heat transfer mechanism between the brush and holder. It was found that the brush holder cooling system is capable of removing approximately 30% of the heat due to brush losses for brushes operating at 1.55×10^6 A/m^2 (1000 A/in^2) current density and >1 m/sec (14,000 ft/min) sliding velocity. The remainder of the loss must be carried away by the rotor.

2.3.3 Current Progress

A literature search was performed to obtain information pertaining to high power density solid brush current collectors. The following Table 2.2 shows a listing of the publications found.

TABLE 2.2

ARTICLES FROM THERMAL LITERATURE SEARCH

1. Sukhoroslov, L. A. and Lozhkin, L. V., A Model Representing the Temperature Conditions of the Brush-Commutator Assembly of Electric Machines, Elektrotekhnika, Vol. 43, No. 1, January 1972, pp. 59, 60.

2. Rotter, R., The Influence of Brush Friction on Commutator Heating, Elektrscha Bahnon, Vol. 47, 1976, pp. 105-112.

3. Krenth, Hans Peter, On The Relationship Between Shut-Down Power and Contact Temperature at the Brush Trailing Edge, Elektrotechnik and Maschinenban, Vol. 89, 1972, pp. 283-287.

4. Rubanenko, I. R. and Grossman, M. I., The Distribution of Heat Between Brushes and Commutator, Elektrotekhnika, Vol. 40, No. 4, April 1969, pp. 58, 59.

5. Voloshin, N. V., Baru, Yu. A. and Titou, D. M., The Influence of Commutator Temperature on Commutation of D.C. Machines, Izv Vuz Elektromekhanika, No. 7, July 1968, pp. 811-813.

6. Rubanenko, I. R., Grossman, M. I., The Heat Conductivity of Electrical Machine Brushes, Elektrotekhnika, No. 5, May 1969, pp. 38-39.

7. Karasev, M. F. and Seregin, V. A., The Effect of the Commutator Temperature on Commutation in D.C. Machines, Elektromekhanika, No. 7, 1969, pp. 738-740.

All of the articles that were in a foreign language have been translated into English. The information contained in the articles plus the thermal data generated in previous report periods will be used to generate new brush system concepts that will place less thermal burden on the rotor cooling system.

2.4 Debris Removal and Atmosphere Control

2.4.1 Objectives

The long-term effects of debris accumulation must be countered in practical machines by a removal system. The degree of accumulation is expected to be much less than that experienced in prior machines with carbon brushes, due to the reduced wear anticipated. In the long term, however, brush debris can present an insulation shorting path which has to be prevented. Concepts for removal of the wear particles will be based on expected machine atmosphere exchange rates, particle size and generation rate, debris composition, and available filtering techniques.

The gas atmosphere system must respond to the following parameters:

- Desired gas and pressure which establishes the propensity for arc formation.
- Desired vapor addition which reduces brush friction and enhances brush life.
- Desired gas exchange rate which controls brush debris and off-gassing products.

2.4.2 Prior and Related Work

Work at the Westinghouse Research and Development Center, as well as other divisions, has indicated the necessity to provide a controlled gaseous environment in the current collector area to enhance brush performance.

2.4.3 Current Progress

The most probable machine cover gas is carbon dioxide with water vapor added as a lubricant. Other cover gas possibilities include nitrogen and argon with additives of water vapor and/or hydrocarbon vapors. The cover gas will be used to transport the brush debris that is airborne out of the machine. Particles too large to be suspended by the gas will be allowed to fall to the bottom of the machine where the insulation is such that electrical short circuits are prohibited.

A schematic of the debris removal system is shown in Figure 2.21. The gas stream existing from the machine first flows through a valve that controls the amount of flow through the machine. The gas is then passed through a filter that removes the debris particles. Following the filter, the gas flows through a centrifugal blower that pressurizes the gas to overcome the circuit flow resistance. A heat exchanger is used to cool the gas since the machine as well as the blower add heat to the gas. The gas then passes through a filtering bed of activated charcoal that will filter out unwanted organic vapors. The vapor additive is then restored to a desired level in the vapor addition chamber. The gas is then returned to the machine.

Figure 2.22 is a photograph of a debris removal system that was made for testing on the Machine Environment Brush (MEB) test stand. The apparatus in the figure is capable of 0.047 m^3/sec (100 ft^3/min) volume flow. The testing of this system has just begun. The desired flow as well as the complexity of the gas take-off and injection inside the machine will be determined next.

Dwg. 6434A38

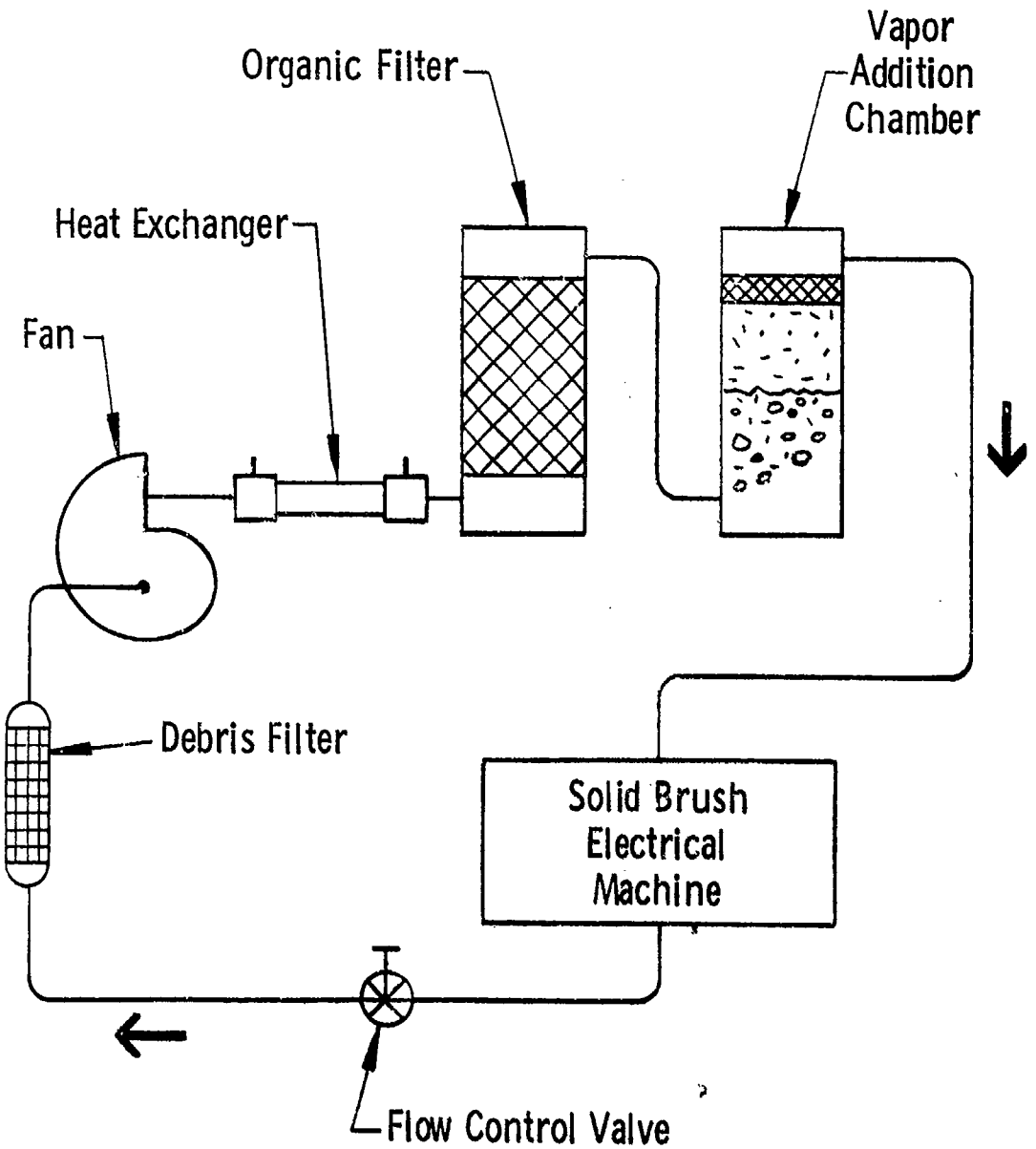

Fig. 2.21 – Debris removal system

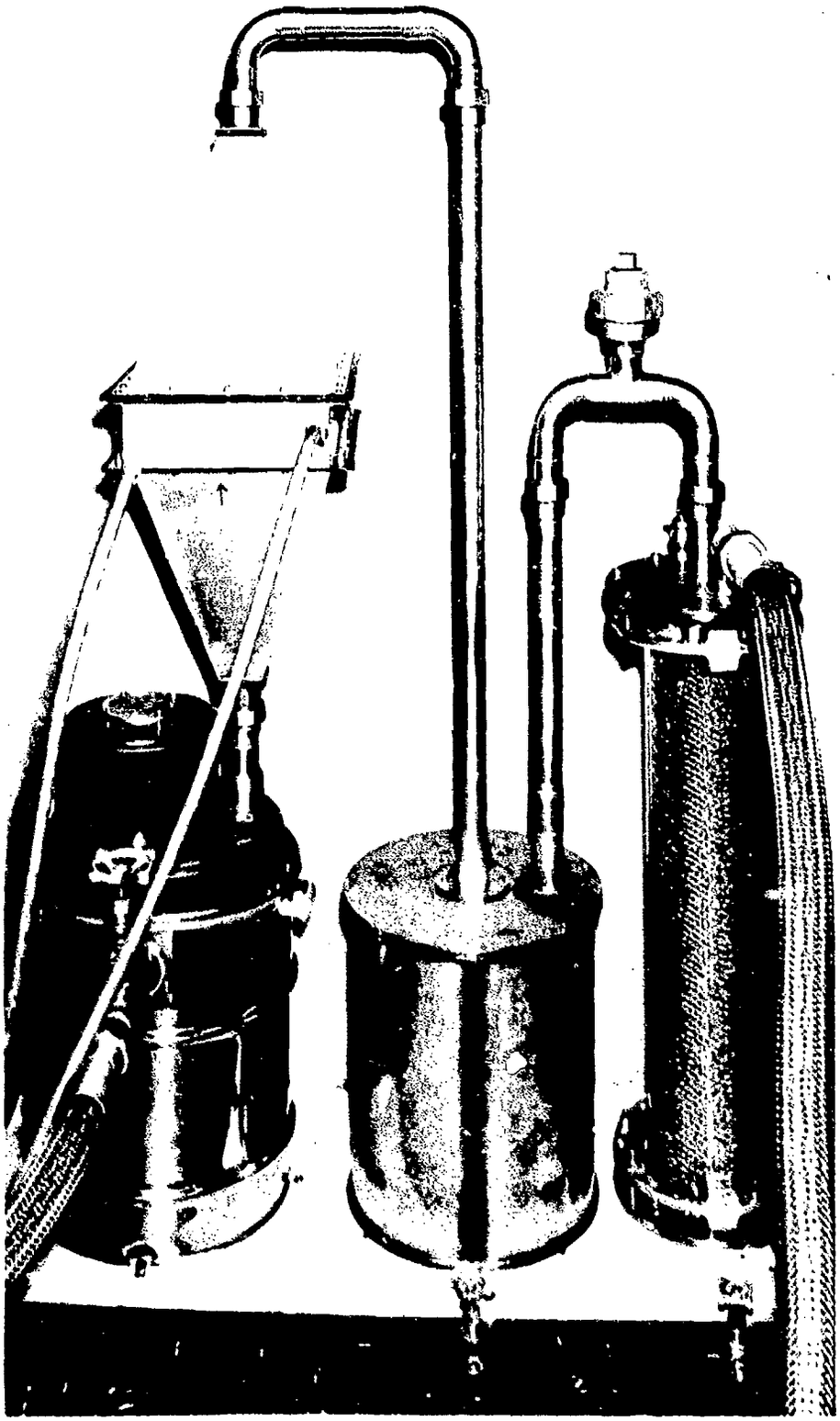

FIGURE 2.22. Debris removal system prototype.

REFERENCES

2.1 Woda, K., "Carbon Brushes and Brush Holders", Elin-Zeitschrift, 1975, pp. 95-107.

2.2 Sckerl, Walter, "Method for Objectively Evaluating Railway Motor Brush-Holding Loading Systems and Its Use in Some Known Constructions", Elektrische Bahnen, Vol. 46, No. 1, 1975, pp. 16-22.

2.3 Bar, G., "The Action of Static Forces on Brush-Holding Arms and Their Influence on Brush Pressure and on the Behavior of Sliding Contacts During Operation", Energielechnik, Vol. 8, No. 2, 1973, pp. 104-110.

2.4 Maslov, P. F., et al., "A Study of the Vibration of Brushes Relative to the Commutator", Elektrotekhnika, No. 4, 1973, pp. 31-33.

2.5 Maslov, P. F., Tuktayev, I. I. and Khlystov, M. F., "Analysis of Vibration of the Brushes of Traction Motors", Elektromekhanika, No. 10, 1971, pp. 1123-1130.

2.6 Davidovich, Ya. G. and Drizdo, M. L., "Criteria for Stable Mechanical Operation of Brushes", Elektromekhanika, No. 2, 1970, pp. 173-176.

2.7 Kollenberger, W., "The Effect on the Mechanical Stability of Shafts Fitted with Sliprings of the Pressure Exerted by Carbon Brushes", Brown Boveri Review, Vol. 56, No. 8, August 1969, pp. 356-367.

2.8 Bosov, A. A. and Kurasov, D. A., "On Mechanical Stability of Brush Contacts", Elektromekhanika, No. 7, 1968, pp. 730-735.

2.9 Lopata, Andrezej, "Self-Excited Vibrations of the Brush in the Brush-Commutator Syste, Roxprawy Inzynierskie, Vol. 23, No. 1, 1975, pp. 133-142.

2.10 Volkmann, W., "The Motion Stability of Carbon Brushes Under the Influence of Aerodynamic Processes, Bulliten SEV, Vol. 64, 1973, pp. 639-644.

2.11 Muller, H. D., "Contribution to Mechanical Problems Concerning the Transfer of Current Between Carbon Brushes and the Commutator in Electric Railroad Motors, Elektrie, Vol. 25, 1971, pp. 273-274.

2.12 Denisov, V. A. and Shaternikov, V. Ya, "Devices for Controlling the Mechanical Factors of Commutation in Electric Commutator Machines", Elektrotekhnika, No. 5, November 1971, pp. 25-32.

2.13 Skorospeshkin, A. I., Zinner, L. Ya. and Kozlov, A. A., "Device for Investigating the Dynamic Operating Conditions of the Commutator Surfaces and the Brush Vibrations, Elektromekhanika, No. 9, September 1970, pp. 983-987.

2.14 "Design and Development of a Segmented Magnet Homopolar Torque Converter", Final Technical Report Submitted to Advanced Research Projects Agency, Department of Defense, September 1976, Contract Number DAHC/5-72-C-0229.

2.15 "Research Program for a 3000 HP Segmented Magnet (SEGMAG) Motor and Generator", First Annual Report for Period Ending 31 May 1977, Office of Naval Research, Contract N00014-76-C-0619.

2.16 P. Reichner and O. S. Taylor, "Shunts for High Current Density Brushes", to be presented at the Ninth International Conference on Electrical Contact Phenomena, September 11-15, 1978.

2.17 R. Holm, Electric Contacts, Springer-Verlag, New York, 1967.

2.18 A. E. Emanuel, H. C. Doepken, and P. C. Bolin, "Design and Test of A Sliding Plug-In Conductor Connector for Compressed Gas-Insulated Cables", IEEE Transactions on Power Apparatus and Systems, Vol. PAS-95, No. 2, March/April 1976.

2.19 J. F. Archard, "Contact and Rubbing of Flat Surfaces", Journal of Applied Physics, Vol. 24, No. 8, August 1953, pages 981-988.

2.20 J. F. Archard, "Single Contacts and Multiple Encounters", Journal of Applied Physics, Vol. 32, No. 8, August 1961, pages 1420-1425.

2.21 Marks' Standard Handbook for Mechanical Engineers, Seventh Edition, McGraw Hill, 1967.

2.22 O. S. Taylor and P. Reichner, "The Effect of Variation in Contact Force on Solid Brush Power Loss", to be presented at the 24th Annual Holm Conference on Electric Contacts, September 11-15, 1978.

SECTION 3

BRUSH INTERFACE AND MATERIALS RESEARCH

3.1 Contact Interface Investigations

3.1.1 Objectives

To obtain direct information on contact interface conditions in high current sliding current collection systems through the use of advanced diagnostic techniques and to undertake carefully controlled experiments in specified environments to assist in the development of an improved high current density brush model.

3.1.2 Prior Work

Although from time to time over the last twenty years, occasional investigations have been undertaken into the nature and conditions at current transferring sliding interfaces, relatively little quantitative information is available on the prevailing conditions compared with, for example, other fields of solid state or surface science. As a consequence, although we have been able to develop a speculative model of the sliding surface,[3.1] there are many uncertainties which remain to be resolved.

Basically it is considered that application of the contact force to the brush-slip ring system results in the generation of a true area of mechanical contact (A_t) which is appreciably smaller than the apparent area of contact (A_b), which is the brush area. The ratio of these two areas may be as much as one hundred to one ($A_b/A_t \geq 100$). At the true area of contact formed by the elastic and plastic deformation of the asperities on the brush/ring surfaces, not only is mechanical contact taking place, but electrical current transfer must also occur. The relatively limited area of contact gives rise to a major contribution to

the electrical resistance as a result of constrictions. In addition, in general, a contribution will also be present due to the adsorbed or reacted film on the areas of contact. If such a film is sufficiently thin ($\tilde{>}$ 30 Angstroms) electron tunneling may take place without major losses. However, thicker films, (e.g., oxidized) may result in significant resistance, leading to increased losses and, depending on the applied voltage, to electric field breakdown effects.

Effects which take place at these local areas of contact thereby play a major role in determining the electrical behavior of contacts and, in a similar way, are major contributors to the interface frictional and wear effects.

Because adsorbed vapors and gases and reacted films, even though only Angstroms in thickness, may play such an important part in the interface behavior, relatively few techniques for obtaining direct information have been available until recently. What little direct information that is available appears to indicate that adsorption of gas and vapor molecules onto edge and basal sites on graphite crystallites may determine the interface behavior. The attachment of the graphite crystallites to the underlying surfaces structure depends on whether the interface is covered with an oxide layer, the attachment being increased in some cases and decreased in others. Attachment of the graphite crystallites appears, from x-ray diffraction studies, to follow a "shingle-like" structure.

3.1.3 Current Progress

3.1.3.1 Contact Model

Based upon theoretical studies and the evaluation of experimental results of a range of conventional powder-metallurgy materials operating at 0.8 MA/m^2, an attempt has been made to improve the understanding of phenomena which take place at the contact interface. The results of this work have been largely reported in a paper which has recently been submitted to the forthcoming International Conference on Electric Contact Phenomena, to be held in Chicago in September 1978. This paper is reproduced here as Appendix 3.1, with the results being as indicated there.

Perhaps the most notable features are that the constriction resistance appears to dominate the electrical performance, with the film resistivity apparently being very small ($< 6 \times 10^{-13}\ \Omega \cdot m^2$). Presumably this is a consequence of the operation of brushes in a non-air environment in which significant oxide films are not formed. Evaluation of the frictional behavior, based on the assumption that shearing of an adsorbed water vapor layer is responsible, lead to an estimate of the film thickness as being one to two monomolecular layers. This appears to be consistent with a small film resistivity.

Perhaps the most notable feature of the experimental studies which remains unexplained was the marked change in wear rate that was observed as the metal-to-lubricant ratio of the brush was changed from a metal mass fraction of 0.45 to 0.90. For this change, the wear rate changed by an order of magnitude, from 0.7 mm^3/Mm to 70 mm^3/Mm. At the lower end of this range, the wear rate is comparable to that achieved in boundary lubrication. To date, a fully satisfactory explanation for this large change in the wear rate has not yet been evolved, although extensive analytical work which is at present being undertaken appears promising. Experimental studies, using Auger spectroscopy and scanning electron microscopy, are also underway in an attempt to obtain some direct experimental evidence which will enable this phenomena to be better understood.

3.1.3.2 Experimental Investigations

In order to characterize and analyze the contact interface, one needs an analytical technique which is capable of sufficient spatial resolution to select the areas of interest and which has the required depth resolution of 10-20 Å. Auger electron spectroscopy (AES) is such a technique. The instrument used for the investigations to be described is of the scanning type and has a primary beam diameter of $\sim$ 3 μm. The depth analyzed is variable with the material and depends on the energy of the Auger electrons which is being collected. A measure of the analyzed depth is provided by the parameter known as the "inelastic mean

free path" or "escape depth" (symbol λ). For the copper LMM line ($\sim$60 eV) in metallic solids, $\lambda \tilde{=} 7$ Å and for the copper KLL line for 920 eV, $\lambda \tilde{=} 13$ Å (reference 3.2).

Five slip rings, 83 mm (3.25") in diameter, which had been run under standard conditions on the bench testers, have been analyzed using AES. Unless indicated otherwise, the whole slip ring was transferred from the test site to the Auger laboratory in a vessel under CO_2-over pressure. Transfer from this vessel to the ultra-high vacuum (UHV) chamber of the Auger spectrometer took from five to ten minutes, during which time the slip ring was exposed to the ambient air. Although this procedure did not prevent adsorption of moisture and other contaminants present in the laboratory air, it did prevent long exposure effects such as slow oxide formation on copper.

Figure 3-1 shows the geometry inside the UHV chamber. The slip ring (center) is mounted on a vertical shaft which can be rotated through 360°. Vertical motion of the shaft is also available so that each point of the sliding surface can be accessed. The annular opening directly to the right of the slip ring contains the entrance slit of the cylindrical mirror analyzer (CMA). The primary electron beam emerges through the central orifice. A sputtering gun points down towards the analysis spot from the top of the photograph. Typical sputtering conditions with argon gas yield, at 2 kV acceleration potential, removal rates between 20 Å/min and 200 Å/min (ion current densities $\sim$ 20 $\mu A/cm^2$ - 200 $\mu A/cm^2$).

The results of the AES analyses to date are summarized for each slip ring below. Some general conclusions are presented.

Slip Ring SA52 8/76 (Helical Groove)

This slip ring was not stored in CO_2 prior to analysis. The slip ring material was brass (62 Cu-34.75 Zn-3.25 Pb nominal). The surface of the slip ring was strongly enriched in Zn and Pb compared to the bulk composition. This was true both inside and outside the brush

tracks. Semiquantitative analysis using normalized peak heights (Reference 3.3) for Cu, Zn, and Pb, yielded the following estimates of the concentrations at various depth levels:

Depth (Å)	Cu wt %	Zn wt %	Pb wt %
0	10	76	14
100	38	53	9
1000	69	28	3

The presence of the low energy LMM transitions for copper and zinc (∿ 60 eV) and the N00 spectrum of lead (∿ 90 eV) on the as-received surfaces in the brush tracks indicates that a certain fraction of the metal surface was covered by less than a few monolayers of adsorbates (<10 Å). Evaluation of this slip ring demonstrated the success of the experimental apparatus and techniques.

Slip Ring SA51 8/76 (Helical Groove)

The slip ring material was OFHC copper. It was tested under copper-graphite brushes. The oxygen spectrum on the as-received surface contained an extra peak at 515 eV, which is usually not resolved in the oxygen spectrum of adsorbed oxygen on metals, although it may show up as a shoulder on the high energy side of the main KLL transition at 510 eV. The splitting in two peaks was attributed to chemisorption of oxygen to copper, rather than adsorption in the physical sense. Other contaminants included sulfur, chlorine, and nitrogen. The sulfur LMM spectrum is a triplet typical for Cu_xS (Reference 3.4). The amount of chlorine present was highly variable from location to location, and it was not associated with any identifiable salts. In one area, Ag was detected.

The presence of the low energy copper transition at ∿60 eV again confirmed that, in the brush track, free metal surfaces were present with less than 10 Å of adsorbate coverage.

Slip Ring SA50-2 (Smooth)

The slip ring material was OFHC copper. The contact surface was plated with 2.5 μm of ruthenium. The use of a silver (graphite)-ruthenium combination was suggested by the earlier work of Rabinowicz. The ring was run in test B1-230 under 75 w % Ag/C brushes (SG 142). The analysis showed that the ruthenium coating was of excellent quality. No copper could be detected and no flaws were present. There was considerable Ag/C transfer to the slip ring surface in the brush tracks. The photographs in Figure 3.2 show two opposite halves of the slip ring. It can be seen that two distinct transfer patterns were present: a line pattern in the direction of the slip and, superimposed on it, a spot pattern containing many more or less circular features aligned in the sliding direction. The spot pattern was absent over a length of about one quadrant (Figure 3.2(b)). The cause of the spot formation is not yet clear.

The ruthenium coating was rich in nitrogen and sulfur. Some sodium, chlorine, and silicon were also detected. These impurities may be due to the plating process. The spots analyzed as silver, carbon with a low oxygen content, whereas the adjacent areas within the tracks consisted primarily of ruthenium, oxygen, and impurities (nitrogen, sulfur, chlorine).

Slip Ring SA50-2 (Smooth)

This OFHC-copper ring was coated with 6 to 10 μm of tantalum. The testing conditions were as for SA50-3 (test B1-231). The tantalum coating was of poor quality and consisted mostly of carbides and oxides. In the brush track, the coating was abraded and copper exposed. The wear of the coating was more extensive in the bottom half of the track, indicating uneven loading on the brushes. Away from the brush track, no chlorine or sulfur were found, which indicated that the OFHC copper

was the source for these elements when they were detected on the copper surfaces (as opposed to the CO_2-atmosphere containing these elements). The poor quality of the tantalum coating was probably due to the fact that it was deposited by a sputtering technique. The oxides formed during deposition by reaction with residual oxygen in the sputtering atmosphere. The carbides may have formed during the run because of arcing.

Slip Ring SA50-4 (Smooth)

This OFHC copper ring was not coated. It was run under the same conditions as SA50-3 and SA50-4 (Test 229). In the as-received condition, the copper LMM spectrum and the oxygen spectrum again revealed the chemical bonding of oxygen to copper. After 15 sec sputtering (~25 Å removed), the LMM spectrum of copper assumed the characteristic shape of metallic copper and the oxygen spectrum became that of adsorbed oxygen. The transfer of Ag/C from the brush to the slip ring took place according to the same patterns noted for SA50-3.

3.1.3.3 Preliminary Conclusions

AES has definitely confirmed that the area in the brush tracks contained a significant fraction of clean metal covered by less than ~10 Å of adsorbed elements. When the slip ring material is an alloy, it is important to know whether the alloying elements segregate at the surface. This may affect both the friction/wear properties and the electrical properties of the contact. For pure OFHC-copper slip rings, it has been established that sulfur and chlorine segregate to the surface. This may actually be beneficial as far as frictional resistance is concerned (Ref. 3.6). With regard to the role played by the humidity of the environment, no clear conclusions can be drawn at this time, one of the difficulties being the exposure of the slip rings to ambient air during handling. In situ film formation and analysis would be preferable (see Section 3.4). Concerning the transfer of brush material to the slip ring, preliminary results indicate that the addition of silver to

the brushes causes a larger amount of the debris to stick to the slip ring surface. The heavier deposits occur in the spot patterns for reasons which have not yet been clarified.

3.2 Multi-Element Brush Research

3.2.1 Objectives

To develop a physical model of a multi-element brush, to develop and optimize multi-element brush materials, including metal-coated carbon and graphite fiber materials, and to evaluate candidate materials at current densities up to 7.75 MA/m^2 by the end of FY1979. The best candidate materials will then be evaluated in a demonstration unit at the same current density.

3.2.2 Prior Work

In some of the very earliest (ca. 1900) electrical brushes metal wire brushes were employed to make electrical contacts with commutators or slip rings. However, high friction and wear rates were experienced and such devices were discarded in favor of carbon based materials. In recent times, significant advances have been achieved by operating metal coated carbon fiber brushes in air and controlled atmospheres at current densities of 1.55 MA/m^2 (1000 A/in^2) and above. Additional work in this area is reported here. However, consideration of the fundamental effects which are present in such brushes has led to the conclusion that the optimum number of elements in such a brush may be in the range 10^2 to 10^5. It is to determine whether this is the case that the present program has been undertaken.

3.2.3 Current Progress

A multi-element contact model was developed and was used to describe the effects of changes in the number of fiber elements and the load current magnitude on contact performance "efficiency". This efficiency is presented in terms of the interface power loss per ampere of load current transferred. Within the present limitation of one

existing fiber diameter, set somewhat by the manufacturers of carbon and graphite fibers, the optimum numbers of fibers comprising a multi-element electrical contact for different current loads was predicted.

Several methods for depositing metal on carbon and graphite fibers have been evaluated, and the most promising one was selected to produce metallized fiber for brush fabrication. Two methods of fabrication were used to produce brushes, with packing factors deliberately varied from 0.25 to 1.0. To date, several of the fabricated brushes have been tested at current densities to 4.5 MA/m^2 in air and in helium atmospheres of varied humidity. Future effort will be directed towards testing brushes at higher current densities (to 7.75 MA m^2) and towards optimization of fiber metallization and brush fabrication methods.

3.2.3.1 Physical Model of Multi-Element Brush

The advantages of brush segmentation have been demonstrated in the use of split brushes and in the improved performance capability of smaller brushes. These improvements relate to the increase in real contact area and mechanical freedom to follow the rotor surface. In an attempt to maximize this increase in the number of contact points and, therefore, in the real contact area, the large step was made to fiber brushes consisting of elements numbering in the millions. The primary advantages of brush segmentation are:

1. Reduced contact volt-drop.
2. Reduced electrical contact power loss and heat density.
3. Improved dynamic mechanical response.

These advantages are apparent in the tests of experimental fiber brushes.

However, it would be desirable to investigate fewer, but larger sized subdivisions to determine whether an optimum size will provide improved performance. Other possible advantages of fewer subdivisions include easier fabrication, easier analytical representation of the mechanical and thermal systems, and better correlation with conventional brushes if the same material can be used. An initial attempt to analyze the performance of such a brush is given below.

3.2.3.1.1 Contact Electrical Resistance

For metallic contacts, the components of contact resistance follow an inverse power relationship to applied force:

$$r_1 = C_1 f^{-k_1} \tag{3.1}$$

$$r_2 = C_2 f^{-k_2} \tag{3.2}$$

where r is the component of contact resistance, f is the contact force, and C and k are constants which depend on material properties and the nature of the surface. The subscripts are "1" for constriction and "2" for film.

If two or more sets of these contact elements are electrically connected in parallel, they will share the current just as parallel resistors in a circuit. For n identical elements with a total force F = nf, the overall resistance will be

$$R = (r_1 + r_2)/n \tag{3.3}$$

From Equations (3.1), (3.2), and (3.3), the resistance becomes:

$$R = C_1 F^{-k_1} / n^{1-k_1} + C_2 F^{-k_2} / n^{1-k_2} \tag{3.4}$$

or

$$R = R_1/n^{1-k_1} + R_2/n^{1-k_2} \tag{3.5}$$

where R_1 and R_2 are the constriction and film resistances for a single element brush under the total force, F. For certain contact geometries, Holm[3.7] has found values of $k_1 = 1/3$ and $k_2 = 2/3$ for light (elastic) loading and $k_1 = 1/2$ and $k_2 = 1$ for heavier loads where plastic flow determines the real contact area. The gross shape or conformability of the individual contacting members may influence the distribution and number of contact points at a given load. For closely mated or flexible bodied members, the number of contacts may increase with load, and this will result in larger apparent values for k.[3.8,3.9] The flexibility of

the asperities, the average separation distance, and the conformability of the contact members will determine this relationship. The proper values of k are best determined empirically for the specific brush-slip ring combination selected.

The improvement in contact resistance associated with brush subdivision is illustrated in Figure 3.3. The resistance relative to that for a single contact (n = 1) is shown for both the film and constriction components and for both the theoretical elastic and plastic loading assumptions. It can be seen that the predicted constriction resistance is reduced to 10%, or less, of its initial value with only 100 elements, when the contact is assumed to be plastic or elastic, respectively. The reduction in film resistance with increasing n is noted to be more dependent upon the nature of the contact (the value of k_2) and would be independent of subdivision for plastic contact theory.

For high metal-content brushes in a controlled (non-oxidizing) environment, the film component of resistance has been found to be small compared with the constriction resistance for conventional brush sizes. (see Appendix 3.1). On that basis, one may predict a major improvement in electrical performance of the brush interface for segmentation into as few as 10 elements. Also, 90% of the gain should be achieved with less than 1000 elements if the elastic values for "k" apply, even with the presence of thin surface films.

As an example, examine a silver-graphite brush (75% Ag by weight) with the following operating conditions:

k_1 = 1/3 (elastic contact)
C_1 = $2/312 \times 10^{-3}$ (for F in lb)
F = 2.15 lb (11 psi, with an apparent contact area of 0.195 in^2)
ρ = 15×10^{-6} Ω cm
L = 1 in
k_2 = 2/3
C_2 = 0.173×10^{-3} (for F in lb)

If the brush is segmented, the contact resistance (Ω) may be found from Equation (3.4) as

$$R = 1.79 \times 10^{-3}/n^{2/3} + 0.104 \times 10^{-3}/n^{1/3}$$

The second term, the film resistance, is seen to be relatively small. The brush body resistance for the solid brush, which is also small, is

$$R_b = \rho L/A = 32.3 \times 10^{-6}\ \Omega \quad (3.6)$$

If the packing factor varies with number of elements, then the body resistance for the segmented brush could be considered to be a function of subdivision, but still a small value.

For elastic contact theory, Figure 3.4 shows the predicted reduction in total resistance (essentially contact resistance) for the silver-graphite brush, with increasing segmentation. With only 50 to 100 elements, a 90% reduction is predicted.

In order to evaluate this mathematical model, a brush holder has been constructed which will accept brush elements with a square cross-section of 1.52 mm x 1.52 mm. Fifty-four of these will be required to give the contact area of the standard solid test brush. This element size permits the use of conventional brush fabrication techniques so that the material will be as close to that of the full-size brush as possible.

The segmented-brush holder is shown in Figure 3.5 with some of the unfinished brush elements. The holder is built-up to provide a variable number of rows of 5 elements each. This was done to simplify machining and to permit flexibility in testing. The holder provides a large increase in surface area for heat conduction from the brush to the holder; about seven times that for the standard full size brush for the same contact surface area. With this configuration, it is expected that a significant portion of the current will pass directly from the brush to the holder, but individual shunting will be provided in initial tests to assure that all elements are functional. The elements will be flexibly mounted to the brush mechanical loading pad to permit independent action.

3.2.3.1.2 Friction and Wear Factors in Subdivision

The reduced contact heat generation and improved cooling associated with subdivision is expected to reduce the contact temperature for a given brush current density. This is expected to reduce the wear rate although the friction coefficient may increase somewhat. On the other hand, the probable increase in real area of contact could increase

the friction and wear coefficients. However, this may be compensated by a reduced contact force requirement because of the previously gained lower contact resistance. The required force may also be less because of the improved mechanical response to slip ring irregularities.

It is likely that the distribution of metal and graphite (or other lubricant) is also important, as is the grain size of these components. The use of independent lubricants sources on the slip ring surface with solid metal brushes is not as effective as the same materials intimately intermixed. Since there is no present model which defines this effect, both experimental and analytical effort in this area may improve the understanding of the contact interface.

Although a relatively high friction coefficient has been observed with fiber brushes, it is not clear at this time if this is due to the increased real area of contact or the difference in material from that of the conventional solid brushes. Testing of the segmented brush described above may help to clarify this relationship. In the simplest theory, the friction and wear based on adhesive theory for homogeneous materials would be proportional to the real area of contact. For n elements with a total load F, the total real area A and thus the friction, may be determined from the expression for the individual elements for elastic and plastic theory:[3.7]

Elastic

$$(A/n) \alpha (F/n)^{2/3}$$

$$A \alpha n^{1/3} F^{2/3} \qquad (3.7)$$

and since the assumed relationship for the friction coefficient is

$$\mu \alpha A/F$$

then:

$$\mu \alpha n^{1/3} F^{-1/3} \qquad (3.8)$$

Plastic

$$(A/n) \alpha (F/n)$$

$$A \alpha F$$

$$\mu = \text{constant (independent of F and n)} \qquad (3.9)$$

Similarly, the wear (e.g., m^3/m travel) is proportional to area and would be

Elastic

$$W \alpha n^{1/3} F^{2/3} \tag{3.10}$$

Plastic

$$W \alpha F \text{ (independent of n)} \tag{3.11}$$

The light load on the individual elements of a fiber brush would suggest that elastic contact theory should apply. However, the predicted increase in friction coefficient according to Equation (3.8), for the very large number of contacts, is much greater than experimentally observed. This may be explained in at least two ways. First, it need not be inconsistent to model the electrical constriction area as that based on elastic contact for light loads while at the same time utilizing plastic contact theory for friction and wear. The few electrically deformed contact spots which establish the electrical constriction may themselves be composed of asperities which are plastically deformed. Then, because of the close proximity of these subcontacts, they will act as one electrical constriction with an elastically determined nominal area, while the shear area is that of the real plastically-deformed asperities.

The second explanation would be that the model must be more complex and must include the lubricity of the graphite as well as the higher shear strength of the metallic joints. In this content, a new approach to brush interface modeling can be based upon the difference in wear rate coefficient between the graphite and metal components of the brush material. If the wear rates are defined as:

$$W_m = C_m p_m v \tag{3.12}$$

$$W_g = C_g p_g v \tag{3.13}$$

where W is the linear wear rate (e.g., in/hr), C is a constant for the brush-slip ring material combination and temperature, p is the contact

pressure for each material component, v is the contact sliding velocity, and the subscripts m and g refer to the metal and graphite components. Since the wear rate must be the same for both components, and the velocity is the same, the pressure on each component would thus be inversely proportional to the wear constant C for that component. On this basis, one would expect a higher contact pressure under the graphite than under the metallic portion of the brush. This would be modified, of course, by the lubricant separating the metallic surfaces or if the metallic material is wiped over the brush interface area. Correlation of this model is presently being investigated using experimental data for brushes with various percentages of graphite-metal mixtures.

3.2.3.2 Fiber Brushes

The main subtasks during this period were:

- To continue establishment of techniques for coating fibers with metal.
- To establish a simple base-to-fiber joining technique and establish the interface resistance characteristics.
- To continue testing fiber brushes at high current densities (1.55 MA/m^2 to 7.5 MA/m^2).

3.2.3.2.1 Prior Work

A batch method was developed to produce metallized surfaces on nominal eight micron diameter carbon fibers. This consisted of initial substrate surface conditioning (cleaning), followed by a thin chemically deposited nickel coat and a final electrolytically deposited silver plating. Typical thickness of deposited metals was about one micron. Yields averaged 20,000 fiber/feet. Optical and electrical methods were used for evaluating the quality of the metallized carbon fibers. Combined, these methods assured that good metal coverage and the desired coating thickness were achieved.

Test brush samples of approximately 400,000 individual fibers were prepared. The fibers were first compressed into a rectangular cross section of 1.3 cm^2, yielding a theoretical packing factor of 0.25, then joined at one end to silver-plated copper support bases with low melting point solders. Each brush had a free fiber length of approximately 20 mm.

A test rig was commissioned for evaluating the sample fiber brushes. Preliminary tests were run in cover gases of nitrogen, helium, carbon dioxide, and air. Generally, the positive (anodic) brush voltage drop was found to be higher (up to 3 times) than the negative, being somewhat higher on copper slip rings as compared to silver. The contact voltage drop tended to increase less than linearly on silver slip rings as the current density was increased. The friction coefficient also tended to be constant or rise slightly with increasing current density (up to 0.8 MA/m^2). Wear was low for brushes of both polarities.

3.2.3.2.2 Current Progress: Metallization of Carbon and Graphite Fiber

Of several metallization processes tested, one was selected for plating highly conductive metal layers on the surfaces of 8 μm diameter carbon and graphite fibers. Although the plating method was originally developed for batch processing, yielding 20,000 fiber-feet per hour, it has recently been semi-automated to achieve a higher yield, 280,000 fiber-feet. Most of the fibers processed to date have been carbon, plated with approximately 0.1 μm nickel and 1.0 μm silver.

Plans for the future include automation of the metallization installation by incorporating continuous electroplating. Resulting from this, hourly production of metal-coated fiber will be increased to about 500,000 fiber-feet. Emphasis will be placed on improving the coverage and continuity of the deposited metal, which will result in brushes of higher quality.

3.2.3.2.3 Current Progress: Brush Fabrication

Initially, brushes were constructed by joining the metallized fibers to solid copper bases with lead-tin alloy solder. Good wetting of the fiber-brush base interface was achieved, resulting in typical

interface resistances near 17 μΩ for brushes containing 400,000 fibers, surface areas of 1.25 cm^2, and a packing factor of 0.25.

Several brushes were constructed with internal gas cooling ducts, which penetrated into the fiber bundle. Test results indicated that these ducts will permit at least 20 liters per minute cooling gas flow through the brush fibers. Additional cooling capacity (higher flow rates) can be provided, if necessary, by increasing the gas inlet pressure.

Other methods of brush fabrication have also been developed. The criteria used to evaluate these methods include (1) loose packing and flexibility of the fibers must be maintained at the face end of the brush, and (2) the fibers must be joined or contained in a base, possessing good electrical contact (low resistance) with each other and the base.

The first attempts to produce silver-copper alloy bases were moderately successful, but were not considered to be suitable for large-scale production. The problem areas centered around handling of the hair-like fibers, special fixturing, and wicking during heating or brazing operation, and shrinkage during cooling.

A subsequent, more simple technique for fabricating fiber brushes was developed, and it employed a swaging operation. This has been quite successful, enabling large brush areas, with integral cooling channels (if required) to be assembled from individual modules. This procedure is to squeeze a copper tube around the fiber at the base end of the brush. All samples are presently being fabricated by swaging the full length of the outer-tube assembly, machining away sections of the copper tube to expose the underlying fibers. The fibers are then severed at the mid-plane of the exposed length, forming a pair of brushes. Other techniques are considered applicable for the consolidation of the base. These techniques would require equipment design changes which are not necessary here to complete the present multi-element brush evaluation.

A more detailed description of the fiber-base joining procedure is as follows. A predetermined number of fibers were straightened to their full length and submerged in methanol. Wetting of the fibers by this means improves their handling and bundling. Fiber bundles were then inserted into previously deoxidized copper tubes. Presently, a 400,000 fiber bundle is inserted into a 1.9 cm diameter, 18 cm long tube. The excess methanol is blown out of the tube and the remainder is evaporated by heating the tube. This fiber-tube assembly was then swaged to the desired inside diameter, which determines the fiber packing factor. The packing factor is defined as the ratio of the total fiber cross section area to the swaged tube inside diameter cross section area. Figure 3.6 illustrates fiber spacing in a brush base having a 70% packing factor.

An electrical test was used to determine the effects of swaging (packing) on the fiber-base joint resistance. To that end, a 2.5 cm section of the swaged copper tube was machined away from the central zone of each fiber-tube assembly, exposing the fibers as previously discussed. The remaining copper ends of this assembly, which form the fiber joining bases, serve here as the current terminals of a four-terminal resistance measurement system. With current established, voltage drops were measured with needle probes across each of the two fiber-to-tube joints. From these measurements, calculations of joint resistance were made. The results of testing a number of fiber-tube assemblies are shown below.

3.2.3.2.4 Current Progress: Fiber Brush Test Results

Effort was concentrated during the period on testing brushes at a current density of 1.55 MA/m^2 (1000 A/in^2), with a silver-plated copper slip ring running at a peripheral speed of 15 m/s and with an apparent mechanical loading of about 7 kPa (1 lb/in^2). Each test brush nominally contained 400,000 silver-coated carbon fibers. The effective fiber length of each brush was about 1/2 cm. Bulk temperature of the fibers varied from 18° to 52°C, depending upon the level of cooling provided. Testing is still in progress, but the following results have been achieved.

TABLE 3.1

SWAGING EFFECT ON FIBER-BASE CONTACT RESISTANCE

No. Of Fibers	Packing Factor	Fiber-Base Resistance, μΩ (1)	(2)
80k	.34	183	100
80k	.42	141	103
80k	.73	83	61
80k	.90	38	-
120k	.50	34	27
120k	.99	27	-
400k	.25	164	-
400k	.51	25	13
400k	.73	8	7

(1) As processed.

(2) Post heat treatment: 750°C, 10 min, H_2 atm

- Test runs were made wherein single brushes of each polarity were constrained to slide in independent tracks on the slip ring surface. During these experiments, which were 5 to 17 hours in duration, an air environment was employed and its dew point was deliberately varied in the range -6 to -17°C (3700 to 1400 ppm_v moisture). The brushes operated with low combined electrical and mechanical losses, averaging 28 to 40 W/brush (0.14 to 0.21 W/A). The power loss showed no dependency on humidity in the range studied. Initially, upon starting each run, the brush power loss was typically 1.5 to 2 times higher than its steady-state or average value. The lower steady-state power loss level was reached after about one hour of operation.

- In other similar experiments, the influence on fiber brush performance over a wider range of moisture concentrations was evaluated, -1 to -50°C dew points (5800 to 40 ppm_v), for test environment gases of air and helium. Again, as noted before, the combined electrical and mechanical brush-ring interface loss showed little dependency on the humidity level. The average power loss varied from 41 to 37 W/brush when run in either gas, tending to the lower loss value at higher humidity levels. As tested, the average brush-ring friction power loss was about 2.8 to 3.6 times higher when run in increasingly humid air, as compared to operation in helium. However, the average electrical loss was 2.5 to 1.6 times lower in air than in helium. The net result, as previously mentioned, was that the combined power losses resulting from operation in the two gas environment are about the same. A strong adverse polarity effect on performance was observed when the fiber brushes were operated in air atmospheres at moisture levels greater than -20°C dew point (1000 ppm_v). With increasing humidities, the electrical loss at the positive brush steadily increased, while the negative polarity brush loss remained essentially constant. At the highest air humidity, a positive to negative electrical loss ratio of 3 was recorded. This suggests that fiber brush operation in air environments should be carried out under "dry", rather than "wet" conditions. In contrast, fiber brush operation in helium gas environments (over the wide humidity range) was not influenced to any decided degree by the brush polarity.

- Based on the combined testing in air and helium environments, life was estimated for the positive and negative polarity brushes to be 2520 and 3290 h/cm, respectively. Additional testing is required to determine the brush life characteristics in each of the gas environments separately. More recently, preliminary testing has been demonstrated at up to 4.65 MA/m^2 (3000 A/in^2) with fiber brushes in air.

3.3 Monolithic Brush Material Research

3.3.1 Objectives

The overall objectives of this task were (1) to develop, manufacture, and evaluate new monolithic brush materials and structures which provided high electrical conductivity, low friction and low wear (target date - by the end of the third quarter of FY 1978); (2) to undertake parallel evaluation experiments on developed monolithic brush materials under varying conditions of atmosphere, additive, temperature. load force, and slip ring speeds up to 3.1 MA/m^2 (2 kA/in^2) (target date - same as (1)); and (3) to operate the preferred monolithic br·sh material in a machine environment tester at current densities up to 3.1 MA/m^2 and collector surface speeds of 25 to 75 m/s (scheduled in the third quarter of FY 1978 to the end of FY 1979).

Several primary approaches for the new monolithic brush materials were pointed out in the contact proposal. During this reporting period, efforts were primarily made on the preparation and evaluation of metal (copper/silver)-coated graphite, and the preparation of oleophilic graphite and phosphate-impregnated graphites for the metallization. The objectives were to develop a process of metallization of graphite powders which after pressing and sintering, provided a maximum conductivity for a given metal content in the metal-graphite brush material. The oleophilic graphite and phosphate-impregnated graphites are modified graphites which provide higher lubricity and lower wear rate than ordinary graphites, respectively, as were suggested in the literature.

Evaluation of developed monolithic brush materials were continued and focused on silver-graphite and copper-graphite materials of varying metal contents, types of graphites, and processes of fabrication of the materials. Effects of additives including "cleaning action" material in copper-graphite brushes and dichalcogenides in silver-graphite brushes, to the brush performance were primarily studied.

3.3.2 Prior Work

A number of brush test rigs were commissioned to evaluate candidate contact system materials, including brushes, rings, gas environments, and vapor additives. The rigs varied in size from relatively small laboratory-type screening testers to considerably larger machine environment-type test stands. Based on initial screening tests, a few silver- and copper-graphite brush materials were selected for advanced testing under higher speed and higher current conditions and with greater numbers of parallel connected brushes. The metals in these materials were combined with the graphite by compacting and sintering of mixed powders or by direct infiltration into preformed graphite blocks. The infiltration technique permits only a limited amount of metal to be combined with conventional base graphite materials. Although copper-graphite brushes fabricated in this manner performed very well when loaded to current densities of 0.8 MA/m^2, they wore at high rates at higher electrical loads. There is no apparent limit to the amount of metal that can be combined with graphite when processed by the powder metallurgy technique. Relatively good contact performance was achieved with silver-graphite brushes processes by this technique when tested on laboratory testers to current densities of 2.3 MA/m^2.

3.3.3 Current Progress

3.3.3.1 Material Production

3.3.3.1.1 Metal-Coated Graphites

A process has been developed for coating graphite powders of sizes down to 38 μm with copper or with silver. The metal contents ranging from 20 to 97 weight percent of the coated powder have been achieved by simple and multiple chemical platings. Detailed process of metallization of the powders and fabrication of the metal coated powders into a solid brush material as well as evaluation results of the sintered materials are described in a paper and is presented in Appendix 3.2 of this report.

The objective was to obtain a sintered metal-coated graphite composite which provided a continuous, three-dimensional metal matrix throughout the composite body. Such a new type of structural material would permit a maximum usage of metal conducting constituent and graphite solid lubricant and is a desirable brush material for carrying high current density and operating under high peripheral speeds. Metallographs of the sintered metal-coated graphites revealed the structure of continuous metal matrix. Compared with metal-graphite brush materials fabricated by conventional powder metallurgy and metal infiltration techniques, the electrical resistivities of the present materials are consistently much lower than the commercial materials of the same metal contents and the advantage becomes progressively greater at lower metal contents. These concluded that the present sintered metal-coated graphite provided higher conductivity and more efficient usage of metal constituent than metal-graphites fabricated by other techniques. However, for practical application, those problems including the proper selection of graphite grades and graphite particle sizes, the addition of binders, and other fabrication conditions need to be further explored in order to obtain a new brush material of high electrical conductivity, low friction, and low wear rate.

3.3.3.1.2 Oleophilic Graphite

Oleophilic graphite is a modified graphite which possesses a high ratio of surface-to-edge sites. It was prepared by grinding large flakes of one natural graphite in a liquid hydrocarbon medium. The reduction of graphite powder dimensions by such grinding is illustrated in Table 3.2.

Several oleophilic graphite products were coated with copper and with silver by chemical plating (see W29, W30, and W32 in Table I of the paper in Appendix 3.2).

3.3.3.1.3 Phosphate-Impregnated Graphites

Phosphorous-containing compounds are known to be effective oxidation inhibitors for graphite. The addition of small amounts of phosphorous compounds into a carbon brush has been suggested for lowering the wear rate of the brush in electric contacts. Some experimental work on wear and friction measurements has been reported by Lancaster,[3.10] but no data on voltage drops in brush contacts have been published. Recent work indicated that, in the presence of ammonium phosphates or phosphorous oxyhalides, the ignition temperature of graphite in air was increased significantly. On the contrary, many metallic oxides were found to be oxidation catalyzers to graphite. Since the amount of phosphate additives in brushes is so small (a few percent) that it is not sufficient to act as an oxidation barrier as it does for graphite moderator in nuclear reactors a conversion of metallic impurities (oxides in the ash content) of graphite into inactive phosphates appeared to be the most likely anti-wear mechanism for the phosphorous-containing additives in carbon brushes. Based on this understanding an investigation into phosphate additives seemed to be worthwhile for carbon brushes to be used in high speed and/or high current machines, where conventional brushes may be worn away rapidly by oxidative processes.

Experimental work was mainly to develop a method of phosphate impregnation. Samples of natural graphite was used. The whole process consisted of the following steps: (1) soaking graphite powders in ammonium hydrogen phosphate solution and drying; (2) initiation of interactions of ammonium phosphate with graphite impurities by heating under inert atmospheres; and (3) driving off excess phosphoric acid from the sample by rapid heating to 900-1000°C under a stream of inert gas. From graphite sample with ash content of 1.0% by weight, for example, a good impregnated product containing 0.49% PO_4 (or 0.16% P) was obtained by this impregnation method. High percentage of phosphate impregnation was found to be undesirable because the metal-coated graphite made from the impregnated product, swelled badly during sintering step of the fabrication process.

TABLE 3.2

DIMENSIONS OF GRAPHITE POWDERS AND OLEOPHILIC GRAPHITE PRODUCTS

	Natural Graphite (-80 +200 Mesh Fraction)	Oleophilic Graphite Products (-200 + 400 Mesh Fraction)
Width	140-140 μm	30-80 μm
Length	250-460 μm	40-200 μm
Thickness	38-100 μm	4-17 μm
Ratios		
Width / Thickness	2.4-3.7	4.7-6
Length / Thickness	4.6-9.2	12-18

3.3.3.2 Materials Testing

Over 40 experimental brush materials were developed and manufactured during the reporting period. Experimental screening runs with many of these, totaling over 160 tests, have shown promising performance, but further optimization of the material compositions is required to provide the best performance capability.

Most emphasis was concentrated on silver-graphite brush materials, fabricated mainly by the conventional powder-metallurgy technique. The variables included mass fraction of silver, type of graphite, and processing of the composite materials. An in-depth discussion of important selected physical properties (density, conductivity, and hardness) and the operating performance (contact resistance, friction coefficient, and wear rate) for these materials is presented in Appendix 3.1 of this report. The objective was to obtain improved brush performance both experimentally and through an improved understanding of the mechanism of brush operation. A discussion of the results from testing similar brush materials under machine environment-type conditions is presented in Section 2 of this report. The goal there was to evaluate the influence of large numbers of parallel brushes with larger total load currents on contact resistance and brush life.

Summary discussions of other candidate brush materials fabricated and tested under screening test conditions during the period are presented below.

- Copper-graphite materials were formulated by the powder metallurgy processing technique for test evaluation, with the goal of finding a replacement for the more expensive silver metal in silver-graphite brushes. The operating performance found for such material brushes is characterized by low friction coefficients but, also, by significantly higher contact voltage drops as compared to similarly processed silver-graphite brushes. Typically, friction coefficients are about 1/3 to 1/2 of those attributed to the silver-graphite brushes and the voltage drops range up to 10 times higher, depending somewhat upon the material composition and processing variables.

Additions of the somewhat abrasive hard carbon to selected copper graphite brushes resulted in a desired reduction in the contact voltage drop (as a result of reduced film thickness), without causing an appreciable increase in the friction-coefficient. However, these additions, when effective, caused an increase in the brush wearing rate. A better fundamental understanding of the reason for the difference in performance between copper- and silver-graphite brushes is required to enhance future material developments in this area.

- Additional metal-graphite materials were fabricated by infiltrating molten metal into basic graphite pore-void structures. The goal here was to utilize the metal component more efficiently (yielding equal or better conductivity with less metal) and, simultaneously, to achieve greater lubricating capability with the larger amount of graphite available to the interface. Both copper and silver metals were infiltrated in base graphite materials, achieving metal mass fractions up to about 0.55.

  Results of screening tests revealed no strong advantage by either silver or copper as the preferred infiltration metal. Very low brush wear (0.2 to 1.2 mm^3/Mm) is characteristic of both metal grades, being lowest for copper-graphite. Both metal grades performed in the medium contact voltage range (0.08 to 0.18V double contact drop) and with medium to medium-high friction coefficients (0.17 to 0.26).

  The contact voltage drop of metal infiltrated brushes was lower than that of similar composition brushes processed by the powder metallurgy technique, however, the opposite is true for the friction coefficients. Thus, the metal appears to be used more efficiently in the former brushes as evidenced by the lower contact resistance, but the graphite employed in those brushes is less effective as a lubricant. More effort is required to achieve an improvement in the brush performance of metal infiltrated metal-graphite grades (lower voltage drop and lower

friction). This may be achieved by devising methods for incorporating larger mass fractions of metal in graphite materials possessing greater lubricating capability.

- Silver-graphite materials were formulated by the powder metallurgy processing technique using oleophilic graphite. The goal here was to utilize the claimed high lubricating qualities of oleophilic graphite to improve the friction and wear characteristics of conventional high metal containing-high current density metal-graphite brushes. Based on our screening test results, low to medium friction coefficients (0.08 to 0.14) were achieved with oleophilic graphite brushes containing silver mass fractions of 0.8 to 0.9. These coefficients are 1/2 to 2/3 the values exhibited by similar material brushes containing natural graphite. This desired lower friction characteristic was achieved with a significant unexplained increase in brush wear, however, and a tendency towards higher interface power losses due to significantly higher contact voltage drops. Because of the latter results, no further work is planned for material development in this area at the present.

- Work was initiated to evaluate brush materials containing small amounts (0.05 mass fraction) of selected dichalcogenides (molybdenum disulfide and niobium diselenide). These are "self-lubricants" not requiring adsorbed vapors for their effective lubricating capability, but they were combined with graphite in their brush materials, which does. Preliminary test results reveal that improved friction and wear performance is achieved when these materials are run in dry, rather than moist, carbon dioxide gas environments. Further work is planned to confirm these results, to investigate a wider range of dichalcogenide additions, and to extend testing to other gas environments and with other slip ring materials.

Supporting work was done to provide increased cooling for future candidate material brushes tested in the laboratory screening tester.

Greater cooling than is presently available is necessary for evaluating brushes under the new, higher current density goal of 3.1 MA/m^2. To that end, an improved ambient gas handling system was designed. The initial objective of this design was to provide sufficient cooling to permit a 100% increase in heat load on the brushes without a significant increase in brush temperature. The system consists of a rotating fan attached to the tester slip ring, surrounded by a stationary shroud. The fan and shroud provide a surface that is 650% greater than the slip ring alone. Fixed guide vanes are employed to provide for a minimum rotating gas velocity profile at the shroud/fan pump inlet. Preliminary brush tests appear to confirm the system design cooling capability. The brush temperature rise associated with present heat loads is reduced by 50% with the increased cooling system.

3.4 University Investigations

3.4.1 Objectives

During the first year of the ARPA-funded investigation into Interface and Material Research on High Current Density Solid Brushes, three University based investigations have been initiated. These are with the following organizations:

Syracuse University, Dept. of Materials Science - Prof. R. Vook, Prof. D. V. Keller, II

MIT, Mechanical Engr. Dept. - Prof. E. Rabinowicz

Northwestern University, Mechanical Engrg. Dept. - Prof. R. A. Burton

The objectives for these investigations, the first two of which are subcontracts and the third being a consultancy-type study, are outlined below.

Syracuse University - Surface Film Composition Studies. The objective is to elucidate, through experimental and theoretical investigations, the basic phenomena which govern the mechanical, chemical, and electrical nature of the surface films which are formed at the interface between sliding solid bodies in which high currents are being transferred.

The use of modern diagnostic techniques (SEM, Auger electron spectroscopy, RHEED, etc.) and to obtain the required information on surface film composition is the central feature of the experimental investigations.

MIT - Materials Science Aspects of High Current Brush Operation. The objective of this program is to determine, by experimentation and analysis, the influence of materials science related phenomena on the successful operation of high current density brushes. The investigations will center around the elucidation of basic factors which affect elastic and plastic contact material behavior, friction, and wear, and the electrical aspects of brush operation. The influence of the properties of metal/lubricant materials will be investigated.

Northwestern University - Thermo-Mechanical Behavior of Contacts. The objective of this study is to apply and extend the results of available theories on thermo-elastic instabilities in sliding contacts to the conditions which prevail in high current density brushes. Super-temperatures occur locally at the asperity contacts on the brush and slip ring at which mechanical interaction and electrical current transfer takes place. Analysis will be undertaken of the stability, growth, and wear behavior of multiple contact spots of this type.

3.4.2 Prior Work

Surface Film Composition Studies. As described in Chapter 3.1, relatively little prior work has been undertaken on surface films at sliding interfaces under conditions that are relevant to those of interest here; i.e., high current transfer in non-air atmospheres. During recent months, studies using scanning electron microscopy and Auger electron spectroscopy have been initiated under this contract (see Section 3.1 of this report).

Materials Science Aspects. A larger number of studies have been undertaken on the conditions which prevail at sliding interfaces, although relatively few of these have been with graphitic or other lamellar

materials of the type required to maintain low friction in current transferring situations. The majority of these studies, while showing some of the complexities of this type of situation, have failed to provide clear scientific explanations which are relevant to our situation.

Thermomechanical Behavior of Solids. Apart from the major studies undertaken by Prof. Burton and his colleagues at N.W.U., relatively few studies have been undertaken in this area that could be applicable to high current brushes. A notable exception is the experiment of Marshall's,[3.11] in which he showed that thermal mounding was present in high current brushes and that, under extreme conditions, only a single point of contact -- which carried all the electrical and mechanical load -- was present.

The extension of the thermomechanical theory to include the effects of current transfer is a major feature of the present program.

Comment

It is apparent that, with few exceptions, there has been little prior work undertaken which is directly relevant to the conditions that apply to high current sliding contacts which operate in non-air atmospheres. As a consequence, the experimental and theoretical investigations that are planned for the present program are essentially breaking new ground and likely to lead to new, not previously obtained, results.

3.4.3 Current Progress

At the time of writing the present report, the programs at the above-mentioned universities have only just commenced, although subcontracts have been placed in all cases. A general preliminary workshop for all program participants was held at the Westinghouse R&D Center on January 18 and 19, and individual program planning meetings have subsequently been held with all participants. Current progress is outlined briefly below.

3.4.3.1 Syracuse University

Effort is at present being concentrated on assembling the experimental equipment necessary to undertake Auger electron spectroscopy studies, reflected high energy electron diffraction studies, etc.

Several items of equipment have been shipped to Syracuse to enable studies to begin.

For the generation and evaluation of slip ring surface films, two OFHC copper slip rings of the type used in the Westinghouse bench screening testers have been forwarded to Syracuse. Since some delay is inevitable in assembling the equipment which will enable these slip rings to be rotated within the Auger system, two additional slip rings that have been operated at Westinghouse have also been shipped for analysis. As with similar slip rings that are undergoing analysis in Westinghouse, these latter slip rings have been operated under high (85 w/o) and medium (55 w/o) silver-graphite powder metallurgy brushes. As indicated in Appendix 3.1, major differences in wear rate have been observed in such circumstances. It is the intention that these studies should discern the reasons for these differences.

To minimize the possibility of contamination during transit, a vacuum-tight stainless steel shipping vessel was designed, built, and used. The rings were maintained in a CO_2 atmosphere during shipping.

Additionally, to enable electrical work to proceed when the modified Auger stage has been completed, a 250 A dc power supply has also been lent to Syracuse University for use on this program.

3.4.3.2 MIT

Effort is presently concentrated on building test equipment for the measurement of friction and wear, with brush materials, and on developing a better background of information in the electrical contact aspects related to these two areas.

To enable the MIT experiments to be undertaken on representative materials, samples of graphite, 50 w/o graphite-silver, 75 w/o silver-graphite, and 75 w/o silver-niobium-diselenide have been shipped to MIT from Westinghouse. These materials have been characterized during screening tests on the Westinghouse bench screening testers.

3.4.3.3 Northwestern University

Initial work, undertaken by Chen and Burton has concentrated on the extension of prior work by Burton to the evaluation of thermoelastic effects in brushes with high currents and high speeds. This is reported here as Appendix 3.3. The results of this idealized, but representative, model of a brush-slip ring interface show that cooling of the slip ring is preferable to cooling of the brush if thermal mounding is to be presented.

More recently, the emphasis has shifted towards an analysis of an orthotropic brush material, such as that provided by fibers embedded in a brush. This will be reported at a later date.

3.5 Demonstration Machine Program

3.5.1 Objectives

To demonstrate the payoff which will accrue to the use of very high current density brushes in the military environment, specifically in the drive train of a heavy vehicle.

3.5.2 Prior Work

In the June 1975 issue of the DIA publication "Electric Vehicle Research, Development and Technology - Foreign (U)", (DST-1850S-403-75), the results of a competitive trial involving four vehicles, including a ACEC-developed electric drive system, as described in Table 3.3 demonstrated the desirability of electric drive for tanks and other tracked vehicles.

TABLE 3.3

TANK CHARACTERISTICS

Test Vehicle	Engine Output	Weight During Tests	Power-to-Weight Ratio
ACEC M-24	162 hp	11,800 kg	13.8 hp/ton
AMX-13	270 hp	14,500 kg	15.5 hp/ton
Standard M-24	220 hp	15,200 kg	14.4 hp/ton
Leopard I	830 hp	34,300 kg	22 hp/ton

In the words of the DIA report:

"The ACEC M-24 tank negotiated all test areas: the standard M-24 failed to clear an 0.8 meter wall during one phase of the test and was stopped by engine overheating; the AMX-13 broke down with gearbox and clutch trouble at the beginning of the speed trials. Only the ACEC M-24 and a Leopard I tank remained. Although the Leopard has a power-to-weight ratio of 22 hp/ton, compared to 13.8 hp/ton for the ACEC M-24, the latter was faster over the first 40 meters.

The following conclusions were drawn from the trials of the ACEC electric-drive tracked vehicle:

- The absence of a conventional mechanical transmission provides greater flexibility of layout and design of the vehicle. Drive sprockets can be placed either in the front or rear of the vehicle.
- Space required is much smaller than for an ordinary transmission.
- Transmission weight is reduced.
- Drive training is much more rapid than for other tracked vehicles.
- Average speed is increased over ground while skirting obstacles.
- Electric transmission is inherently very simple to maintain.
- At low speeds, steering is continuous up to one-track-locked condition, with no dead or shifting spots.
- At high speeds, steering is light and accurate, with no jolting.

The ACEC vehicle employs dc traction motors which represent the present state-of-the-art, with respect to current collection and other machine features. Significant improvement in machine size and weight are anticipated employing the technology projected in the present research program.

3.5.3 Current Progress

While the initial technology assessment task of this demonstration effort was not scheduled to commence during the reporting period, some ground work has been done for the selection of representative vehicle and drive system characteristics. In discussions with U.S. Army Tank Automotive Research and Development Command representatives, it was determined that two tentative models should be further investigated as potential candidates for systems analysis efforts. These systems are the drive train for the High Speed Tracked Vehicle (light) and the transmission system specified for the Advanced Development of a Continuously Variable Cross Drive Hydromechanical Transmission (CVX-60). TARADCOM has provided suitable technical data to permit establishment of electric machine characteristic requirements in preparation for model system configuration definition. The first quarter of the second annual reporting period will produce selection of the representative vehicle.

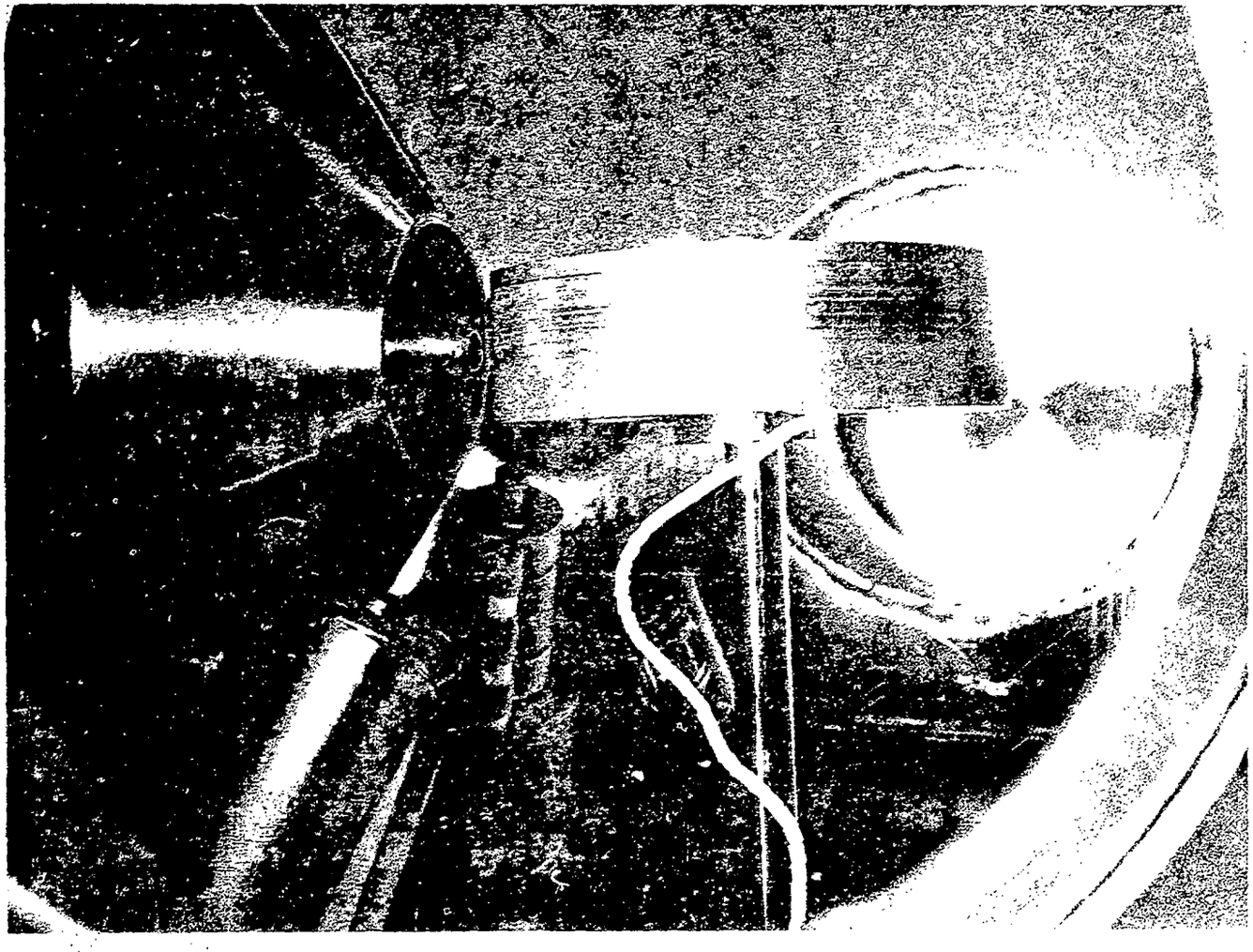

FIGURE 3.1. Slip ring mounted inside Auger ultra-high vacuum chamber.

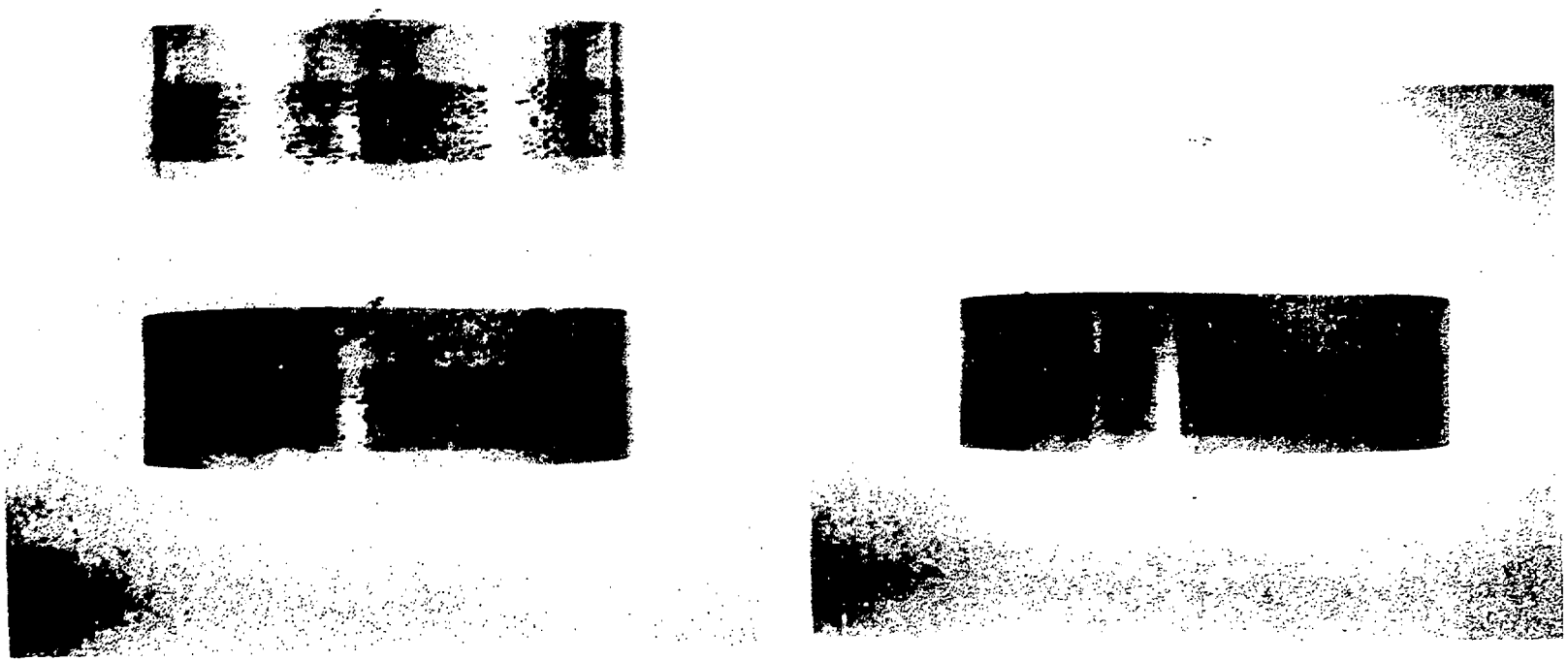

(a) Region 1

(b) Region 4

FIGURE 3.2. Ruthenium-coated slip ring (full size) after operation under 75 w/o silver-graphite brushes (Test B1/230)

Curve 695860-A

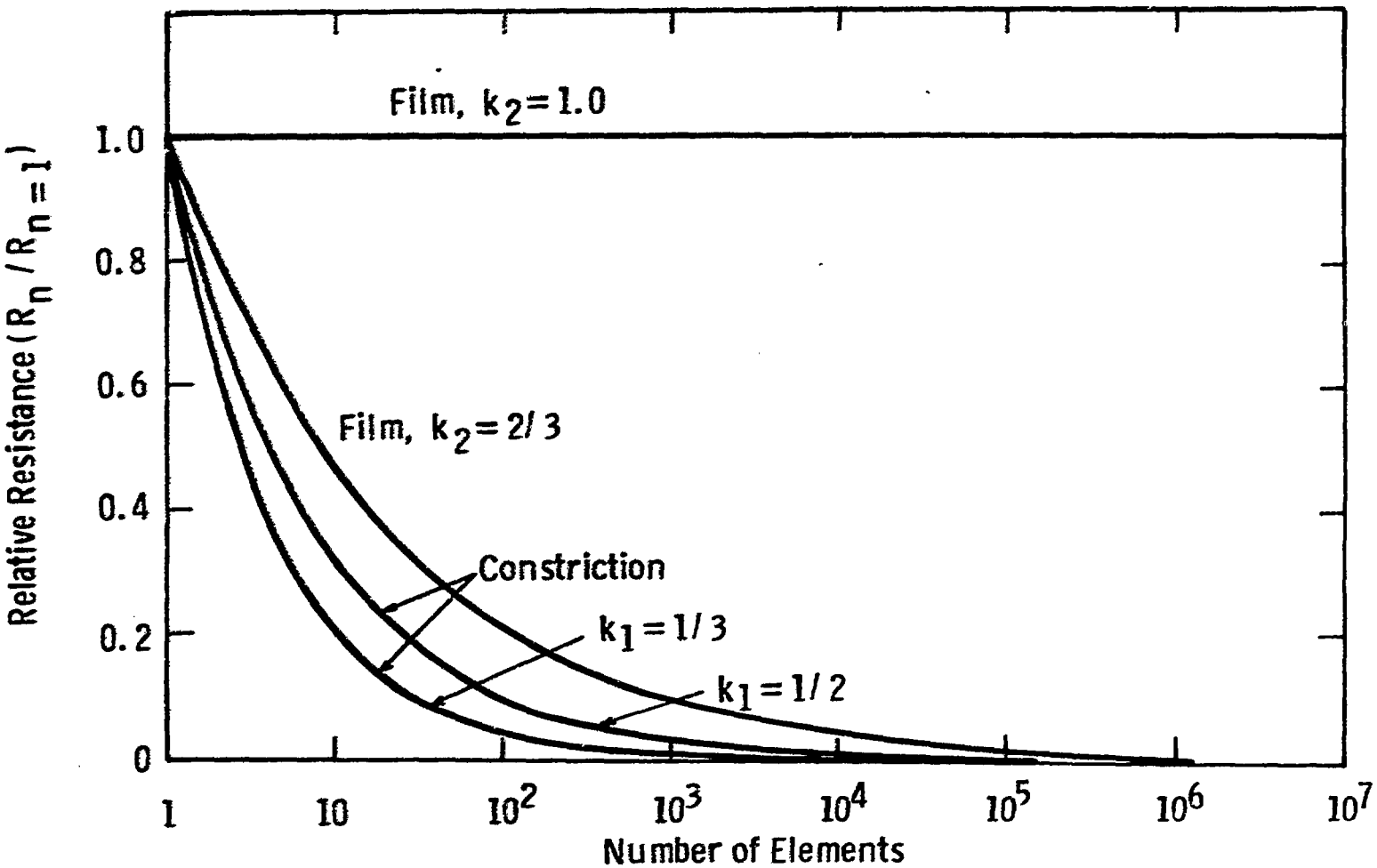

Fig. 3.3—Theoretical effect of brush subdivision on contact resistance (constant total force)

Curve 695859-A

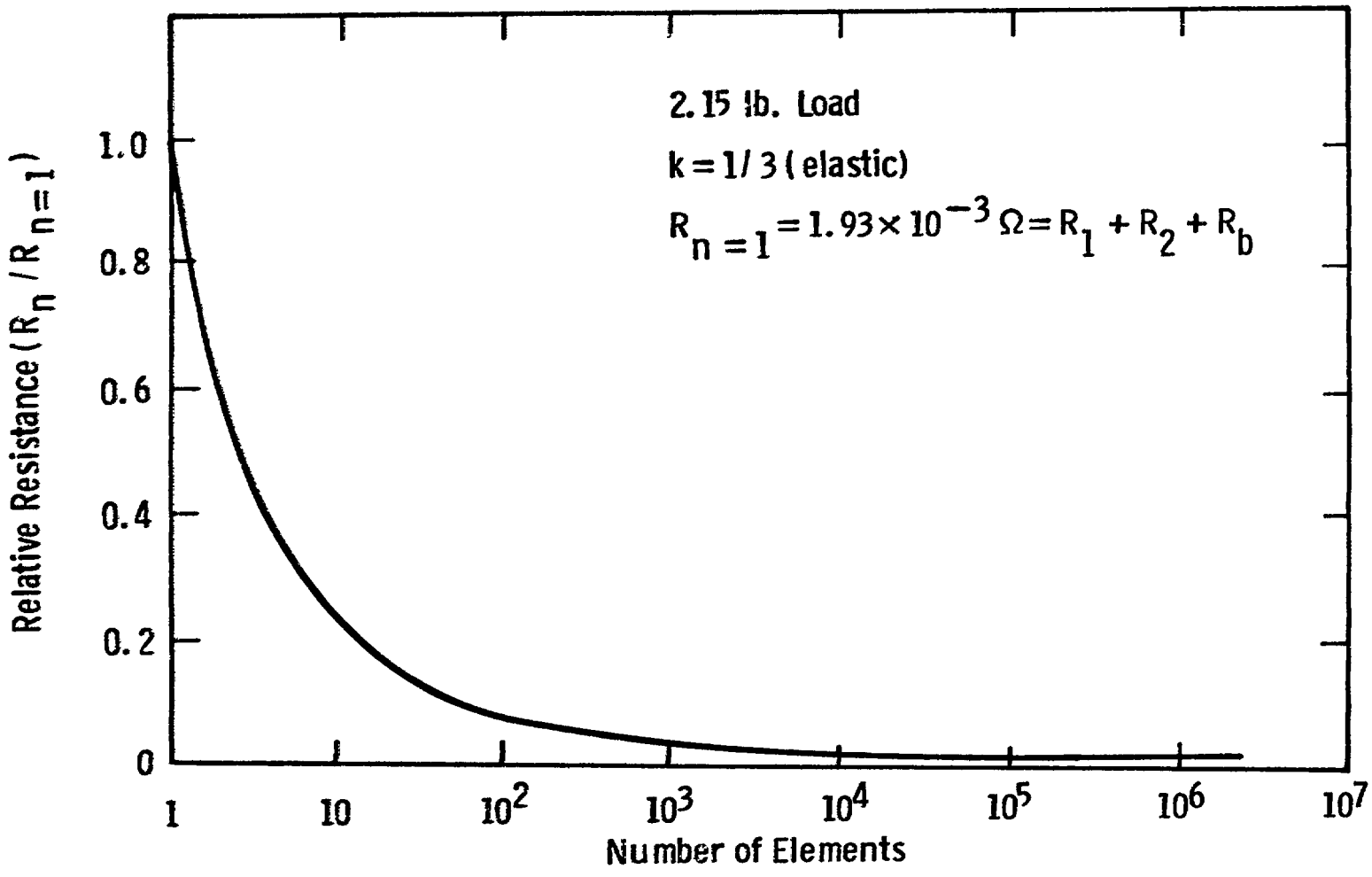

Fig. 3.4—Theoretical effect of brush subdivision on total resistance of a silver-graphite brush

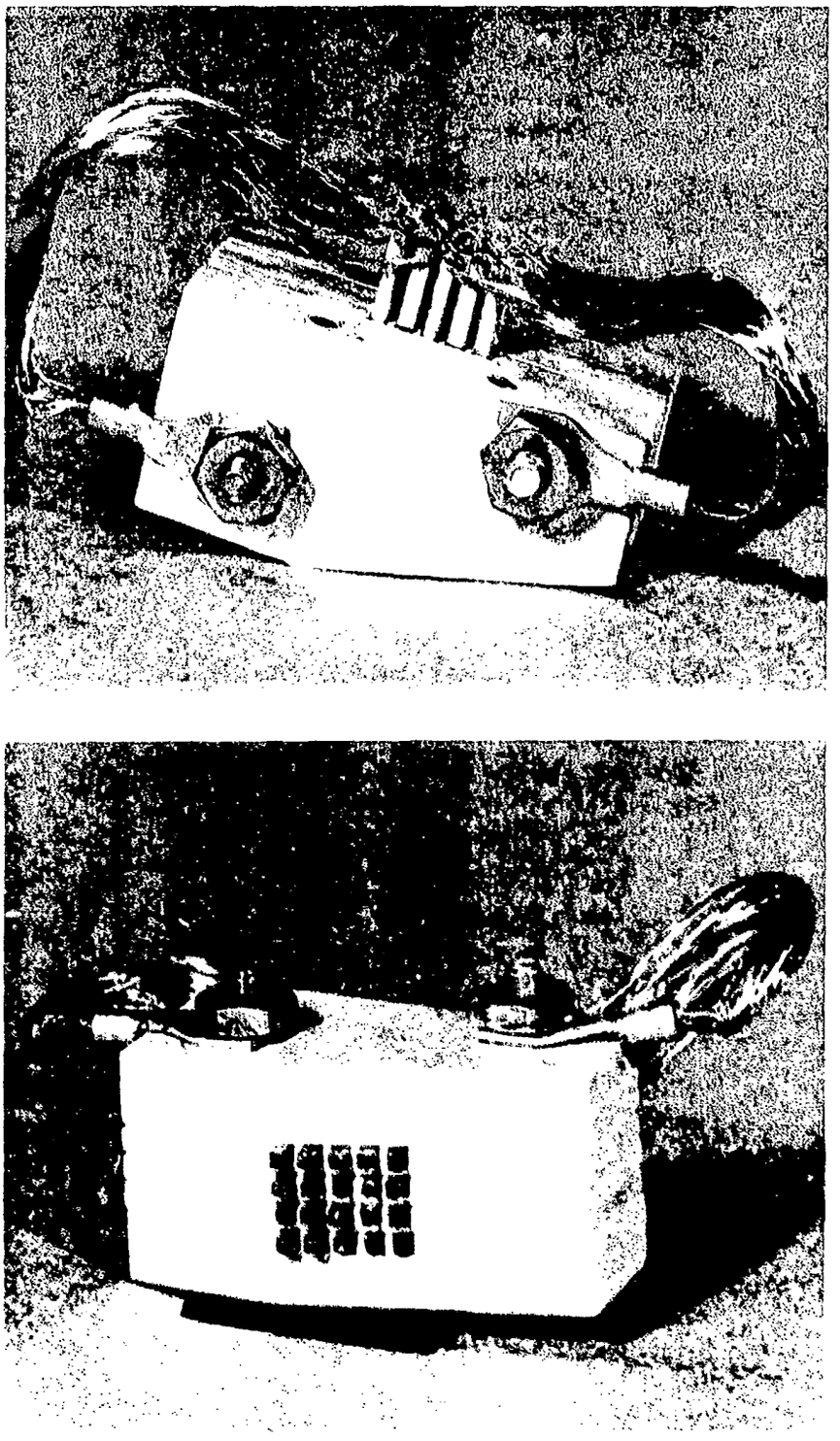

FIGURE 3.5. Segmented-brush holder and elements.

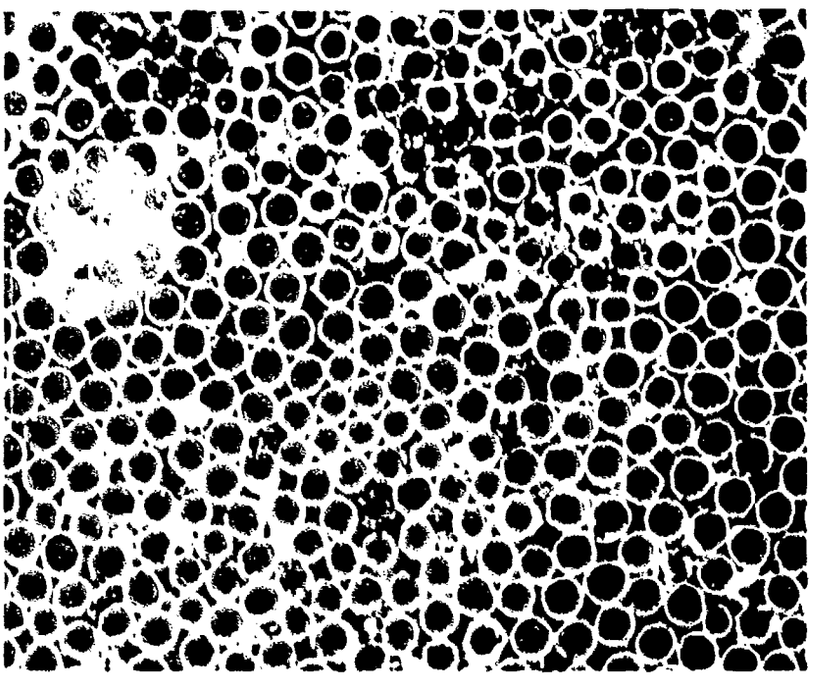

FIGURE 3.6. Fiber spacing with 70% packing factor (original photograph 500X).

REFERENCES

3.1 "Advanced Current Collection Research", Westinghouse Proposal 7M372A-2 to Defense Advanced Research Projects Agency, August 1977.

3.2 J. Schreurs, M. Burke, unpublished results obtained at Westinghouse.

3.3 L. E. Davis, Handbook of Auger Spectroscopy, Physical Electronics Industries, Edina, Minnesota.

3.4 W. T. Seng, I. Greenfeld, Report NSF/RANN/SE/GE 34872/TR 74/1, 1974.

3.5 E. Rabinowicz, private communication.

3.6 D. R. Wheeler, NASA TN D-7894, 1975.

3.7 R. Holm, "Electrical Contacts", Springer-Verlag, New York, 1967 (4th Edition).

3.8 J. F. Archard, "Contact and Rubbing of Flat Surfaces", Journal of Applied Physics, Vol. 24, No. 8, August 1953, pgs. 981-988.

3.9 J. F. Archard, "Single Contacts and Multiple Encounters", Journal of Applied Physics, Vol. 32, No. 8, August 1961, pgs. 1420-1425.

3.10 J. L. Lancaster, "Instabilities in the Frictional Behavior of Carbons and Graphites", Wear, 34, 275 (1975).

3.11 R. A. Marshall, "The Mechanism of Current Transfer on High Current Slip Ring Contacts", Wear 37, 233, 1976.

APPENDIX 3.1

HIGH CURRENT BRUSHES. III - PERFORMANCE EVALUATION FOR SINTERED SILVER GRAPHITE GRADES

I. R. McNab and J. L. Johnson

Paper to be presented at the Ninth International Conference on Electric Contact Phenomena and the Twenty-Fourth Annual Holm Conference on Electric Contacts, September 11-15, 1978, Chicago.

APPENDIX 3.1

HIGH CURRENT BRUSHES. III - PERFORMANCE EVALUATION FOR SINTERED SILVER GRAPHITE GRADES

I. R. McNab and J. L. Johnson

March 8, 1978

Paper to be presented at the Ninth International Conference on Electrical Contact Phenomena and the Twenty-Fourth Annual Holm Conference on Electrical Contacts, September 11-15, 1978.

APPROVED:

J. K. Hulm, Division Manager
Chemical Sciences

Westinghouse R&D Center
1310 Beulah Road
Pittsburgh, Pennsylvania 15235

HIGH CURRENT BRUSHES. III - PERFORMANCE EVALUATION FOR SINTERED SILVER GRAPHITE GRADES

I. R. McNab and J. L. Johnson
Westinghouse Research and Development Center
Pittsburgh, Pennsylvania 15235

ABSTRACT

In this paper, the results of varying the material composition, specifically the metal mass fraction, on the performance of silver-graphite brushes at high current densities (0.8 MA/m^2) in a carbon dioxide atmosphere, have been evaluated. Material properties which were measured included the brush density, electrical conductivity, and hardness. These properties were used in the evaluation of the brush performance when sliding on copper slip rings at a speed of 12.7 m/s. Measured parameters included the contact resistance, friction coefficient and wear rate. The results of this analysis indicate that the resistive behavior was dominated by constriction effects, with the number of contact spots apparently ranging from 2 to 15. The film contribution to the total resistance was small, the resistivity being less than 6×10^{-13} $\Omega \cdot m^2$. Friction measurements indicated a specific shear strength of 10 to 24 MN/m^2 which, if caused by an adsorbed water film would correspond to a film thickness in the range from about 2 to 4 Angstroms. Wear rates well into the microwear regime have been observed, even at the high current densities used here. However, a satisfactory explanation for the strong dependence of wear on metal content (from 0.7 mm^3/Mm to 60 mm^3/Mm) as the metal mass fraction varied from 0.4 to 0.9 has not yet been evolved.

INTRODUCTION

Earlier papers have described the results of high current density (0.8 MA/m^2) metal-graphite brush operation as a function of the brush and slip ring materials,[1] and gas atmospheres with vapor additives.[2] It was shown that the brush performance, as measured by the observed contact voltage drop, friction coefficient and wear rate, was dependent on all of these parameters. This earlier work also showed that the brush performance was markedly dependent on the proportion of metal in the brush material. In this paper, the results of a detailed study into the effects of varying the brush material composition on brush performance are given.

The primary variable in this study was the mass fraction of silver in the brush, which was varied from 0.45 to 0.90. To eliminate variations arising from other causes, all the brushes tested here were supplied by one manufacturer and most were processed in a similar way using the same raw materials. (Three samples which were processed differently, using different materials, are identified.) Details of the manufacturing processes are not available, although it is known that the brushes tested here form part of a standard range of powder-metallurgical products.

To minimize the possible introduction of uncertainties arising from test procedure variations, all the brush grades were tested, sequentially, on the same test equipment, using fixed operating procedures and measurement techniques. A controlled, non-air (carbon dioxide) environment was used, thereby eliminating variations which could have resulted from day-to-day changes in atmospheric conditions -- such as temperature, pressure, humidity, and gaseous or particulate contamination. Since a non-oxidizing gas was used, the build-up of significant oxide films on the surfaces of the brush and slip ring were also eliminated, and the influence of complex film formation and behavior (e.g., "fritting") on contact behavior was much reduced.

BRUSH MATERIAL PROPERTIES

Prior to the start of brush testing on slip rings, several brush material properties were measured, including density, hardness, and electrical resistivity. In general, the density and resistivity values were obtained without problems, using conventional techniques, and they exhibited relatively little variation from brush to brush. In contrast, the hardness measurements proved to be subject to wide variations, even on different portions of the same brush. This almost certainly arose because of the complex nature of the two-phase brush material.

Measured values of the apparent brush density (δ_{app}) as a function of the mass fraction of silver (θ_m) (manufacturer's data) are given in Figure 1. Data for the majority of brush grades, processed in the same way (A), are shown as circled points, but the data for three grades, processed differently (B), are shown as triangular points. The "A" materials data fall on a (solid) line which can be extrapolated to 9640 kg/m^3 for $\theta_m = 1.0$ and to 2010 kg/m^3 for $\theta_m = 0$. These limiting densities, which are not the same as those expected for pure graphite (practical ultimate 2200 kg/m^3) and pure silver (10,500 kg/m^3) occur because of the finite porosity of the

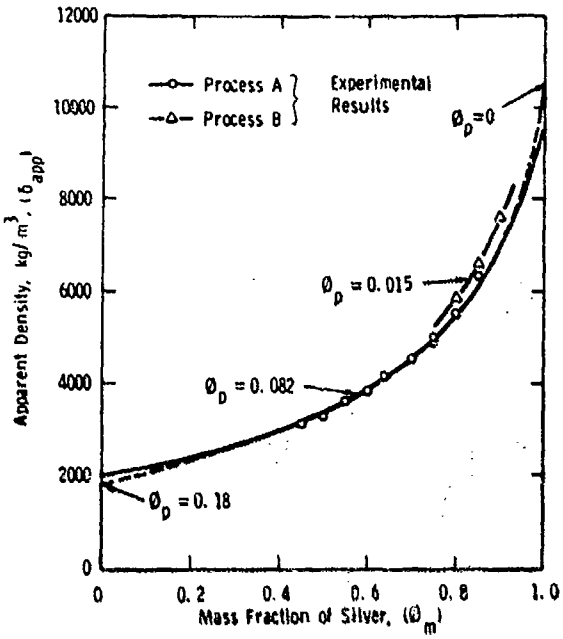

FIGURE 1. *Apparent brush density for silver-graphite brushes, with fractional porosity ($\emptyset p$) as indicated.*

processed brush materials. Based on the manufacturer's data for the mass fraction of silver, the measured apparent brush density (δ_{app}) and the known density of bulk silver (δ_{Ag}), the volume fraction of silver ($\emptyset_v$) can be obtained from Equation (1):

$$\emptyset_v = \frac{\delta_{app}}{\delta_{Ag}} \cdot \emptyset_m \qquad (1)$$

Similarly, the volume fraction of pores ($\emptyset_p$) can be derived from Equation (2), where δ_{Gr} is the ultimate density of graphite:

$$\emptyset_p = 1 - \frac{\delta_{app}\,\emptyset_m}{\delta_{Ag}} - (1 - \emptyset_w)\,\frac{\delta_{app}}{\delta_{Gr}} \qquad (2)$$

Derived values of $\emptyset_p$ for the "A" processed materials fall in a narrow range with a mean and standard deviation of 0.082 ± 0.010, confirming the common processing. Values of $\emptyset_p$ for the "B" processed materials were much lower: 0.015 ± 0.005, confirming the higher density values shown on Figure 1. The solid line passing through the circled points on Figure 1 is for the constant porosity value of $\emptyset_p = 0.082$ for the "A" materials. In practice, it is likely that the porosity will vary with the mass fraction of silver and the dashed extrapolation of the central portion of the curve in Figure 1 illustrates the authors' best estimate of the extremum values.

Although it would be expected, as shown in Figure 1, that the apparent brush density is a function of the mass fraction of silver, it is not physically likely that the same will be true for the brush electrical resistivity, or conductivity. Indeed the electrical conductivity is likely to be dependent on the volume fraction of metal, and (although undetermined here) geometrical factors relating to the size, shape, and degree of interconnection of the silver constituent.[3] Figure 2 shows the measured (at 20°C) brush

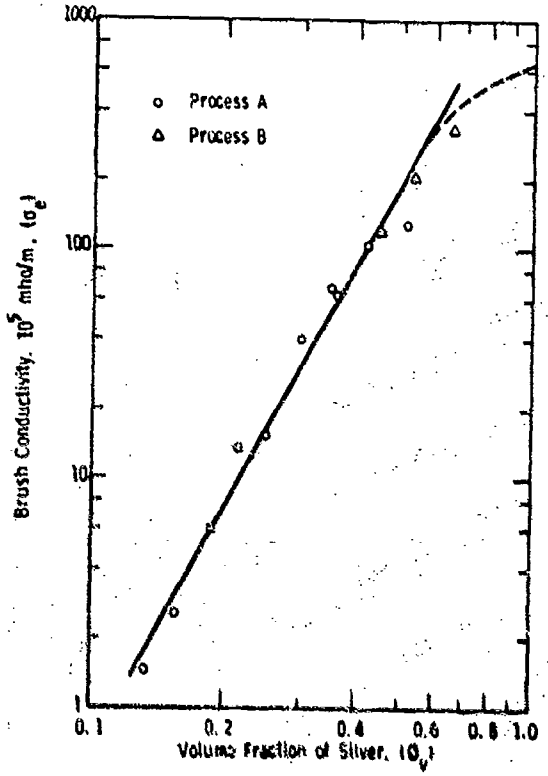

FIGURE 2. *Electrical conductivity for silver-graphite brushes (20°C).*

electrical conductivity (σ_e) plotted on a logarithmic scale as a function of the volume fraction of silver ($\emptyset_v$). It is apparent that to a very good approximation, for the range of materials evaluated here, the electrical conductivity (Mmho/m) can be represented as a power function of the volume fraction of silver, of the form:

$$\sigma_e = 224\,\emptyset_v^{3.56} \qquad (3)$$

where the value of the constants in Equation (3) are obtained from a least squares linear regression fit to the observed data shown in Figure 2. At present, a theoretical basis to explain this parametric variation is not available, so far as the authors are aware.

At high volume fractions of silver, the linear relationship shown on Figure 2 must break down, probably following a variation close to that

shown by the dashed portion of the curve.

Following the recommendations of Holm, Holm and Shobert,[4] attempts were made to ascertain the brush contact hardness for use in subsequent evaluations of the brush performance. Because of the complex behavior of graphite, (as discussed, for example, by Clark, Connelly and Hirst)[5] which, even in the absence of a metal constituent, is known to be a brittle but elastic material, this evaluation is not simple. Thus, behavior which is neither totally elastic, nor totally plastic, is to be expected, with the apparent hardness being a non-linear function of the applied force. For the present purposes, an estimate was made of the indentation hardness for each of the materials by making standard Rockwell measurements (on the 15W scale with a 3.175 mm dia indenter). Even for a single brush material, relatively wide variations in hardness were observed and Figure 3 shows that

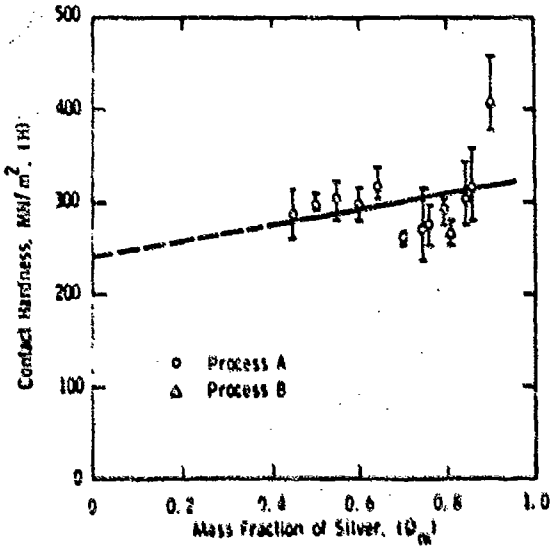

FIGURE 3. Indentation hardness for silver-graphite brushes.

the resulting contact hardness values showed a considerable spread, with a relatively slight overall dependence on the metal content of the brush. The solid line shown in Figure 3 represents the least squares linear regression fit to the measured data.

BRUSH SLIP RING TEST APPARATUS AND CONDITIONS

The brush testing reported here utilized the apparatus described in an earlier paper, and shown in Figure 1 of Reference 1. The major relevant test conditions are summarized in Table 1.

BRUSH TEST RESULTS

Experimentally determined values of the brush slip ring contact resistance, friction and brush wear are shown in Figures 4 to 6. The individual points represent actual measured values with the solid curves being the best fit to the experimental points. In all cases, a significant dependence of the measured properties on the mass, or volume, fraction of silver was observed. In the case of the contact resistance, a rapid, monotonic decrease with increasing fraction of silver was observed, as shown in Figure 4, with measured values ranging from 5000 μΩ to 26 μΩ (that is, by a factor of about 200) as the metal content of the brush increased from ϕ_m = 0.45 to 0.90. It is likely, as discussed below, that this strong dependence is closely related to the electrical conductivity of the brush material, which had a similarly strong dependence on metal content.

TABLE 1. TEST CONDITIONS

Slip Ring Speed	:	12.7 m/s (8.3 x 10^{-2}m, dia)
Slip Ring Material	:	Copper (silver bearing)
Slip Ring Surface	:	Helical Groove
Brush Face Area	:	10^{-4} m^2
Brush Angle	:	15° trailing
Brush Force	:	8.3 N
Brush Current	:	78A dc
Gas Atmosphere	:	Carbon Dioxide
Humidity Dew Point	:	20C
Number of Brushes	:	One Positive; One Negative (common track operation)

Over the same range of materials, the measured friction coefficient, shown in Figure 5, varied much more slowly -- rising approximately linearly from 0.09 to 0.28, that is, by a range of about three.

The measured wear behavior of the tested brush materials is shown on Figure 6. Although relatively little experimental data is available, there is some evidence for two distinct wear regimes, as illustrated by the two lines having different slopes, with the division between the two occurring at a mass fraction of silver of about 0.65. Below this value, the wear rate was of the order of 1 mm^3 per 10^6 m of slip ring travel (ranging from 0.7 to 1.3 mm^3/Nm), an extremely low wear rate. Above this value of ϕ_m, the wear rate increased much more rapidly -- from 1 mm^3/Nm to 70 mm^3/Nm as ϕ_m increased from 0.65 to 0.90.

BRUSH PERFORMANCE EVALUATION

The observed brush performance was evaluated with a view to gaining an improved insight into the mechanisms of current transfer, friction, and wear for high current contact systems. The ultimate objective is the development of improved contact materials and brush systems through a better understanding of the critical aspects of brush performance. One of the most important aspects of an evaluation of this type is that it should provide a consistent explanation for all of the observed aspects of brush performance, although this may not prove simple, and is relatively rarely found in the literature.

During the present evaluation, it has been found difficult to provide a complete explanation of brush behavior; further measurements of brush properties, brush performance, and microinterface structure are required before an unequivocal description can be obtained. The procedure followed here has been to derive an explanation of brush performance in which the number of assumptions has been kept to a minimum.

It has been assumed, subject to further measurements, that since the specific depth* of the indenter was not less than 0.03 during the hardness measurements, the observed values of hardness corresponded to the indentation hardness. According to Shobert,[6] in sliding contacts the true area of mechanical contact (A_t) can be estimated by the use of the expression:

$$A_t = F/\xi H \qquad (4)$$

where ξ relates the average pressure at the beginning of plastic deformation to the indentation hardness and is usually about 1/3. For the present experiments, the applied brush force, F, was 8.3N.

Contact Resistance

The total brush resistance (R_T) is composed of two terms: the constriction resistance (R_c) and the film resistance (R_f). The usual expressions (see Holm[7] and Shobert[6]) are:

$$R_T = \frac{0.4\,(\rho_b + \rho_s)}{(nA_t)^{1/2}} + \frac{\rho_f}{A_t} \qquad (5)$$

where ρ_b and ρ_s are the brush and slip ring electrical resistivities, n is the number of contact spots, ρ_f is the film resistivity, and a contact spot ellipticity of three has been assumed. In the evaluation of the constriction resistance in Equation (5), it has been assumed that the contact spots are sufficiently far separated that interaction effects may be neglected; Greenwood[8] discusses the case where this correction has to be included.

Based upon the values of A_t from Equation (4), the measured values of ρ_b and ρ_s (corrected for temperature effects) and the measured values of brush resistance as a function of metal content, the following comments may be made. At low metal contents, where the film resistance under the experimental conditions employed here is probably negligible, the brush resistance decreases less slowly with increasing metal content than would be expected from the brush resistivity data. In addition, at high metal contents, the measured resistance falls logarithmically to relatively low values. If the film resistance had made a significant contribution to the total brush resistance, this would not have occurred.

The only simple consistent explanations we can derive for these observations are that:

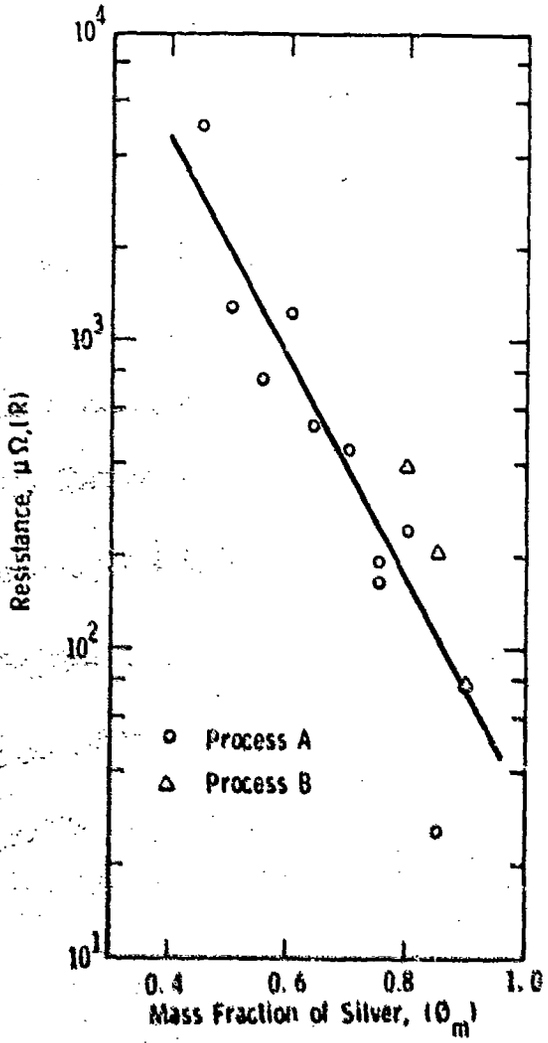

FIGURE 3. Electrical contact resistance of silver-graphite brushes in humidified carbon dioxide.

1. The film resistance is negligible at high metal fractions, with the film resistivity being less than about 6×10^{-13} ohm-m^2. The film resistance is probably also small at low metal fractions, although the present measurements do not allow this to be determined.

2. The number of contact spots decreases monotonically with increasing metal content, ranging from about 13 at $\phi_m = 0.4$ to about 2 at $\phi_m = 0.9$. Since the brush hardness does not vary strongly over this range of metal content, this result apparently indicates that the number of contact spots is dependent on the composition of the brush material, being larger for graphitic material and progressively smaller for an increasing metal content.

*Specific depth = depth of penetration ÷ radius of indenter.

Friction

The observed friction coefficient data has been evaluated using three alternative, though not necessarily mutually exclusive, approaches.

First, a "law of mixtures" type of rule has been employed in an attempt to explain the observed variation of μ with metal content. Since ϕ_v is the volume fraction of silver, the area fraction of silver (subject to geometrical and/or surface effects) should be proportional to $\phi_v^{2/3}$ with the area fraction of graphite being proportional to $(1 - \phi_v^{2/3})$. If the friction coefficients for graphite and silver are μ_{Gr} and μ_{Ag}, respectively, the overall friction coefficient should then be:

$$\mu = \phi_v^{2/3} \mu_{Ag} + (1 - \phi_v^{2/3}) \mu_{Gr} \qquad (6)$$

Using $\mu_{Ag} = 0.3$ and $\mu_{Gr} = 0.07$, the variation given by Equation (6) is, as shown on Figure 5, in good agreement with the observed data.

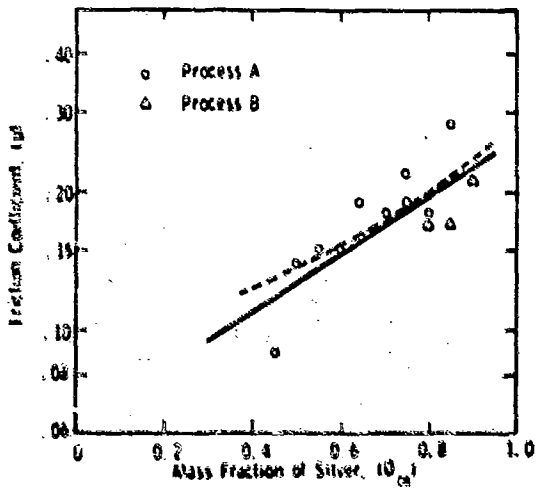

FIGURE 5. Friction coefficient of silver-graphite brush-copper ring combinations in humidified carbon dioxide. Solid: experimental; Dashed: calculated.

A second approach is to use the observed friction coefficients, and measured brush hardness values, to define a film shearing strength (τ) which is given by[4]

$$\tau = \mu H \qquad (7)$$

Based on the measured values of μ and H, we find τ to be a monotonically increasing function of ϕ_m, in the range from 10 to 24 MN/m^2 as ϕ_m increases from 0.4 to 0.9. These values of τ are close to those quoted by Shobert for boundary lubrication (10 to 20 MN/m^2) and appreciably lower than the values which apply when metal-to-metal friction occurs. For the latter case, $\tau = H/2$, giving $\tau = 130$ MN/m^2. The derived values of τ are also significantly higher than the 1 to 5 MN/m^2 which corresponds to the inherent shearing of graphite platelets and is the result of van der Walls forces.

Based on the possibility that there may be adsorption of water vapor on the brush and slip ring surfaces, as suggested by Shobert and used by Pardee,[9] the friction coefficient may be related to the shearing of a pseudo-hydrodynamic fluid film through the expression:

$$\mu = \frac{\eta A_t v}{Fh} \qquad (8)$$

where η is the fluid viscosity, v is the peripheral velocity, h is the film thickness, and the other symbols have their previous definitions. Using A_t from Equation (4) in conjunction with Equation (8) has permitted the ratio (η/h) to be evaluated. On the assumption that monomolecular adsorbed water films have viscosities which are similar to those of liquid water, the film thickness may then be found. Using $\eta = 3.6 \times 10^{-4}$ N·s/m^2 (for water at 80°C) we find that h decreases monotonically with increasing metal content of the brush from about 4.2×10^{-10} m at $\phi_m = 0.4$ to about 1.8×10^{-10} m at $\phi_m = 0.9$. At $\phi_m = 0.7$, $h = 2.5 \times 10^{-10}$ m, corresponding to (an average) separation of the brush and slip ring surfaces by a single monomolecular film of adsorbed water. According to the theories of quantum tunneling through thin films, film thicknesses of this order would yield film resistivities of 2×10^{-13} ohm·m^2 and less for a surface work function of 4 electron volts (see Shobert[6]). This is in good agreement with the conclusions reached here as a result of the analysis of the resistance measurements. It seems plausible to assume, although with no direct supportive evidence at present, that the decrease in film thickness with increasing metal content is related to the decrease in the amount of surface graphite available for adsorption.

Contact Wear

Although subject to some discussion, it is probable, in non-oxidizing atmospheres and after "bedding-in" of the brushes has been achieved, that adhesive wear is the predominant wear mechanism. For this case, Archard[10] has suggested that the volume wear (w) may be related to the true area of contact and the sliding distance (s) by the expression:

$$w = \text{constant} \times A_t s \qquad (9)$$

Defining a new constant, $\underline{z} = 2 \times 10^5 \times$ the constant in Equation (9), Holm gives this equation as

$$\frac{w}{s} = (5 \times 10^{-6} z) \frac{F}{H} \qquad (10)$$

Values of $z < 2$ are generally defined as mildwear. For the values of (w/s) given in Figure 6 and the hardness values measured for the brushes investigated here, we find average z values ranging from 0.001 at $\phi_m = 0.4$ to 0.13 at $\phi_m = 0.9$. That is, all values were well in the mildwear regime, with

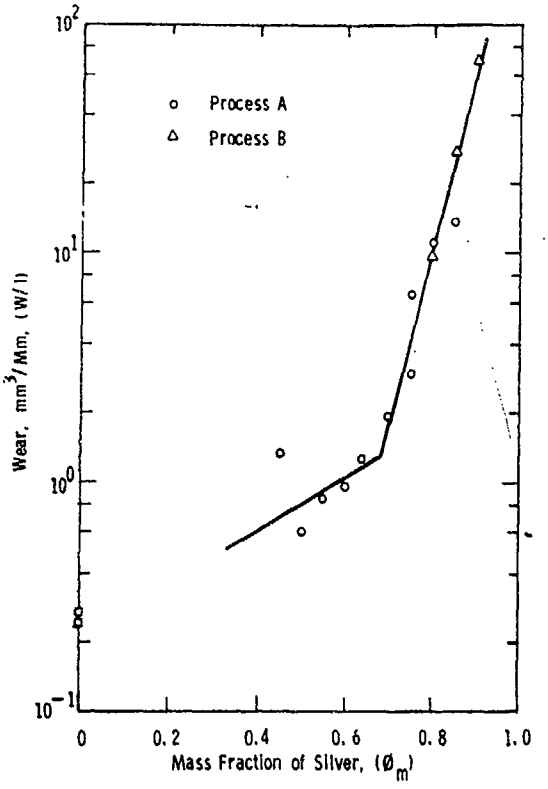

FIGURE 6. *Wear performance of silver-graphite brushes in humidified carbon dioxide.*

the lower values being in agreement with data quoted by Holm.[7]

It should be noted that, in contrast to the prediction of Archard's equation, the brush wear rate increased with increasing hardness. However, in agreement with the work of Rabinowicz,[11] on various metal-metal combinations, we find that, on average, increased friction coefficients are associated with increased wear rates.

Archard's Equation (9) was derived on the assumption that wear was proportional to the meeting of asperities on the two contact surfaces. On this basis, one may expect the wear rate to be strongly dependent on the thickness of the adsorbed film -- perhaps exponentially for a Gaussian distribution of asperity heights. Note that the wear rate in Figure 6 increased more rapidly at a brush metal content ($\emptyset_m$ = 0.7) for which the film thickness became less than a monomolecular layer.

DISCUSSION AND CONCLUSIONS

In the previous section, we have attempted to obtain a consistent explanation of the brush performance observed with a range of silver-graphite brushes. The major conclusions that were reached are as follows:

1. The brush contact resistance was dominated by constriction effects with the number of contact spots ranging from 15 at $\emptyset_m$ = 0.4 to 2 at $\emptyset_m$ = 0.9.
2. The film resistance was negligible, with the film resistivity at high metal contents being less than 6 x 10^{-13} Ω·m².
3. Measured friction coefficients appeared to be consistent with a model in which a "law of mixtures" might apply.
4. Derived values of the specific shear strength (ψ) fell in the range noted by Shobert as being applicable for boundary lubrication. ψ was significantly higher (up to 10 times) than the value for shearing of graphite platelets, and significantly lower (1/15 to 1/6) than the value for metal-to-metal friction.
5. Based on an assumed viscosity for water, a film thickness in the range 4.5 to 2.0 x 10^{-10} m has been derived. This value is in agreement with the value derived from film resistance considerations.
6. All measured values of the wear rate (w/ℓ) fell into the microwear regime, although a large (100 to 1) increase in wear rate was observed as the metal content $\emptyset_m$ changed from 0.4 to 0.9.
7. In contrast with the predictions of Archard's equation, the observed wear rate increased with increasing brush material hardness, although this was in agreement with Rabinowicz's measurements of friction and wear with various metal combinations.
8. At present, a clear explanation for the rapid increase in wear rate with metal content is not available, although it may be related to the adsorbed film at the interface.

In general, it appears that a relatively good explanation of observed behavior has been achieved for the electrical resistance and friction behavior, but that an explanation for the wear behavior is lacking, at present. The finding that the thickness of an adsorbed water film decreases with increasing metal content appears to be reasonable, since it is likely that adsorption will be preferentially onto edge sites on graphite crystallites. Perhaps the most inexplicable feature at present is the rapid decrease in the number of contact spots with increasing metal content. In general, because of the improved thermal conductivity of brushes with a high metal content, we would have expected thermal mounding to be less severe as the metal content of the brush increased.[12,13] Similarly, an increased wear rate presumably gives rise to increased production of wear debris which, having characteristic dimensions greater than the film thickness we have assumed here, should have a pronounced effect on the current transfer mechanism. However, for an assumed typical debris particle having dimensions

of 0.1 mm x 0.1 mm x 2 x 10^{-5} mm (volume = 2 x 10^{-7} mm^3), the observed wear rate (w/ℓ) of about 1 mm^3/Mm corresponds to the production of one wear particle only once per slip ring revolution. Thus, the wear process is a relatively rare event and, on the average under the conditions of these experiments, has a relatively minor effect on the conduction process.

ACKNOWLEDGMENTS

The work reported here was performed under Advanced Research Projects Agency Contract N00014-76-C-0683 and monitored by the Office of Naval Research.

REFERENCES

1. J. L. Johnson and L. E. Moberly, "High Current Brushes. I - Effect of Brush and Ring Materials", 23rd Holm Conference on Electric Contacts, Chicago, November 1-3, 1977.
2. P. K. Lee and J. L. Johnson, "High Current Brushes. II - Effects of Gases and Hydrocarbon Vapors", 23rd Holm Conference on Electric Contacts, Chicago, November 1-3, 1977.
3. R. N. Beech and M. S. T. Price, "Copper-Graphite Materials", Industrial Carbon and Graphite, Soc. Chem. Ind., London 1958, p. 448-462.
4. E. Holm, R. Holm, and E. I. Shobert, II, "Theory of Hardness and Measurements Applicable to Contact Problems", J. App. Phys. 20, 319, 1949.
5. W. T. Clark, A. Connelly, and W. Hirst, "The Friction and Wear of Electrographite", Brit. J. Appl. Phys. 14, 20, 1963.
6. E. I. Shobert, II, "Carbon Brushes -- The Physics and Chemistry of Sliding Contacts", Chemical Publishing Co., New York, 1965.
7. R. Holm, "Electric Contacts", Springer-Verlag, New York, 1967.
8. J. A. Greenwood, "Constriction Resistance and the Real Area of Contact", Brit. J. App. Phys. 17, 1621, 1966.
9. R. P. Pardee, "Moisture Dependence of Silver-Graphite Brushes in Air, Nitrogen, Helium, and Carbon Dioxide", IEEE Trans. PAS. 86, 616, 1967.
10. J. F. Archard, "Single Contacts and Multiple Encounters", J. App. Phys. 32, 1420, 1961.
11. E. Rabinowicz, Private Communication, 1977.
12. R. A. Marshall, "The Mechanism of Current Transfer in High Current Slipring Contacts", Wear 37, 233, 1976.
13. R. A. Burton, "Thermoelastic Effects in Sliding Contacts", Collected Papers, Vol. I, Northwestern University, 1976.

APPENDIX 3.2

HIGH CURRENT BRUSH MATERIAL DEVELOPMENT
I. SINTERED METAL-COATED GRAPHITE

P. K. Lee

Paper to be submitted to Twenty-Fifth Annual Holm Conference on Electrical Contacts, 1979.

APPENDIX 3.2

HIGH CURRENT BRUSH MATERIAL DEVELOPMENT
I. SINTERED METAL-COATED GRAPHITE

P. K. Lee
Electrotechnology Department

Westinghouse Research and Development Center
Pittsburgh, PA 15235

ABSTRACT

The technique for coating graphite powders with copper or silver by chemical plating and the preparation of the sintered metal-coated graphite composites are described. A process has been developed for coating graphite powders of sizes down to 38 μm. Metal contents ranging from 20 to 97 percent, by weight of the final product, have been achieved by simple and multiple platings. Metallographs of the sintered products reveal the ideal structure of a continuous, three-dimensional metal lattice throughout the composite. The electrical resistivities of the sintered products were measured and are compared with metal-graphite brush materials fabricated by conventional powder metallurgy and metal infiltration techniques. As expected, at the same metal contents, the sintered metal-coated graphite composite always exhibit much lower electrical resistivities than the conventional materials. The difference in electrical resistivity is attributed to the metal structure of the metal-graphite systems.

INTRODUCTION

Conventional monolithic solid brushes for electrical power transfer in sliding contacts are made of graphite, carbon-graphite, or metal-graphite composites. Graphite has unique antifriction properties but also has its deficiencies including brittleness and low strength. The incorporation of metal (copper or silver) in solid brushes tends to correct such deficiencies and also provides high current-carrying capacity and low contact voltage drop and resistance. Solid brushes for certain advanced electrical power sliding contact systems are required to operate under conditions of extremely high current density (155 A/cm^2) and high peripheral speed (70 m/s).[1] Such brushes must efficiently provide excellent electrical and thermal conduction paths in the contact system and exhibit reliably long life. The monolithic-type metal-graphite brush is an obvious initial choice candidate for such systems. However, to meet the practical requirements of low electrical resistance and low friction drag, efficient utilization of the brush conducting and lubricating constituents in the metal-graphite brush structure is necessary.

It has been noted that,[2] to obtain maximum electrical conductivity in a metal-graphite material, the metal constituent must be united to form a continuous three-dimensional lattice, holding within itself "islands" of graphite. Matrices of unconnected metal must be avoided. At a low metal content such a structure can only be produced when the metal is in the form of thin continuous films over the surface of the graphite particles. Two main techniques are known for making conventional metal-graphite brushes. The powder metallurgy technique[2,3] involves the solid-state sintering of

premolded mixtures of metal powder and graphite powder or hot pressing of the powder mixtures. The metal infiltration technique,[4-6] which is now widely used for making composites consisting of a low melting metal and a refractory metal or material, involves pressure infiltration of molten metal into the open pore volume of a graphite or carbon-graphite skeletal structure. However, neither technique will provide the most efficient usage of the metal constituent. A uniform mixture of metal and graphite powders through mechanical mixing is difficult to obtain, because of the great difference in densities of the components. Also, during mixing, graphite powder is smeared over the metal particle surfaces, reducing the chance for direct metal-to-metal contacts upon subsequent pressing and sintering. By infiltration technique, since the thermal expansion coefficients of metal and graphite may differ by a factor of three or more, the metal filaments in graphite skeletal structure may not be continuous when cold. Metallographs of conventional metal-graphite brushes manufactured by these two techniques revealed such metal discontinuities.

Recent studies of copper-graphite composites[7-9] indicated that new materials produced by powder metallurgy techniques from mixtures of copper powder and copper-coated graphite powder, showed significant improvements in electrical resistivity, antifriction, and antiwear properties when compared to the ordinary products made from conventional mixtures of copper and graphite powders. Copper coating of the graphite particles, up to an extent of 50 percent by weight, was reported to be obtained by an electrolytic plating technique.[7] Further improvement in coating techniques were achieved by a combination of chemical plus

electrolytic plating.[10] A high plating efficiency was obtained in these experiments only with relatively large graphite particles, in the range of 100-160 μm. While such large particles may be useful for making self-lubricating bearings or seals, they are much larger than the graphite grain sizes generally used in practical brushes. Again, mixtures of copper powder and copper-coated graphite powder cannot be uniform due to the wide density differences. In addition, the flake-like graphite particles cannot be evenly plated by electrolytic deposition because agglomeration is generally unavoidable.

To achieve the efficient usage of the metal conducting constituent in brush material structures, sintering of powders composed only of metal-coated graphite particles has been the approach followed here. High metal content has been obtained by multiple chemical plating. Problems of complete metal coverage over the finer graphite powders have been solved by thoroughly cleaning the graphite surfaces and by variation of plating conditions, based on available kinetic information[11-15] on electroless copper deposition. In addition, known techniques for silver plating[16] powdered materials have been modified for preparation of silver-graphite brush materials.

The techniques for coating graphite particles down to 38 μm sizes with copper and with silver, and the preparation of the sintered metal-coated graphite composites are described in this paper. The metallographic structures of such composites are also described, and

their electrical resistivities are compared with metal-graphite brush materials fabricated by conventional powder metallurgy and metal infiltration techniques.

EXPERIMENTAL

Materials and Preparation

Graphite Powders -- Two grades of graphite powders, natural graphite and electrographite, were used in the experiments. For coating practice, powders were screened into the following fractions of different particle sizes (in microns): 150-180, 75-150, 38-75, 38-45, and <45.

Plating Solutions -- Solutions were made with reagent grade chemicals and deionized water. The silver-plating solution was cautiously prepared just prior the plating experiment, based on the amount of silver nitrate required for that experiment. For example, 100 ml of triethanolamine was dissolved in 100 ml of water and the solution was cooled to 6 to 7°C. At this temperature, 34g of silver nitrate was gradually added in portions of 5 to 6g to the solution with constant stirring. The temperature of the solution was kept below 10°C. The solution was filtered through a dense filter paper by mild suction before use.

Apparatus and Procedure

Chemical Plating -- The chemical plating system consisted of an all glass container and stirring device. The glass container (beaker) was placed in a water bath for temperature adjustment and control. Plating

experiments were performed under an exhaust hood. Before metal plating, the graphite powder surfaces were sensitized and the powder sample was mildly rinsed with water. A calculated amount of plating solution was measured into the plating container and its temperature and concentration adjusted; chemical reduction was then effected by the action of formaldehyde solution. The reducing agent was added to the solution immediately before or after the graphite powder was dispersed into it. Vigorous stirring (mixing) was continued until the end of plating when the evolution of tiny hydrogen bubbles ceased or the copper solution became colorless. The metal-coated powder was washed with water by decantation, and then filtered, washed, and finally dried by washing with acetone.

In multiple plating, the coated graphite obtained by decantation from the first plating operation, was dispersed into a second plating container with a new batch of plating solution and the plating operation repeated. As the coated powder became heavier, an amber bottle with a wide mouth was used as the plating container. The bottle was carefully capped and vigorous mixing of the contents was obtained by plating the bottle on an ordinary ball-mill roller.

Electrolytic Plating -- Graphite powders were also coated with copper by electrolytic plating for comparative studies. These experiments

were carried out in a tilted rotating cylindrical plastic container. A shallow copper disc fitted to the inside bottom of the container, served as the cathode. Another copper disc was added to the outside bottom and attached to the cathode through the center for current passage. The outside copper disc was also anchored to the shaft of a motor for rotation. The anode plate (copper or platinum) was suspended from the top of the container into the electrolyte or plating bath. The tilting angle and the rotating speed were adjusted to ensure sufficient agitation in the powder sitting in the container. Electrolytic copper plating was performed at room temperature.

Fabrication of the Metal-Coated Graphite Materials

Fabrication of metal-graphite materials from the metal-coated graphite powders includes two major steps: molding in a hydraulic press and sintering under a hydrogen atmosphere. Before molding, the powders were dried in a furnace for one hour under a stream of hydrogen gas to drive any moisture out of the powder and to reduce the surface oxides on the copper-coated powder. The dried powders were wetted with hydrocarbons (petroleum ether, for example) and mixed in a capped bottle on a laboratory mixing roller for at least one hour. Samples were then charged into rectangular dies and molded under pressure into cubes of 1.7 cm side length. The molded blocks were finally sintered for one hour in a hydrogen atmosphere. The molding pressures, as well as the sintering temperatures for different metal-coated powders were determined from a series of separate experiments in order to optimize the electrical resistivity and the microstructure of the resulting materials.

Evaluation of the Sintered Materials

The microstructures of the sintered metal-coated graphites were examined metallographically. The electrical resistivity of the sintered cubes or bars was measured along the directions parallel and perpendicular to the molding pressure as an evaluation of the efficiency of utilization of the metal conducting constituent in the material structure.

RESULTS AND DISCUSSION

Chemical Metal-Plating of Graphite Powders

A series of experiments were made on chemical plating of graphite powders of various particle sizes, from 180 μm down to 38 μm, with copper and with silver. Efforts were mainly made to obtain a complete metal coverage of the powder (as observed under optical microscope), by controlling the chemical plating conditions. Typical results are summarized in Table I.

It was found that successful plating (complete metal coverage and high plating efficiency) of graphite powders by the chemical plating technique depended upon two main factors: cleanliness of the powder surfaces and particle size of the powder. Pretreatment of the graphite powders by heating in a furnace under hydrogen atmosphere was found to be very beneficial to improve the metal coverage during plating. The surface impurities and any organic or grease contaminations from the original graphite processes are believed to be removed by such heat treatment.

TABLE I

TYPICAL RESULTS OF CHEMICAL PLATING OF GRAPHITE POWDERS

Run No.	Graphite Particle Size μm	Metal Content In Final Product %
	Copper Plating	
W 2	150-180	36.6
W 15	75-150	41.5
W 22	<45 (E*)	53.0
W 29	38-45	--
	(Multiple Plating)	65.8
	Silver Plating	
W 5	150-180	22.8
W 9	75-150	34
W 18	45-75(E)	51.9
W 32A	38-45	
	(Multiple Plating)	86.0
W 32B	(Product of 32A)	
	(Multiple Plating)	97.5

*(E) indicates electrographite. Others were natural graphite.

Heat treated powders, with particle sizes within 75 to 180 μm, can be plated without difficulties. However, for powder sizes down to the 38 to 75 μm range (Run Nos. W18, 22, 29, and 32 in Table I), complete plating coverage can only be obtained by using a larger quantity of solution (50% more than for large particles) and by plating in a dilute bath at a slightly lower temperature. Since finer powders exhibit larger surfaces per unit weight and since chemical deposition of metal from solution occurs only at catalytic regions of the substrate surface, increased exposure to the sensitizer and activator in the plating process resulted in an increased coverage of the adsorbed sensitizing species and, hence, of the catalyst (generally silver or palladium in copper plating) on the graphite surfaces. The chemical plating process is autocatalytic and the metal deposition rate is proportional to the metal concentration in the plating solution as well as to the total surface area of the powders in the plating system. Rapid deposition would lead to a non-uniform plating and coverage. Apparently, the use of a more dilute plating solution and a control of the ratio of total surface area of the powders to the volume of plating solution are the key factors for complete plating coverage on fine powders. Lowering the plating temperature helps the metal deposits to grow more uniformly, however, the surface reduction would not initiate over a long period when the temperature was inadequately low.

A thick metal-coating on fine graphite powders was obtained by multiple chemical plating (W29, 32A, and 32B in Table II). With this technique, the desired percentage of metal coating on graphite powders was easily achieved by controlling the amount of plating solution in the last plating step. The growth of the metal deposits was random and three dimensional. One electron-micrograph of a typical silver-coated product (W32B, 97.5% Ag by weight, initial particle size 38-45 um) is shown in Figure 1. The heavy silver coating is porous and polycrystalline but the particles are well covered by the silver deposits.

Chemical Plus Electrolytic Metal-Platings

Several experiments were made in which graphite powders were copper plated by chemical plating and then followed by electrolytic plating. Attempts were made to obtain a thick, uniform metal coating on the graphite particles. The graphite powders were lightly coated chemically, with copper to 36 to 37% by weight. Without drying, the copper coated powders were transferred into the electrolytic bath and the plating continued electrolytically. By this technique, a more compact metal coating was obtained but the plating process was time consuming. For example, after plating a 20g sample for 1-1/2 h, the copper coatings only increased to 58.8% by weight (Run No. W1) in one experiment and to 61.7% by weight (Run No. W3) in another experiment. Several problems were encountered in electrolytic plating and were not solved. Agitation of the graphite powders in the electrolytic container bath was very ineffective because of the flake nature of the powders and because of the wide range of particle sizes of the powders. Agglomeration of the particles

on the surface layer of the powders was unavoidable when plating for a short period of time. That is, a uniform and thick metal coating could not be obtained by the electrolytic technique.

Effects of Fabrication Conditions

To optimize the fabrication conditions (molding pressure and sintering temperature), one sample of copper-coated graphite powder (W15, 41.5 w/o copper) and one sample of silver-coated powder (W9, 34 w/o silver) were separately molded and sintered into solid blocks at several different pressures and temperatures. The apparent densities and electrical resistivities of the sintered materials were measured. It was found that the apparent density of the material generally increased with the molding pressure. However, the electrical resistivity varied differently with both pressure and temperature. For all materials tested, the electrical resistivity decreased with increasing molding pressure when sintering temperature was the same. But the electrical resistivity measured in the direction perpendicular to the molding load tended to increase slightly at the highest pressure investigated. Under the high molding pressure, the metal coatings of the graphite powders could be damaged to a certain extent, resulting in exposure and comminution of some graphite particles in th interparticle contacts. As the sintering temperature increased, a volume growth in the direction of the molding load became noticeable. The electrical resistivity of the material molded at lower pressure but sintered at higher temperature was generally much higher than that molded at higher pressure and sintered at lower temperature.

Characteristics of the Sintered Metal-Coated Graphite Materials

The microstructures of the sintered metal-coated graphite materials were examined metallographically. Typical examples are shown in Figures 2 (W15, 41.5 w/o copper), 3 (W9, 34 w/o silver), and 4 (W32F, 97.5 w/o silver). Figures 2 and 3 show the structure of graphite materials having low metal contents but for which the micro-photographs clearly show a continuous, three-dimensional metal lattice throughout the bulk structure.

The electrical resistivities of the sintered metal-coated graphite materials were measured and the values plotted as a function of the metal content are shown in Figures 5 (sintered copper-coated graphite) and 6 (sintered silver-coated graphite). In these figures, the resistivities of commercial copper- and silver-graphite brushes fabricated by liquid metal infiltration and powder metallurgy techniques are also included for comparison. The overall electrical resistivity of the present materials is constantly much lower than the commercial materials and the advantage becomes progressively greater at lower metal contents. For example, the electrical resistivity for the sintered silver-coated graphite materials is 6.0 μΩ-cm at 75% silver and 44 μΩ-cm at 50% silver, compared to 18 μΩ-cm and 410 μΩ-cm, respectively, for the commercial silver-graphite brush materials. With a low metal content, the metal particles in conventional brush materials are widely spaced while in the present materials a continuous metal phase is retained. This explains the differences in electrical resistivity and also emphasizes the need for rigid control of the ultimate arrangement of the metal and graphite in brush materials.

ACKNOWLEDGMENT

The author wishes to thank Mr. R. E. Gainer, Jr., for his assistance in fabrication of the product materials and Mr. D. G. Martin for his assistance in making the resistivity measurements. This work was supported by the Advanced Research Projects Agency of the Department of Defense (Contract No. N000-14-76-C-0683) and monitored by the Office of Naval Research.

P. K. Lee

P. K. Lee
Tribology & Magnetofluidynamics

APPROVED: _____

I. R. McNab, Manager
Tribology & Magnetofluidynamics

APPROVED: _____

C. J. Mole, Manager
Electrotechnology Department

REFERENCES

1. C. J. Mole and E. Mullan, "Design Trends in Homopolar Machines Since the Mid 1960's", Seminar on Energy Storage, Compression and Switching, Canberra, Australia, November 1977.
2. R. N. Beech and M. S. T. Price, "Copper-Graphite Materials", Industrial Carbon and Graphite, Soc. Chem. Ind., London, 1958, p. 448-462.
3. M. Humenik, Jr., D. W. Hall, and R. L. Van Alsten, "Graphite-Base Cermets", Metal Progr., Vol. 81 (4), pp. 101-108, April 1962.
4. C. Scott and W. Deats, "Impregnating Carbon Electric Brushes with Molten Metal (e.g., brass) Under Pressure", U.S. Patent 1,053,880, February 18, 1913; "Electric Contact Material", U.S. Patent 1,053,881, February 18, 1913; Chem. Abstr., Vol. 7, pp. 1141, April 1913.
5. Le Carbone-Lorraine, "Improvement of Parts Intended for Sliding Electric Contacts", Belg. Pat. 446,346, Aug. 31, 1942; Chem. Abstr., Vol. 39, pp. 608, 1945.
6. P. Schwarzkopf, "Theory of the Powder Metallurgical Infiltration Process", Z. Anorg. Chem., Vol. 262, pp. 218-222, May 1950.
7. O. F. Lupanov, D. S. Yas, V. B. Podmokov, and M. S. Dyadenko, "Apparatus for Electroplating Graphite Granules with Various Metals", Legka Prom., No. 4, pp. 31-32, 1968; Chem. Abstr., Vol. 69, 112779S, 196
8. D. S. Yas, L. A. Osvetimskii, N. S. Dyadenko, A. A. Zaporozhets, and N. A. Belentsova, "Copper-Graphite Materials with Copper-Clad Graphite Granule Additions, I. Effect of Bare and Copper-Clad Graphite on the Strength Characteristics of Copper-Graphite Materials", Porosh. Met., No. 5 (101), pp. 70-75, May 1971.

9. D. S. Yas, V. I. Pavlenko, A. A. Zaporozhets, and N. S. Dyadenko, "Copper-Graphite Materials with Copper-Clad Graphite Granule Additions, II. Antifriction properties of Copper Graphite Materials with Various Amounts of Copper-Clad Graphite Granules", Porosh. Met., No. 4 (124), pp. 17-21, April 1973.

10. V. I. Pavlenko and D. S. Yas, "The Copper Plating of Graphite Powders in the Manufacture of Copper-Graphite Materials", Porosh. Met., No. 2 (158), pp. 9-13, February 1976.

11. T. F. Yudina, V. Ya Omelchenko, and L. L. Kuzmin, "Chemical Copper Plating of Powdered Materials", Izv. Vyssh. Ucheb. Zaved., Khim. Khim. Tekhnol., Vol. 13 (9), pp. 1331-1335, 1970.

12. R. Sard, "The Nucleation, Growth, and Structure of Electroless Copper Deposits", J. Electrochem. Soc., Vol. 117 (7), 864-870, July 1970.

13. J. Dumesic, J. A. Koutsky, and T. W. Chapman, "The Rate of Electroless Copper Deposition by Formaldehyde Reduction", J. Electrochem. Soc., Vol. 121 (11), pp. 1405-1412, November 1974 and related references quoted.

14. K. N. Golovnya, N. M. Dyatlova, and N. N. Balashova, "Kinetics of the Chemical Plating of Metals and Dielectrics from Solutions Based on Complexons", Elektrokhim (Soviet Electrochem), Vol. 5 (No. 6), pp. 703-705, June 1969.

15. E. I. Saranov, N. K. Bulatov, and S. G. Mokrushin, "Autocatalytic Reduction of Copper by Formaldehyde", Zash. Metal. (Protection of Metals), Vol. 4 (No. 2), pp. 161-166, March-April 1968.

16. V. Ya. Omelchenko, L. L. Kuzmin, B. M. Smelyanskii, and Yu. E. Zusman, "Chemical Method of Silvering Powdered Materials", Zh. Prik. Khim., Vol. 44 (No. 7), pp. 1491-1495, July 1971.

FIGURE 1. Electromicrograph of silver (97.5 w/o)-coated graphite particles (graphite particles, 38-45 um).

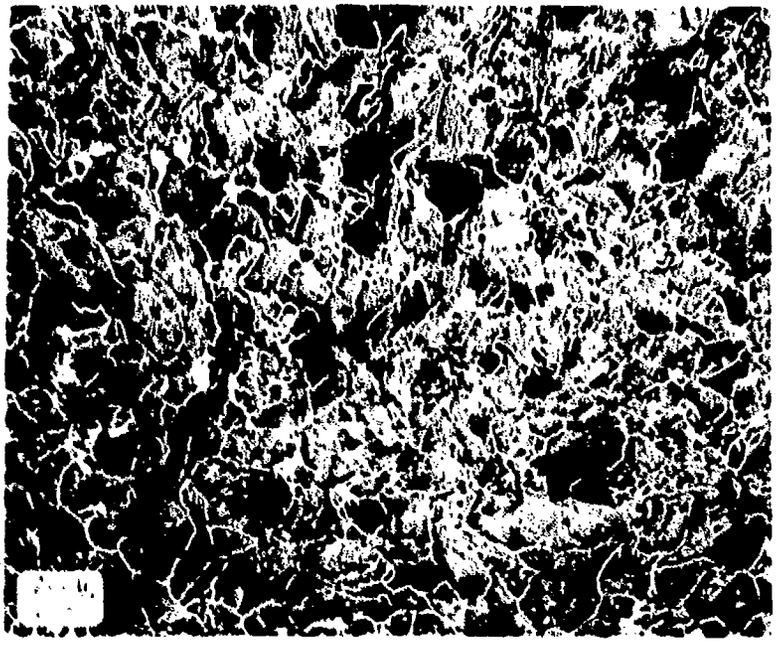

FIGURE 2. Metallograph of sintered copper (41.5 w/o)-coated graphite (cross-sectional face perpendicular to molding load; graphite particles 75-150 um).

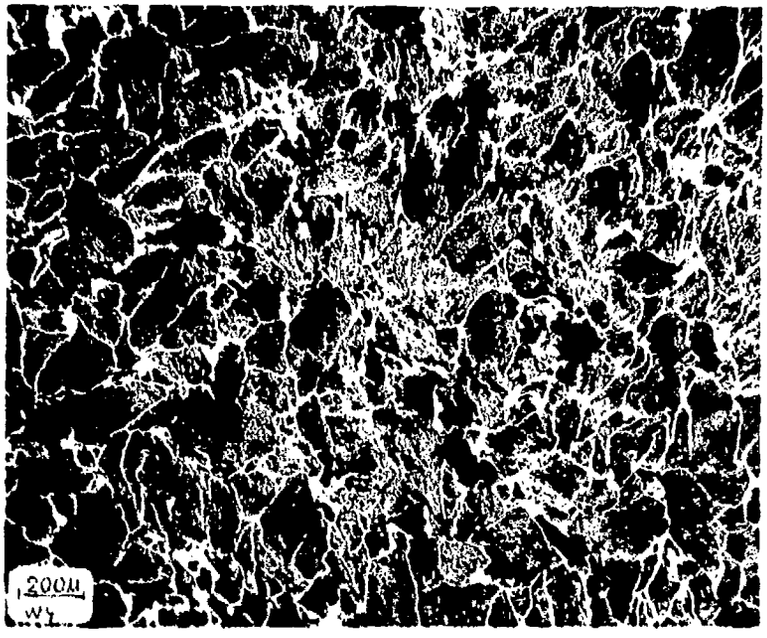

FIGURE 3. Metallograph of sintered silver (34 w/o)-coated graphite (cross-sectional face perpendicular to molding load; graphite particles 75-150 µm).

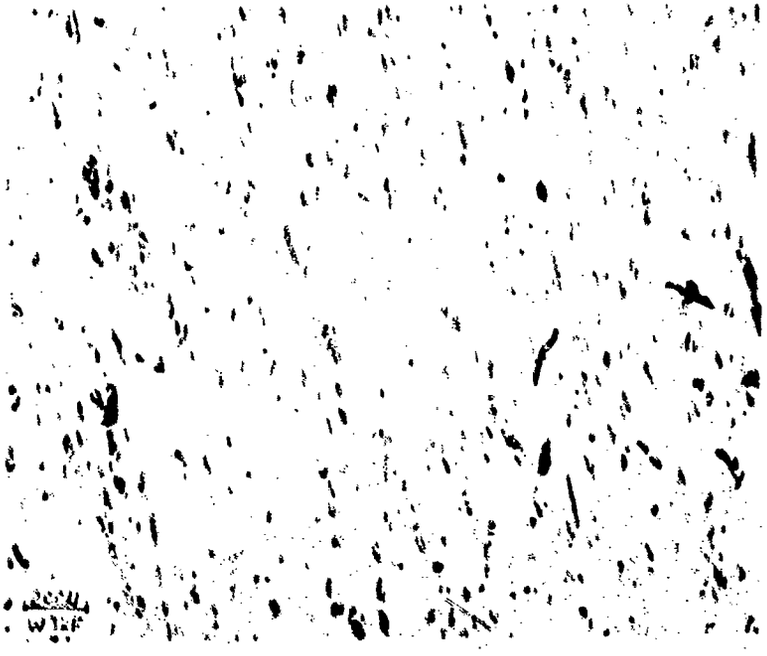

FIGURE 4. Metallograph of sintered silver (97.5 w/o)-coated graphite (cross-sectional face parallel to molding load; graphite particles 38-45 µm).

Curve 693543-A

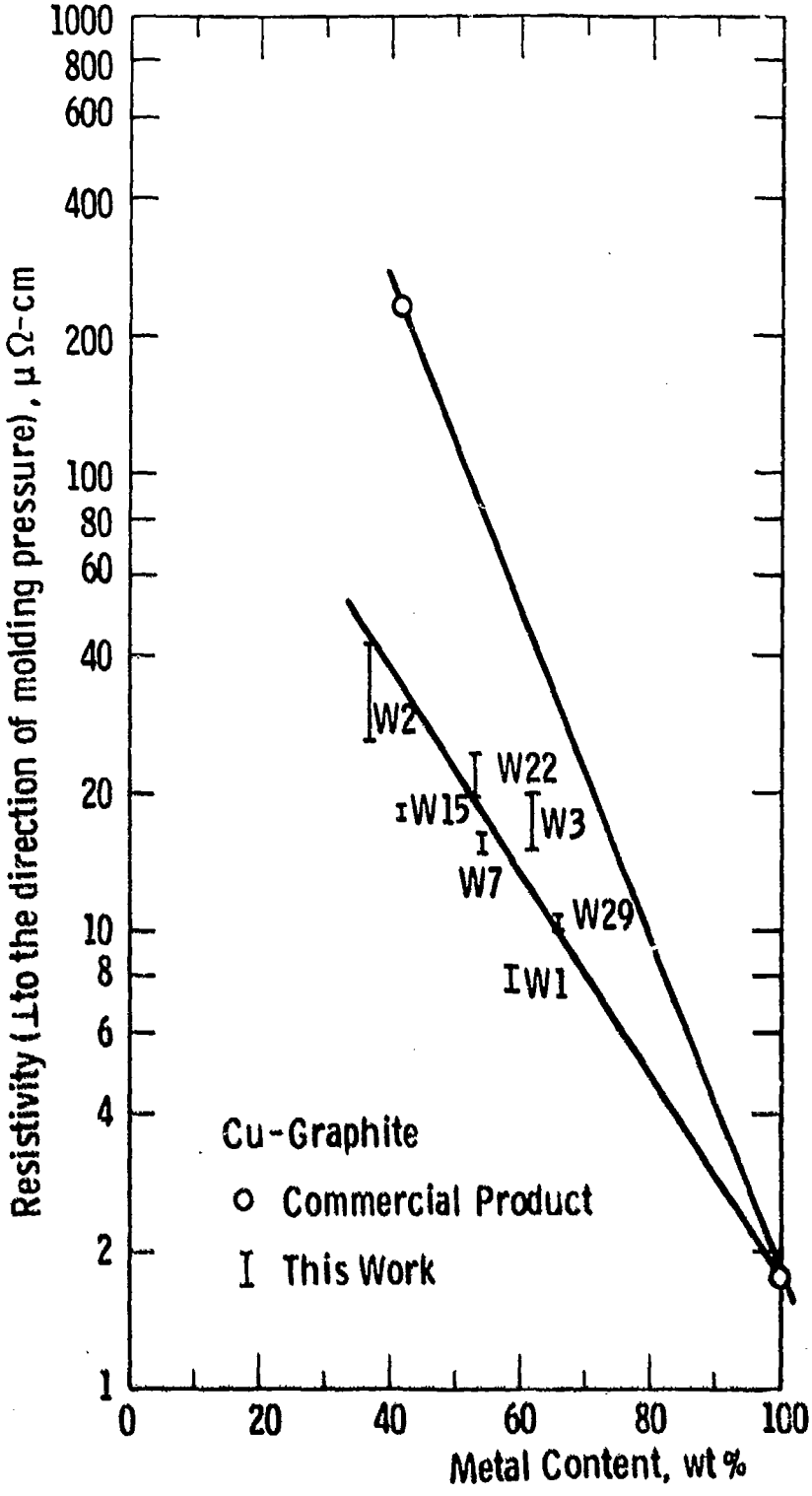

FIGURE 5. Resistivities of sintered copper-coated graphite materials as a function of metal content.

Curve 693544-A

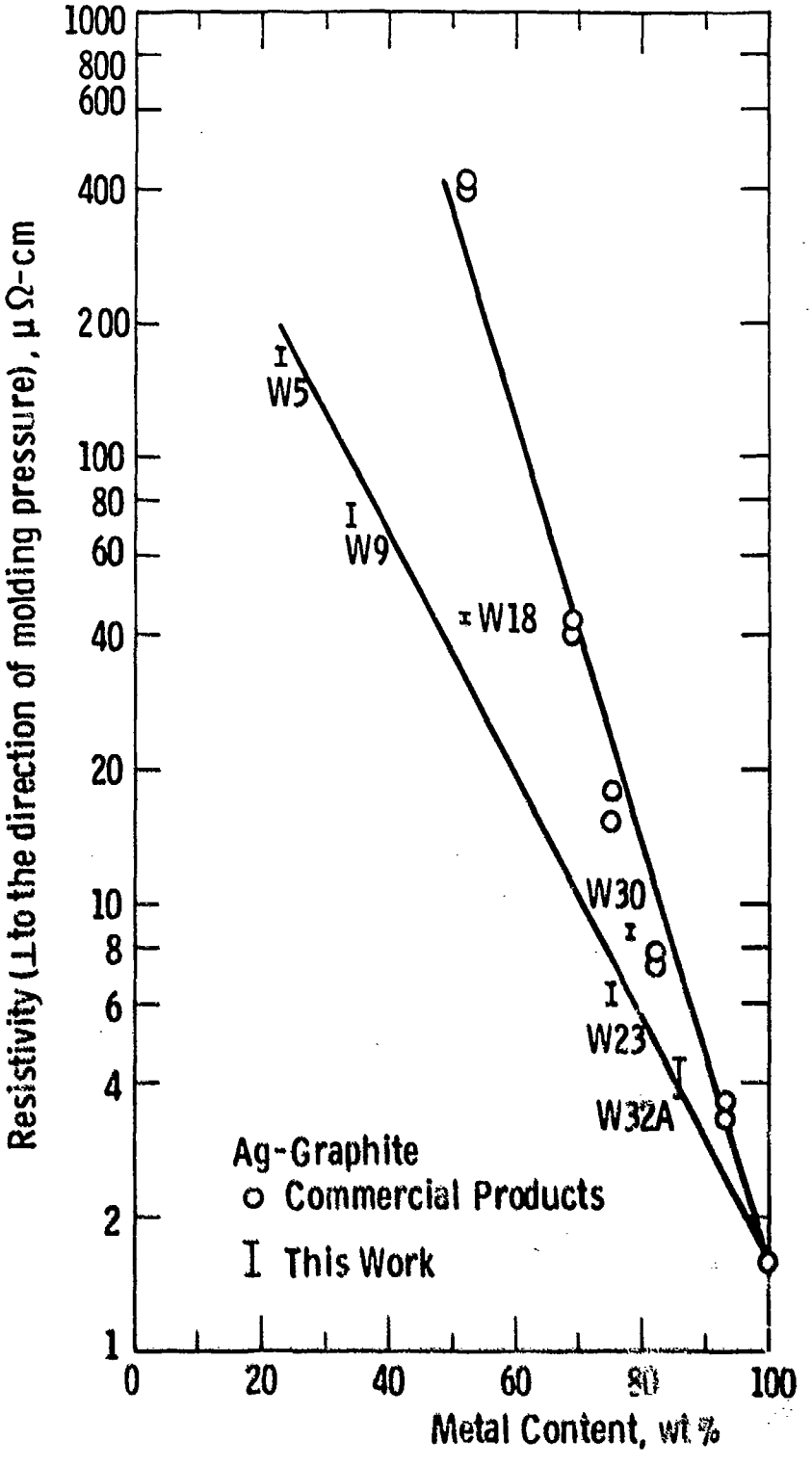

FIGURE 6. Resistivities of sintered silver-coated graphite materials as a function of metal content.

APPENDIX 3.3

THERMOELASTIC EFFECTS IN BRUSHES WITH HIGH CURRENT AND HIGH SLIDING SPEEDS

C. P. Chen and R. A. Burton

Paper to be presented at the Ninth International Conference on Electric Contact Phenomena and the Twenty-Fourth Annual Holm Conference on Electrical Contacts, September 11-15, 1978, Chicago.

Revised
1 April 1978

APPENDIX 3.3

THERMOELASTIC EFFECTS IN BRUSHES WITH HIGH CURRENT AND HIGH SLIDING SPEEDS

by

C. P. Chen and R. A. Burton**

**Department of Mechanical Engineering and Astronautical Sciences, Northweste University, Evanston, Illinois 60201.

THERMOELASTIC EFFECTS IN BRUSHES WITH HIGH CURRENT AND HIGH SLIDING SPEEDS

by

C. P. Chen and R. A. Burton
ME/AS Dept., Northwestern University
Evanston, IL 60201

Abstract

Experimental results in the literature indicate that electric brushes may deform, leading to point contact with the slip ring at high current levels. The present work provides theoretical support for these observations and a quantative statement showing how operating variables influence this behavior. The analysis is restricted to a two dimensional model of the brush, with isotropic and constant material properties. The most unexpected result is that, for steady current flow, cooling of the exterior of the brush increases the tendency to deform unfavorably.

INTRODUCTION

The electrical brush may, in idealized form, be thought of as a wafer shaped object making contact with the moving surface of a steadily turning cylindrical body, or slip ring. The line of contact would be parallel with the axis of the cylinder, and the sliding would be perpendicular to this line. Even when no current passes through the line of contact, frictional heating may deform the brush, causing contact to transform from a uniformly loaded line to one or more discrete patches. This is the result of the formation of thermal asperities which move slowly across the contact zone. These thermal asperities are often several multiples of the height of the initial roughness or waviness of the brush face, and the peak of each corresponds to a small region or patch of contact with the slip ring, which may be highly stressed as well as hot. Several studies have clarified the nature of the transition to patch-contact in the absence of current flow,[1,2] and Dow has verified the theoretical predictions experimentally.[3] Kilaparti[4] has investigated the role of wear and other factors at work in the limited zone of contact.

Approaching the problem from the electrical side, Marshall has shown that a similar formation of heated contact patches occurs in brushes carrying high levels of current.[5,6] McNab[7] has reviewed the problem of brush wear and has noted ambiguities in the literature as to the combined effects of current, load and speed. Undoubtedly these interactions are complicated by the formation of patch contact.

The present study is intended to provide an analysis which incorporates both frictional heating and current flow, and establishes how these and other factors interact to determine contact patch size, stress level and temperature.

STATEMENT OF THE PROBLEM

A two dimensional brush of unit thickness will be assumed, of roughly the configuration shown in Fig. 1. It is approximately in the form of half a circular disk and has a flat side or edge. Near the center of the edge is the contact patch of width $2a$. The outer circular boundary will be taken as an isopotential line over which a uniformly distributed current passes into the brush. Current exits through the contact patch. Assuming the electric field is quasistatic it will obey LaPlace's equation; and once the potential distribution is determined, the distribution of electrical heating may be found.

The resultant temperature field can be obtained in two steps. First a solution is obtained for the condition that electrical heat only flows out through the contact patch, and that all other boundaries are adiabatic. Next a solution is found for heat flow into the contact patch and out through the curved surface of radius R. By superposing these two solutions, suitably scaled, any combination of heat flows through the patch and outer surface can be produced.

Once the temperature fields are specified, the thermal displacement of the boundary can be calculated. In many instances a rounded bulging-out of the contact patch will be predicted, and through application of Hertz's theory of contact of cylindrical bodies the conditions can be found where the contact patch would indeed be pressed smoothly against the slip ring surface with a contact-free gap to either side.

METHOD OF ATTACK

Because the thermal and electrical problems can easily be solved in an axisymmetric configuration (see Fig. 2), it has been found practical to transform these solutions into a very close approximation of the chosen configuration, by conformal transformation. Once the temperature fields are so generated, a simple integral equation can be applied to determine the deflection of the edge of the wafer.

A Green's function for edge deflection can be generated through determination of the deflection distribution produced by a small patch of elevated temperature at an arbitrary position in a semi-infinite plate. This can be found by adaptation of the equations for stress and deflection in a heated axisymmetric body[8] in plane stress. In Fig. 3 is shown the body with the uniform temperature patch of radius ϵ. Disregarding for the moment the broken-line construction also on the figure, we note that for points external to the patch the stresses and deflections are given by:

$$\sigma_r = -\alpha E T \epsilon^2 / 2(x^2 + y^2)$$

$$\sigma_\theta = \alpha E T \epsilon^2 / 2(x^2 + y^2)$$

$$u_r = (1+\nu)\, \alpha T \epsilon^2 / 2\sqrt{x^2 + y^2} \qquad (1)$$

Using the method of images as shown by the broken lines in Fig. 3, we may superpose the fields produced by two temperature sources equidistant from the x-axis, and find that on the x-axis:

$$\sigma_y = 2\sigma_r \cos 2\theta$$

$$\sigma_{xy} = 0$$

$$U_y = 0 \qquad (2)$$

By application of the integral equation derived in Ref. (9) for edge displacements of a plate having an edge load σ_y, we find the normal displacement of the edge, δ, to be:

$$\delta = \frac{2}{\pi E} \int_{-\infty}^{\infty} \sigma_y(\xi) \ln|\xi - x| \, d\xi \tag{3}$$

where ξ is a dummy variable. Integrating and letting $\pi\epsilon^2 = dA_i$, one finds that δ_i is the deflection of the plate edge at $x = 0$, caused by a temperature patch $T_i dA_i$, at the position x_i, y_i.

$$\delta_i = \frac{4\alpha T_i}{\pi^2} \left\{ \frac{\pi y_i}{2} + |x_i| \ln|y_i/x_i| \right\} \frac{dA_i}{x_i^2 + y_i^2}$$

When there is a continuous distribution of temperature in the body the influences may be summed to give

$$\delta = \frac{4\alpha}{\pi^2} \int_A \left[\frac{\pi y}{2} + |x| \ln|y/x| \right] \frac{T dA}{(x^2 + y^2)} \tag{4}$$

As it stands this equation gives the displacement at the origin of the coordinate system, but a simple geometric transformation will cause it to apply at $x = \xi$.

$$\delta(\xi) = \frac{4\alpha}{\pi^2} \int_A \left[\frac{\pi y}{2} + |x-\xi| \ln\left|\frac{y}{x-\xi}\right| \right] \frac{T dA}{y^2 + (x-\xi)^2} \tag{5}$$

It is of practical interest that the second term in the brackets has only a small influence on relative displacements in the contact patch.

TEMPERATURE SOLUTIONS IN THE AXISYMMETRIC PLATE

For the case of simple conduction through the cylindrical surface of radius ϵ, see Fig. 2, LaPlace's equation for temperature will be satisfied by

$$T_c - T(r) = (Q_b/K\pi)\ln(r/\epsilon) \tag{6}$$

where Q_b is the heat flow moving radially outward, T_c is the temperature of the inner cylindrical surface and T(r) is the temperature at arbitrary r interior to R.

Turning now to the question of electric current flow, one finds by analogy

$$e_c - e(r) = \frac{\rho I}{\pi} \ln(r/\epsilon) \tag{7}$$

Noting that electric heat generation will be given by

$$q = \frac{1}{\rho}\left(\frac{de}{dr}\right)^2 \tag{8}$$

it follows that the total electrical heating between r and R is given by

$$Q(r) = \frac{I^2\rho}{\pi} \ln\left(\frac{R}{r}\right) \tag{9}$$

irrespective of the direction of current flow. The maximum magnitude of Q would be

$$Q_{e\ell} = \frac{I^2\rho}{\pi} \ln(R/\epsilon) \tag{10}$$

and would be realized as heat flow through the inner surface, if all heat flow were blocked at the boundary, R. Under the same boundary condition, we may write at any r,

$$-K\frac{dT}{dr} = Q(r) = \frac{I^2\rho}{\pi} \ln \frac{R}{r}$$

and it follows that

$$T(r) - T(R) = \frac{Q_e}{2K\pi} \frac{[\ell n(r/R)]^2}{\ell n(R/\epsilon)} \tag{11}$$

This may be rewritten as

$$T(r) - T(R) = \frac{Q_e}{2K\pi} \left\{ \ell n(R/\epsilon) + 2\ell n(\epsilon/r) + \frac{[\ell n(\epsilon/r)]^2}{\ell n(R/\epsilon)} \right\} \tag{12}$$

CALCULATION OF SURFACE DEFLECTION

As stated above, solutions in the W-plane were to be obtained from the axisymmetric Z-plane solutions by conformal transformation. To this end the Zhukovsky transform may be applied.

$$W = Z + 1/Z \tag{13}$$

This may be rewritten as

$$Z = [\ W + \sqrt{W^2 - 4}\ ]/2 \tag{14}$$

Hence for any W, expressed as a complex number $x + iy$, there will be a Z, which can be expressed as $re^{i\varphi}$. Knowing r, one may use Eq. (6) or (12) as appropriate, to obtain the temperature at the point and at the corresponding W-point. The use of the transform on the electrically heated field is permissible because the quantity

$$q = \frac{1}{\rho}\left[\left(\frac{\partial e}{\partial x}\right)^2 + \left(\frac{\partial e}{\partial y}\right)^2\right] \tag{15}$$

transforms such that

$$q(Z) = q(W)\left|\frac{dW}{dZ}\right|^2 \tag{16}$$

See Ref. (10). Once values of T are known at points in the W-plane it is possible to evaluate the integral of Eq. (5) at various values of ξ. Closed form solution was possible only for the case of simple heat transfer (see Eq. (6)). Consequently, the space was subdivided into a net of points and the influences of each were summed. The simple heat flow solution provided a check on the accuracy of the summation procedure. Results are reported here as the difference in displacement between contact center and edge or

$$\tilde{\delta} = \delta(0) - \delta(1) \tag{17}$$

For the case of simple heat flow radially outward, the exact solution is:

$$\hat{\delta}_{th} = \frac{\ell \alpha Q_b}{\pi K} (0.5708) \tag{18}$$

By numerical integration (for $R/\epsilon = 1000$)

$$\hat{\delta}_{th} = \frac{\ell \alpha Q_b}{\pi K} (0.5715) \tag{19}$$

The close agreement gives confidence in the numerical procedure, so it may be applied to the case of electrical heating with all of the heat passing outward through the contact patch, drawing upon Eq. (12) for the temperatures, and noting that any component of the temperature distribution that is constant throughout the field will not contribute to deformation of the boundary, therefore it will not contribute to $\hat{\delta}$. The result of this numerical integration is

$$\hat{\delta}_e = \frac{\ell \alpha Q_e}{\pi K} \left[-0.5708 + \frac{0.7636}{\ell n(R/\epsilon)} \right] \tag{20}$$

This result is interesting in two respects. First it represents an indentation rather than a protrusion of the surface, and second it is dependent on the size of the brush, R. In the first we note simply that for heat to be removed through the contact patch the lowest temperature must be at the contact surface, hence a deficit of temperature there and the resultant indentation.

The second effect is the result of the fact that the more material through which current is passed the more heat generated.

The combined displacement for electrical heating and brush cooling may be obtained by superposition of

$$\hat{\delta} = \hat{\delta}_e + \hat{\delta}_{th}$$

or

$$\hat{\delta} = \frac{\ell \alpha Q_e}{\pi K} \left[0.5708 \left(\frac{Q_b}{Q_e} - 1 \right) + \frac{0.7636}{\ell n(R/\epsilon)} \right] \tag{21}$$

Since Q_b represents heat passing through the outer surface of the brush it may be thought of as a measure of cooling. If the brush were insulated Q_b would be zero. With some forced cooling Q_b/Q_e might be any value up to or exceeding unity.

COMBINED EFFECTS OF FRICTIONAL AND ELECTRICAL HEATING

Frictional heating of the contact patch is given by

$$Q_f = \mu VP$$

where V is sliding speed, P is contact load and μ is friction coefficient. Recalling that

$$Q_e = (I^2\rho/\pi)\ell n(2R/\ell) \tag{22}$$

one may write

$$Q_{total} = Q_e + Q_f \tag{23}$$

We now note that with isolated slip ring and cooled brush Q_b could have as its upper limit Q_{total}. Hence the maximum value of $\hat{\delta}$, given by Eq. (22) would be

$$\hat{\delta}_{max} = \frac{\ell\alpha}{\pi K}\left[0.5708(Q_{tot}-Q_e) + \frac{0.7636}{\ell n(R/\ell)}Q_e\right] \tag{24}$$

For convenience call the quantity in brackets Y, (in Eq. (24)) making

$$\hat{\delta} = (\alpha\ell/\pi K)(Y) \tag{25}$$

Let us now draw upon the well known relationship for Hertzian contact

$$\hat{\delta} = P/1.72E \tag{26}$$

where $\hat{\delta}$ is the distance the center of the contact is indented relative to the edges of the contact. It follows that if the thermal bump is pressed flat, to assure full contact over the region 2ℓ,

$$\frac{P}{1.72E} = \left[\frac{\alpha\ell}{K}\right][Y] \tag{27}$$

Here it is assumed that the deflection of the slip ring is negligible relative to that of the carbon, therefore only the Young's modulus E of the carbon brush need be considered.

In Eq. (27) it is seen that ℓ increases with brush load P. Increasing of cooling of the brush causes γ to increase and causes ℓ to be smaller for a given load, an adverse condition. Although the derivation is not valid for large ℓ relative to brush size R, nevertheless the condition $\ell = R$ provides a criterion as to when thermal effects are beginning to be important, and for $\ell \ll R$ the equation should serve to predict contact patch size.

To obtain contact temperature one need only to refer to Eq. (5,12) and superpose the magnitudes of $T(r = \epsilon)$, thus giving the elevation of contact temperature above brush temperature T(R). To obtain contact stress note that its mean value would be $P/2\ell$.

ACKNOWLEDGMENT

This research was sponsored by the United States Office of Naval Research.

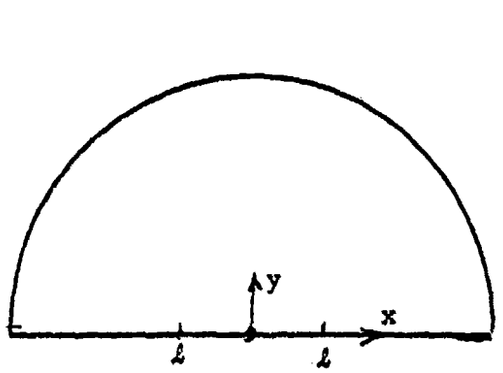

Fig. 1. Idealized configuration of brush. Outer surface R is isopotential, and the contact patch is $-\ell < x < \ell$.

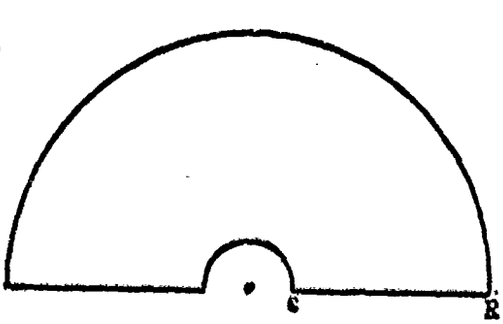

Fig. 2. Axisymmetric configuration, with inner radius c, and outer radius R.

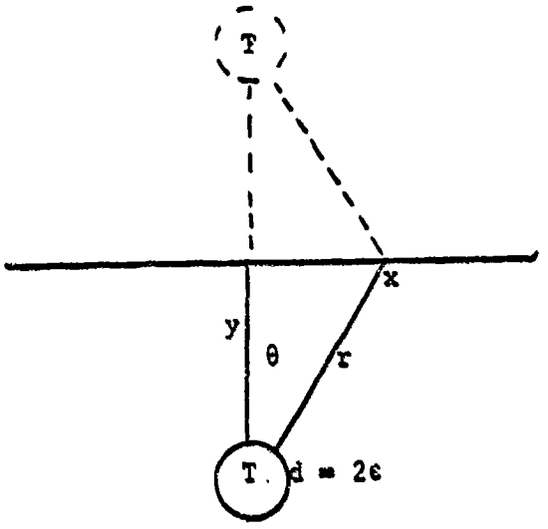

Fig. 3. Illustration for obtaining Green's function for surface displacement produced by small element of elevated temperature T.

REFERENCES

1. T. A. Dow and R. A. Burton, "Thermoelastic Instability of Sliding Contact in the Absence of Wear," Wear, 19, pp. 315-328, (1972).

2. T. A. Dow and R. A. Burton, "The Role of Wear in the Initiation of Thermoelastic Instabilities in Rubbing Contact," ASME Trans., Ser. F, 95, pp. 71-75, (1973).

3. T. A. Dow and R. D. Stockwell, "Experimental Verification of Thermoelastic Instabilities in Sliding Contact," ASME Trans., Ser. F, 261, pp. 359-364, (1977).

4. S. R. Kilaparti and R. A. Burton, "The Thermoelastic Patch Contact Problem for Large Peclet Number," ASME Trans., Ser. F, 100, pp. 65-69, (1978).

5. R. A. Marshall, "The Mechanism of Current Transfer in High Current Sliding Contacts," Wear, 37, pp. 233-240, (1976).

6. R. A. Marshall, "Design of Brush Gear for High Current Pulses and High Rubbing Velocities," IEEE Trans. Power Apparat. Syst., PAS 85, pp. 1177-1188, (1966).

7. I. R. McNab, "Pulsed High Power Brush Research," Electrical Contacts 1977, R. Armington, Ed., Illinois Institute of Technology, Chicago, pp. 107-114, (1977).

8. S. Timoshenko and J. N. Goodier, Theory of Elasticity, Third Ed. New York: McGraw-Hill, 1970, pp. 445-446.

9. Ibid, pp. 107-109.

10. R. Churchill, Introduction to Complex Variables and Applications. New York: McGraw-Hill.

LIST OF SYMBOLS

A	Area of face of brush
E	Young's modulus of brush
e	electrical potential
I	current per unit of thickness of brush
K	thermal conductivity
ℓ	half-width of contact
P	force per unit of thickness holding brush against slip ring
Q	heat flow per unit of brush thickness
q	heat flow per unit of area
r	radial position in transformed Z-plane configuration
R	outer radius of brush
T	temperature
u	displacement
V	sliding speed
W	complex number representing position in W-plane
x	coordinate of position
y	coordinate of position
Z	complex number representing position in Z-plane
α	coefficient of thermal expansion
γ	dimensionless quantity in contact equation
δ	surface displacement
ϵ	$\ell/2$
ζ	position on surface where displacement is given
μ	friction coefficient
ξ	dummy variable
θ	angular coordinate
ρ	electrical resistivity
σ	normal stress
τ	shear stress
ϑ	angular coordinate

D. L. Greene, Manager
Electrical Machines & Systems

J. L. Johnson
Tribology & Magnetofluidynamics

P. K. Lee
Tribology & Magnetofluidynamics

I. R. McNab, Manager
Tribology & Magnetofluidynamics

C. J. Mole, Manager
Electrotechnology Department

J. J. Schreurs
Physical Metallurgy

O. S. Taylor
Electrical Machines & Systems